Aerodynamic optimisation of wind farms using turbulence modelling

Andrew Barnes

A dissertation submitted in partial fulfillment

of the requirements for the degree of

Doctor of Philosophy

of

University of Strathclyde.

Department of Mechanical and Aerospace Engineering

University of Strathclyde

May 10, 2023

I, Andrew Barnes, confirm that the work presented in this thesis is my own. Where information has been derived from other sources, I confirm that this has been indicated in the work.

Abstract

With the need for decarbonisation and more abundant energy sources becoming more immediate, it is necessary to explore and optimise the world's energy generation. The three major sources for this goal are considered to be nuclear, solar, and wind energy, where wind is the more abundant energy source in the UK.

Currently, HAWTs are the standard wind turbine type deployed worldwide, however evidence has demonstrated that VAWTs may be better suited to some major wind energy applications, namely wind farms and floating turbines. The more complex flow problem of VAWTs has slowed their development by requiring greater resources to conduct equivalent simulations.

This thesis addresses how VAWT turbine and array designs are evaluated. It proposes greater standardisation of VAWT designs to maximise efficiency and comparability of research, the importance of field conditions in evaluating VAWTs, and a more refined CFD procedure to enable quicker accurate VAWT simulation.

Through a review of the literature and simulation, an analysis of VAWT aerodynamic design and simulation procedure is conducted. Choice of array design is compared, the impact of CFD procedure on accuracy in different scenarios is evaluated, and the impact of Reynolds Numbers and Turbulence Intensity on VAWT power outputs and wakes, and on simulation accuracy, is analysed.

Analysis of array design demonstrated a potential 80% improvement in VAWT power output from using the Truss array design. The Four-equation turbulence model called Transition SST offers the greatest accuracy for predicting individual VAWT wakes however this was not sufficient for array predictions. Both Reynolds Number and Turbulence Intensity have a significant effect on VAWT wakes and

CFD accuracy so must be accounted for.

Acknowledgements

Firstly, I would like to thank the EPSRC and the States of Guernsey Higher Education Grant for funding my studies, and the University of Strathclyde for covering my moving and equipment costs and helping to solve the numerous funding mishaps.

Thank you to my supervisor Ben Richard Hughes for supporting and guiding me throughout my research career, with special thanks to Dominic O'Connor and Daniel Marshall-Cross who have provided vital guidance during this time. I would also like to thank the rest of the research group: Sheen, Diana, Hasan, and Katrina for accompanying me on this journey.

For providing a welcome distraction from the combination of academia and the pandemic, I'd like to thank my family for not kicking out their eternal student son, Sunny Chen for attempting to understand PhD life, Hao Xu for trying to do the opposite, and G Block for putting up with Guernsey internet.

Research Outputs

Published Research Papers

1. Andrew Barnes and Ben Hughes. Determining the impact of VAWT farm configurations on power output. Renewable Energy, 143:1111–1120, May 2019.

2. Andrew Barnes, Daniel Marshall-Cross, and Ben Richard Hughes. Towards a standard approach for future Vertical Axis Wind Turbine aerodynamics research and development. Renewable and Sustainable Energy Reviews, 148:111221, Sep 2021.

3. Andrew Barnes, Daniel Marshall-Cross, and Ben Richard Hughes. Validation and comparison of turbulence models for predicting wakes of vertical axis wind turbines. Journal of Ocean Engineering and Marine Energy 2021 7:4,7(4):339–362, Jul 2021.

Acronyms

2D	Two Dimensional
3D	Three Dimensional
ANN	Artificial Neural Network
AR	Aspect Ratio
CFD	Computational Fluid Dynamics
CFL	Courant-Friedrichs-Lewy Condition/Courant Number
DES	Detached Eddy Simulation
HAWT	Horizontal Axis Wind Turbine
LES	Large Eddy Simulation
LLFVW	Lifting Line-Free Vortex Wake
PIV	Particle Image Velocimetry
RANS	Reynolds Averaged Navier Stokes
SAS	Scale-Adaptive Simulation
SPIV	Steroscopic Particle Image Velocimetry

TSR	Tip Speed Ratio
URANS	Unsteady Reynolds Averaged Navier Stokes
VAWT	Vertical Axis Wind Turbine
VTM	Vorticity Transport Model

Nomenclature

σ	Solidity
σ_1	Turbulence Profile
c	chord
C_{AP}	Array Power Coefficient
C_n	Normal Force coefficient
$C_{p\text{-}max}$	Maximum Power Coefficient
C_p	Power Coefficient
C_t	Tangential Force Coefficient
D	Diameter
I_{ref}	Reference Turbulence Intensity
N	Number of Blades
P_R	Wind Speed Distribution
r	Radius
Re	Reynolds Number
Re_c	Chord Reynolds Number
Re_D	Turbine Reynolds Number

S	Swept Area
T	Duration (constant)
t	Time (variable)
t/c	Thickness-to-chord ratio
TSR_{opt}	Optimum Tip Speed Ratio
V	velocity
V_{avg}	Average Velocity
V_{cg}	Velocity of a Coherent Gust
V_{e1}	Extreme 1 Year Wind Speed
V_{e50}	Extreme 50 Years Wind Speed
V_{gust}	Velocity of a Gust
V_{hub}	Velocity at hub height
V_{ref}	Reference Velocity
X	Cross-stream Position
Y	Streamwise Position
y^+	Dimensionless Wall Distance
z	Height
z_{hub}	Height of Hub
z_{ref}	Reference Height

Contents

List of Figures

List of Tables

Chapter 1

Introduction

The race to decarbonisation has fuelled the research and development of many renewable energy technologies, with the aim to reduce the carbon emissions of electricity sources whilst also electrifying other forms of energy usage. This poses a major problem in that the world must expand its renewable energy sources at a rate which can keep up with both the increasing proportion of energy usage which comes from electricity and increasing the proportion of electricity which comes from renewable sources, resulting in exponential increases in renewable energy deployment.

One of the most prominent forms of renewable energy in the UK is wind energy due to the relatively good wind resource available both onshore and in suitable offshore waters. According to the Department for Business, Energy and Industrial Strategy, this resulted in wind energy accounting for 19.8% of the UK's electricity production in 2019, the second highest source after natural gas and overtaking nuclear[14]. In the latest energy cost projections by BEIS, the price of new onshore wind projects is also amongst the lowest at £46/MWh, compared to the lowest, solar PV, at £44/MWh and Combined Cycle Gas Turbines at £85/MWh, with offshore wind costing £57/MWh[15]. It should be noted that these cost projections were made before the current energy and materials crisis of 2022 however, and so current pricing is much higher than projected[16].

The standard deployment of wind energy is in the form of Horizontal Axis Wind Turbines (HAWTs) due to previous conclusions that they offer the greatest

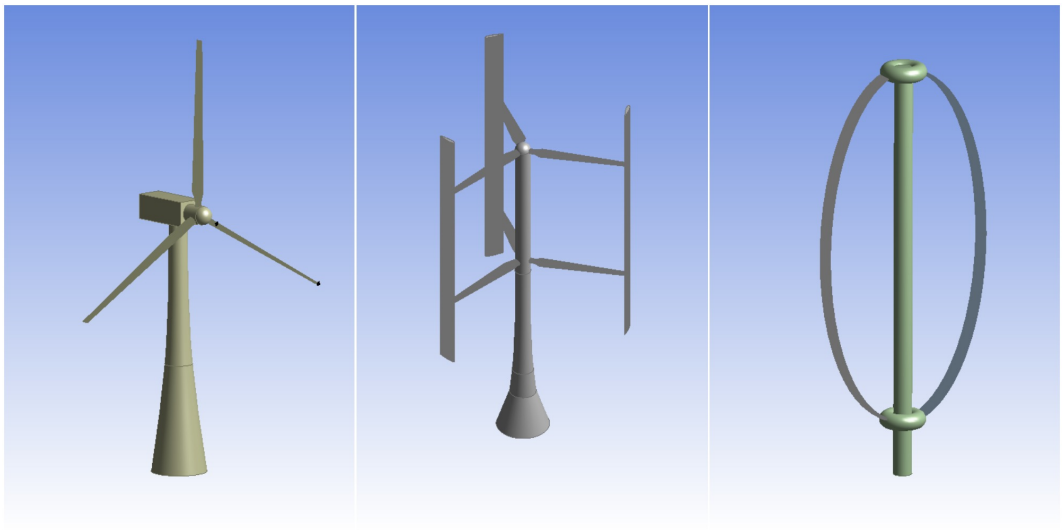

Figure 1.1: The major wind turbine designs, from left to right: HAWT, H-VAWT, Φ VAWT

cost and power efficiency compared to other alternative forms. One other main form of wind turbine exists in the form of Vertical Axis Wind Turbines (VAWTs), which can be split into two further types, lift-based which is often referred to as Darrieus, and drag-based known as Savonius. Out of these two, the lift-based VAWT is the closest competitor to HAWTs because being lift-based allows for Tip Speed Ratios (TSRs) above 1 to be reached, therefore allowing higher power coefficient (C_p) compared to Savonius turbines which are limited to TSR$\leq$1. It should be noted that the power coefficient of wind energy devices is limited by the Betz limit to an efficiency of 59.26%[17], and so it is not possible to develop a wind turbine which outperforms this. Throughout this thesis when the acronym VAWT is used this is referring to lift-based VAWTs. Due to the lack of previous viable commercialisation of VAWTs, the technology can be considered to be novel. Examples of a typical HAWT design and example lift-based VAWT designs are shown in figure 1.1.

In recent years, the assumption that HAWTs are the most effective wind energy technology compared to VAWTs has been questioned for two reasons: Dabiri[18] found that there is the potential for significant gains in C_p of up to 10% for individual turbines during field testing when the array layouts based on closely-spaced turbine pairs are used for VAWTs, in contrast to the decreases seen in HAWT arrays, where in realistic scenarios wind turbines typically exist in arrays rather than

isolated turbines. This resulted in power density per land area usage increasing 6 to 9 fold compared to HAWTs. Secondly, there is increasing evidence that isolated VAWTs can achieve similar C_p to HAWTs[19][20][21][22]. In combination, it may be possible for VAWTs to offer significantly higher power output per turbine to HAWTs.

Excluding this advantage, there may be other advantages to using VAWTs. Dabiri[18] demonstrated that VAWT arrays can achieve higher power density than HAWT arrays which would allow for smaller patches of land to be used effectively for wind energy deployments. VAWTs are also better suited to floating offshore wind in deep waters because the design allows for a low centre of gravity by placing the generator below water level, compared to HAWTs where this must be placed at hub height and so requires a greater effort to balance the system.

One of the main issues which has held back VAWT development is the difficulty of accurately simulating VAWTs due to being a much more difficult flow problem than HAWTs. HAWTs have a constant airspeed at a given point on the blade throughout the rotation whilst VAWTs have a sinusoidal airspeed dependent on the position of the blade, which results in dynamic stall and at low Tip Speed Ratios can result in low Reynolds numbers for the blade. These are more difficult flow problems for simulation techniques such as Blade Element Momentum or Computational Fluid Dynamics (CFD) to accurately predict, and so because these techniques cannot always be relied upon, VAWT simulation procedure continues to require significant investigation.

There is also a relative lack of consensus and development regarding a standardised VAWT design, akin to the 3-bladed HAWT. As a result, research on VAWTs is spread thinly and can be difficult to compare due to the amount of variety between designs. In particular, older VAWT designs used a Φ shape whilst newer designs typically use a H-shape, but because much of the research completed for utility scale VAWTs was during the Φ era, it is not applicable to newer H-bladed designs[1].

Some delay in development may have been caused by preconceived notions

regarding the most suitable scenarios for VAWT deployment, namely that the inherent omnidirectionality makes it more suitable for locations with highly variable and turbulent wind conditions. This is common in urban environments, hence VAWT development has often been focused on small scale turbines which are suitable for deployment on buildings, such as for residential purposes. Omnidirectionality has also resulted on development focusing on simpler designs, on the basis that the lack of need for yaw and pitch control would reduce turbine and therefore energy costs. Instead, there may be greater advantages from more complicated designs for example the use of blade-pitching[23], and larger scales[24]. This desire for simplicity and smaller scales has resulted in relatively limited modern research on more complicated aspects of aerodynamic design, including the relationship between scale and performance characteristics.

From these problems, several research gaps can be identified. There was need for further study of how changes in flow conditions such as Reynolds Number and Turbulence Intensity affect VAWT operation in order to determine the applicability of typical wind tunnel experiments to commercial scale VAWTs, which will also determine the need to adhere to industrial standards such as IEC64100 which are often ignored in the literature. Improvement in the accuracy of CFD and other VAWT simulation methods and procedures was necessary in terms of achieving accurate results with minimal computational resources. Notably, the variation of flow conditions may impact the potential accuracy of simulation methods so understanding any potential interactions is critical. Use of VAWT arrays also required further investigation regarding optimal design procedure and the impact of VAWT geometry, alongside the accuracy of CFD for modelling flow within an array.

By understanding the impact of flow conditions on VAWT performance characteristics, researchers will be able to better design experiments. Similarly, understanding how these factors affect the accuracy of CFD modelling allows for simulations designed to minimise error, and subsequently experimental design may also take this into account to allow their use as validation baselines. By improving CFD procedure, a better balance between accuracy and computational resource require-

ments can be achieved. Given that Large Eddy Simulation (LES) models require very large computational resources to achieve high accuracy, if lower resource Unsteady Reynolds Averaged Navier Stokes models can manage similar, or otherwise sufficient, accuracy reliably this allows for a much greater volume of VAWT aerodynamic simulations, and therefore research, to be conducted by the finite resource of researchers and available computational resources. There was also a lack of any computational validation of using CFD to predict the flow within VAWT arrays, where understanding the causes of any error is vital to the commercialisation of VAWTs given the demonstrated advantages which can arise from VAWT arrays.

This thesis sought to address these research gaps through a review of the literature to determine the best directions for VAWT aerodynamic design and experimental and simulation procedure. Furthermore, a series of simulations using CFD have been conducted in order to evaluate the impact of array design on array power coefficient, including use of optimisation procedures. CFD procedures have been validated against experimental baselines for several different isolated turbine scenarios and an array scenario to determine the most accurate methodologies. The impact of Turbulence intensity on VAWT wakes has also been evaluated using CFD. This methodology is outlined in the flowchart in figure 1.2.

1.1 Thesis Structure

The structure of this thesis is as follows:

Chapter 1 introduces the topic of the thesis and provides context for the research conducted including the need for this research.

Chapter 2 reviews the literature in order to determine research gaps and identify and analyse any potential trends which are evidenced by the literature. Identified research gaps provide a focus for the research whilst any trends which are identified can fill some research gaps. The aims and objectives of the research are stated.

Chapter 3 outlines the methodologies used for the research alongside justifying the use of the methodologies. The methodology for assessing VAWT array performance, including optimisation procedure is shown. The methodology for conduct-

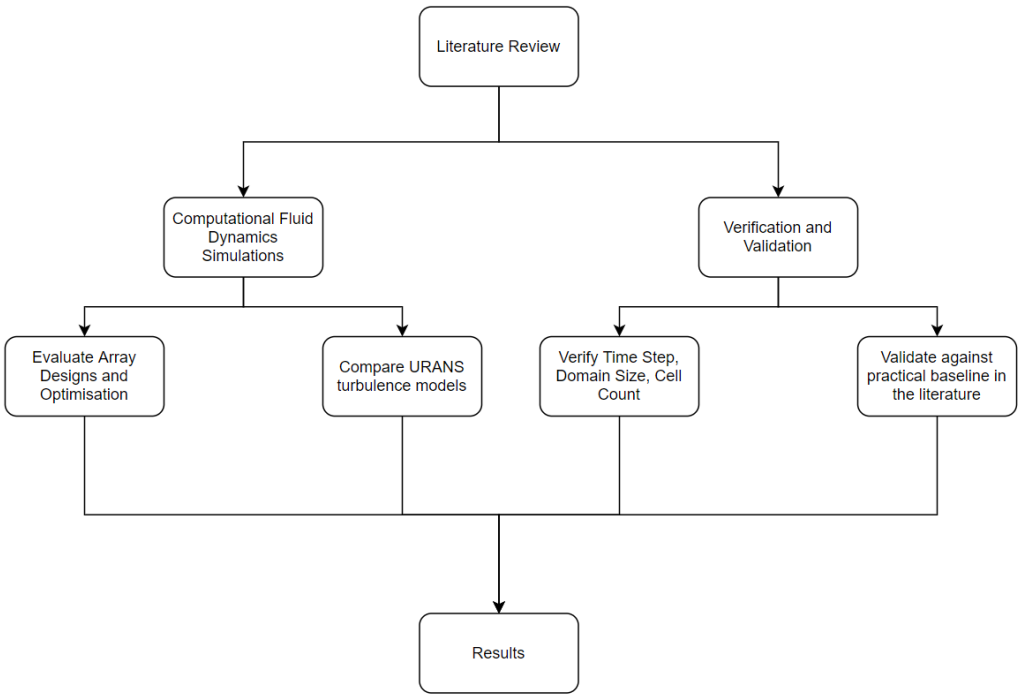

Figure 1.2: Flowchart of Methodology

ing the CFD validations for the chosen scenarios is shown.

Chapter 4 demonstrates the results of the conducted research including appropriate discussion of the value and limitations of the research.

Chapter 5 concludes the thesis and demonstrates how the research has met the objectives outlined in section 2.11 in order to meet the aims outlined in section 2.10. The contribution to knowledge and potential areas for future research are outlined.

Following Chapter 5, all references included in the thesis are listed.

Chapter 2

Literature Review

2.1 Introduction

This review will work towards evaluating current progress towards VAWT array design and consider the accuracy and utility of available VAWT testing methods, including both simulation and practical experiments. In order to inform these, it is also necessary to first fully understand the turbine design in order to predict how changes in this will impact array design and simulation procedures. From this progress, the relevant research gaps will be determined to inform the research conducted in this thesis.

2.2 Design

The design of a VAWT circles around several major passive features, namely the blade shape, Reynolds number, aerofoil, solidity, and aspect ratio. Furthermore there are other passive and active features such as pitch to be considered in more complex turbine designs which can increase power output.

2.2.1 Blade Shape

Numerous blade shapes have been proposed for lift-based VAWTs, aiming to improve efficiency, simplicity, or structural design. The most prominent of these are the Φ design and the H-bladed design or variations upon these.

The Φ design is the classical design used in Sandia testing[25] shown in figure 2.1. A curved blade design is used which should reduce blade tip effects however

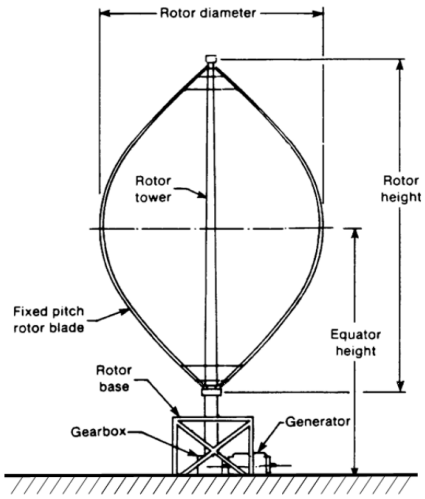

Figure 2.1: Diagram of a Darrieus Φ turbine [1]

this comes with manufacturing difficulties. Compared to newer designs, longer blades are required for the same swept area, and the variable solidity has complex effects on performance. The blades must be either bent permanently into shape, which is a difficult process, or bent in place which reduces lifetime. Because of these issues the design became less popular, however some authors such as Delafin et al.[26] continue to use it due to the experimental data available for larger scale Φ turbines.

H-bladed turbines shown in Figure 2.2 are the most commonly evaluated in modern literature as they solve some issues of the Φ design while also offering greater simplicity. The design allows for evaluation using 2D CFD and the straight blades make manufacturing simpler. In this review, nearly all studies evaluated use H-turbines unless stated otherwise.

Variations of H-turbines have been created such as variable geometry versions which reduce the swept area at high wind speeds, and V-turbines which replace the tower with acutely angled struts. The following blade shapes are all variations upon the H-turbine.

Liu and Xiao demonstrated using a Fluid Structural Interaction simulation that H-turbines with flexible blades increased $C_{p\text{-}max}$ by up to 8%, although performance reduces at higher TSR[27]. Many studies on H-turbines fail to account for this

interaction.

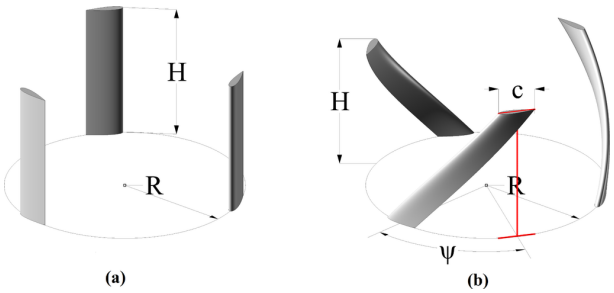

Figure 2.2: Left: H-Bladed VAWT, Right: Helical Bladed VAWT [2]

Helical VAWTs, as shown in figure 2.2, use a blade which curves around the circumference of the turbine in order to reduce the torque ripple. Helical angle choice is important for using this design effectively, with low helical angles having minimal improvement on torque ripple or C_p[28][29], and that turbines with helical angles tending towards 360 degrees/number of blades offer a circle-tending torque rose[2]. Gosselin[30] demonstrates that a high helical angle reduces efficiency of the turbine, however this is likely due to the low turbine AR used which causes worse spanwise propagation of the separation bubble.

Battisti et al.[28] and Scheurich and Brown[31] demonstrated better performance above TSR_{opt}, while Alaimo et al.[2] found reduced $C_{p\text{-}max}$. Scheurich and Brown also demonstrated that helical turbines have improved resistance to unsteady conditions.

It should be noted that variable pitch is incompatible with helical turbines, so a design choice must be made.

Armstrong et al. investigated a turbine with canted blades, a design similar to helical turbines by allowing the blades to experience a variety of angles of attack at one orientation, however without curving the blade around the turbine circumference[4]. Armstrong used tilted blades which would affect results, however no other literature was found for canted blades. $C_{p\text{-}max}$ reduced from 0.32 to 0.29 when transitioning from straight vertical blades to canted tilted blades. Future work should investigate this design without tilting because it potentially offers some benefits of helical blades with simpler manufacturing.

Multi-section turbines also propose to reduce torque ripple by splitting blades spanwise into staggered sections. Gosselin[30] found that while a 2-layered design reduces C_p ripple, C_p overall drastically decreases due to the low blade aspect ratio and wake interference between sections. This means that the design could be viable when a very high blade AR is used for each section. Solidity must also be considered as high solidity turbines cause greater wake interference between blades. These characteristics imply that multi-section VAWTs are best suited to very large scales where low solidity is optimal for efficiency[3][32] and the sectioning has a similar effect to segmenting blades and so will reduce transport costs[33][34]. The ability to manipulate the centre of gravity of VAWTs through the height of the generator is advantageous for very tall multi-section turbines in that this can be used to balance the impact of upper sections on centre of gravity.

Variable blade profiles have the potential to cater for varying conditions along the blade, for example swept blades can be used to reduce tip effects and for larger turbines account for the difference in wind speed due to atmospheric wind shear which results in higher speeds at higher altitudes. Hussain et al. implements a variable aerofoil blade by stretching the NACA 63-415 airfoil thickness-wise with the thicker end at the top of the blades, producing higher $C_{p\text{-}max}$ but a small operating range and higher torque ripple factor compared to constant thickness designs[35]. Hussain et al. did not account for wind shear although this is unlikely to affect performance at the scales used, but means a research gap remains for larger scale turbines where wind shear would become significant. Wind shear would affect the torque profile across the turbine by resulting in higher torque at the top of the blades, with this also resulting in differences in TSR between the top and bottom of the blades, where large turbines could experience a difference of 1-2m/s in wind speed between the top and bottom of the blades based on the IEC64100 wind shear profile[36]. This would mean that blade profile design should tend towards lower sections of the blade being optimised for high TSR whilst higher sections are optimised for lower TSR compared to the TSR experienced at the midplane.

2.2.2 Reynolds Number

The consensus finds performance improvements with increasing Reynolds number (Re) [30][24][28][37][38][39][40][6] with evidence that there is a limit where Re independence occurs[24][41][42][43]. Re positively correlates with $C_{p\text{-}max}$ and expands the operating range due to improved performance at high TSR, therefore VAWTs are less effective in an urban environment due to their small scale and low wind speed causing low Re.

Reynolds number is stated in two ways across studies, relating either to the chord of the blades or the diameter of the turbine. Bachant and Wosnik[42], using an experiment, shows chord Reynolds (Re_c) independence at $2.1x10^5$ with a turbine Reynolds number (Re_D) of $0.8x10^6$. This is in line with Fiedler's experimental study[5] which found chord Reynolds independence at $2.1x10^5$ also. Rezaeiha et al.[43] doesn't show chord Reynolds independence during their testing using 2D CFD. Blackwell et al.'s experimental results using a Φ-turbine shows that this is solidity dependent, with lower solidity turbines showing chord Reynolds independence at as low as $1.54x10^5$ while a turbine with a solidity of 0.3 didn't show independence at the highest tested value of $2.94x10^5$[24]. It should be noted that Bachant and Fiedler both used high solidity H-turbines of 0.48 and 0.4 respectively with both using 3 blades for comparability, while Blackwell used a Φ-turbine with 2 and 3 blades depending on solidity, which would affect results.

2.2.3 Aerofoil Design

The aerofoil used can severely impact performance, however one design won't offer better overall performance. Aerofoils have different responses to wide angles of attack, meaning some are more resistant to dynamic stall and so have smaller torque ripples. Other characteristics of the aerofoil can affect the TSR/C_p curve, impacting TSR_{opt} and $C_{p\text{-}max}$ Reynolds number and therefore scale also alters the TSR/C_p curve of an aerofoil.

The main criteria for aerofoil design are thickness-to-chord ratio (t/c) and camber. Regarding camber, results tend toward a slight camber being advantageous with Asr et al.[44], Danao et al.[45], Claessens[19], Islam et al.[46], and Ferreira[47]

demonstrating ideal camber of less than 4% and typically <2%. Elkhoury et al.[48] found that symmetrical aerofoils perform better which is surprising given the low Re used, as other studies with low Re generate cambered aerofoils[44][47]. Claessens also found that camber becomes undesirable with higher turbulence, which is important because turbulence in the field is higher than used in most studies.

Findings for t/c show larger t/c improving low TSR performance due to delayed stall at the expense of high TSR performance[30][46]. Very high t/c can cause decreased $C_{p\text{-}max}$ due to increased drag[45][46] and is also less desirable at higher turbulence intensities[19]. Asr et al.[44] found higher thickness aerofoils possess better self-starting behaviour and Elkhoury et al.[48] finds that thicker aerofoils perform better in higher solidity turbines. Islam et al.[46] considered the effects of leading edge radius and trailing edge thickness on the performance of a modified LS-0417 aerofoil. An increase in leading edge radius from 2.97% to 4% improved performance while also improving resistance to surface roughness, and decreasing the trailing edge thickness from 0.71% to 0% improved high TSR performance.

Different aerofoil series have been studied, although the typical option is the NACA 4 digit series as this showed good promise in early development and is easy to manipulate. Symmetrical versions are often chosen as the baseline[19][44][45][46][47][49][21], although cambered versions are also used[50]. Mohamed et al. used NACA 6 series aerofoils with the NACA 63-215 and 63-415 offering the best performance[51].

Regarding other series, Mohamed[52] investigated S and FX series aerofoils, of which the S-1046 and FXLV152 showed $C_{p\text{-}max}$=0.4051 and 0.3576 from 0.2964 given by the NACA0018 baseline, however they also had increased TSR_{opt} of 8 and 7 compared to 6 for the NACA0018. These have very high TSR_{opt} values compared to other studies. Mohamed and Islam et al. tested LS aerofoils, the LS(1)-0413[51] and LS-0417[46] respectively. Mohamed found that the LS(1)-0413 performed slightly worse than the NACA63-415 at low TSR but had a wider operating range due to improved high TSR performance. Islam found that the NACA0015 produced better results across the board compared to the LS, S, and NLF aerofoils.

Table 2.1: Studies producing customised aerofoils for VAWTs

Author	Method	$C_{p\text{-}max}$	% Change	Notes
Claessens[19]	Selection	0.48	5%	
Islam[46]	Selection	0.3	20%	
Balduzzi[53] & Bianchini[54]	Virtual Camber	N/A	N/A	
Ma[55]	Multi-Island Genetic Algorithm		27%	
Carrigan[56]	Differential Evolution Genetic Algorithm		6%	Solidity co-optimised
Ferreira[20]	Genetic Algorithm	0.525	4%	
De Tavernier[22]	Genetic Algorithm	0.57	8%	
Bedon[49]	Bézier Curve	N/A	8%	
Chen[21]	Orthogonal Optimisation	0.46	15.5%	
Jafaryar[57]	Response Surface Methodology	0.18	14.2%	

Parakkal et al. investigated Joukowski aerofoils and found that some offered a C_p improvement compared to the baseline NACA0012 and NACA4312[50].

Custom aerofoils are summarised in Table 2.1, with the method of customisation listed, showing no clear reliable advantage from any method. Some studies such as Claessens[19] and De Tavernier et al.[22] demonstrate increased thickness which will improve structural performance.

In summary, choice of aerofoil is dependent on other aspects of turbine design. Optimisation algorithms offer a good method of design, although potentially at a high time cost.

2.2.4 Solidity and Number of Blades

Liang et al. found that chord has a different relationship with C_p compared to the other variables in solidity (equation 2.1): number of blades and turbine radius, which have very similar relationships shown in figure 2.3 [3]. Chord length has a much larger effect on C_p, especially at lower solidity values which are more commonly seen in VAWTs, and the graph demonstrates that optimisation by chord length produces different results to the other solidity variables. At higher solidity values, the trends synchronise however. These may partly be due to the corresponding change in Re with chord length, however the turbine used is modelled on the

one used by Fiedler and Tullis[5] which demonstrates Re independence, and the magnitude of variation from the other conditions is much larger than expected from Re dependence.

$$Blade\,Density = \frac{N}{r} \tag{2.1}$$

From this result, the measure of solidity should be altered to improve comparability between turbines. Equation 2.1 should be used, and accompanied by chord length as an independent variable. Given this hasn't been implemented in most literature, this section will continue based upon the original solidity definition.

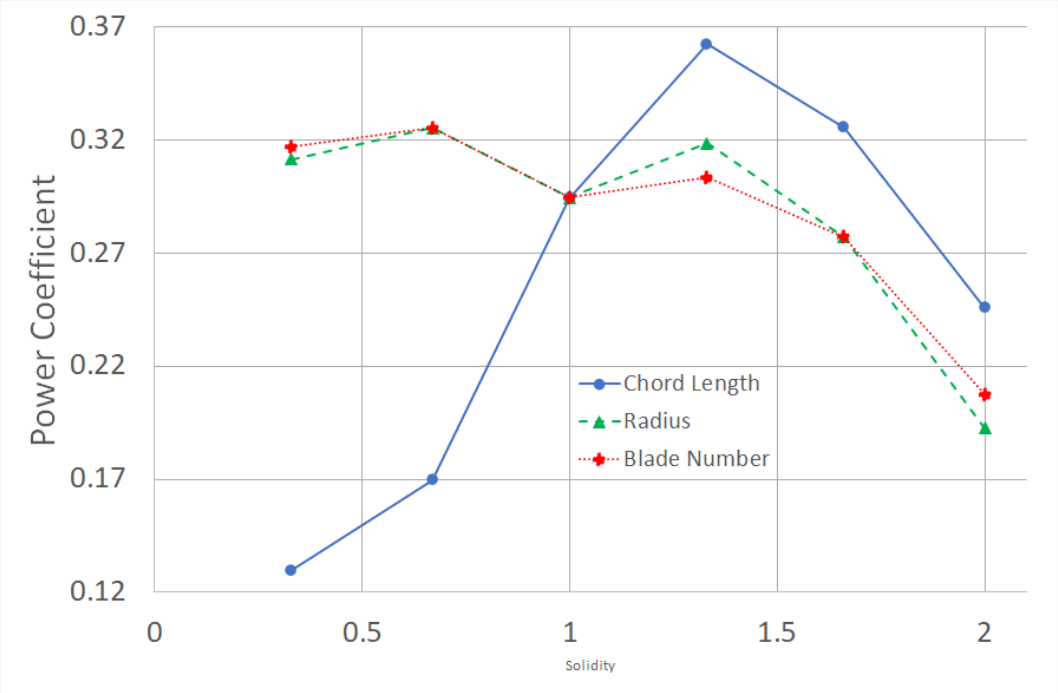

Figure 2.3: Comparing the effects of solidity as a function of chord, blade number, and turbine radius on performance [3]

Liang et al. also finds that ideal solidity range depends upon scale, with larger scale turbines having a smaller ideal range of 0.2-0.6 whilst for smaller turbines it's 0.2-1.28[3]. Meanwhile Sagharichi et al. suggests a range of 0.4-0.6 for fixed pitch VAWTs, however for variable pitch VAWTs even higher solidities of 0.8 offer better performance, particularly at lower TSR[58]. Hand and Cashman found an ideal range of 0.2-0.4 with $C_{p\text{-}max}$ occurring at a solidity of 0.275[32]. The cause of

the lower suggestion by Hand is likely due to the much higher Reynolds numbers tested, in the 10^6-10^7 range compared to 10^5 for Liang and Sagharichi. Resultantly, a negative logarithmic relationship between optimum solidity and Reynolds number is expected, however further modelling is required.

Gosselin[30], Rezaeiha et al.[59], Sagharichi et al.[58], Blackwell et al.[24], and Howell et al.[60] demonstrate that higher solidity is suited to lower TSR operating conditions, with solidity increases causing decreases in TSR_{opt} and improving low TSR performance, while decreasing high TSR performance.

Jain and Abhishek demonstrate that increasing solidity via increasing chord length or number of blades improves $C_{p\text{-}max}$ at lower TSR, and increases blade power ripple[61]. Lee and Lim agree on chord length and shows a smaller operating range[29].

Mohamed[62] and Claessens[19] both agree that increasing solidity aids self-starting behaviour however they disagree about the value required, with Mohamed stating >0.25 is sufficient while Claessens states >0.6. De Tavernier et al.[22] confirms that aerofoil choice affects optimum solidity, explaining the discrepancy.

Both Battisti et al.[28] and Sutherland et al.[1] recommend using 3 blades instead of 2 with Battisti finding C_p increases across the TSR/C_p curve. Sutherland suggests the 3rd blade due to the reduction of torque ripple and ability to use a smaller tower, which reduces costs.

Mohamed[62], Gosselin[30], and Hand and Cashman[32] demonstrate that an optimum solidity exists for maximising C_p. Hand shows that increasing solidity decreased $C_{p\text{-}max}$ compared to the optimum solidity of 0.275, while decreasing solidity also reduced $C_{p\text{-}max}$ but improves high TSR performance. Rezaeiha et al. found that the choice of TSR can change the optimum solidity[59].

2.2.5 Aspect Ratio (AR)

From the early Sandia experiments it was known that increasing AR is the simplest way to increase power production of a VAWT as it doesn't impact other aerodynamic design characteristics[1]. AR is split into Turbine and Blade ARs, where

turbine AR is the ratio between the blade span and diameter, and blade AR is the ratio between blade span and blade chord, with both covered here to show comparability.

Jain and Abhishek[61], Zanforlin and Deluca[39] and Peng et al.[63] have shown that increasing Turbine AR results in increased efficiency with up to 100% increases demonstrated by Peng from 0.67 to 1.43. Gosselin[30] and Hand and Cashman[32] also demonstrate that increasing blade AR positively correlates with efficiency however they disagree on the returns, with Hand showing insignificant increases in C_p beyond AR=10 while Gosselin finds a significant difference between AR=7 and AR=15. Discrepancies are likely due to unknown confounding variables. Both Turbine and Blade AR should be maximised, but traded-off against other design aspects.

Hezaveh et al.'s[64] testing on VAWT wakes demonstrated that low turbine AR slows wake velocity recovery, so array design is also affected.

2.2.6 Pitch

Changing the angle of attack of the blade allows for reduction or prevention of dynamic stall at low TSRs where effective angle of attack is higher, and also by ensuring the blade is at the optimum pitch for maximum power extraction at a given rotational angle. This concept is demonstrated by effective velocity U in figure 2.4.

Pitch can be manipulated in three ways, as a fixed pitch via rotation of the blade at the mounting point, as a fixed pitch with a change in the mounting position and therefore pitching axis resulting in a change in effective angle of attack during rotation (shown in figure 2.5), or as a variable pitch where the pitch is actively changed throughout the rotation of the turbine based upon an algorithm.

Most of the literature shows that small negative fixed pitches, called toe-out pitch, improve performance [4][5][29][65] by up to 29% however there is variation on the degree recommended. Even between Fiedler, Rezaeiha et al., and Lee et al. which all use the same aerofoil, there are large differences. Fiedler recommends -3.9 to -7.8 degrees while Lee and Rezaeiha showed agreement with an optimum of -2 degrees. The major difference between the turbines used by Fiedler and those

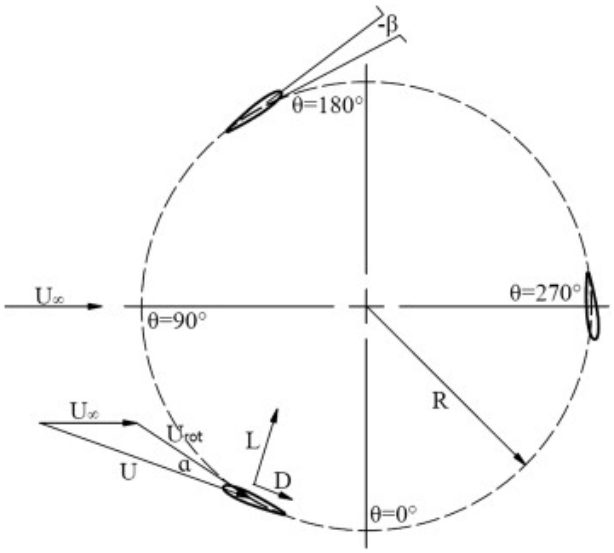

Figure 2.4: Diagram demonstrating pitch angle and effective angle of attack [4]

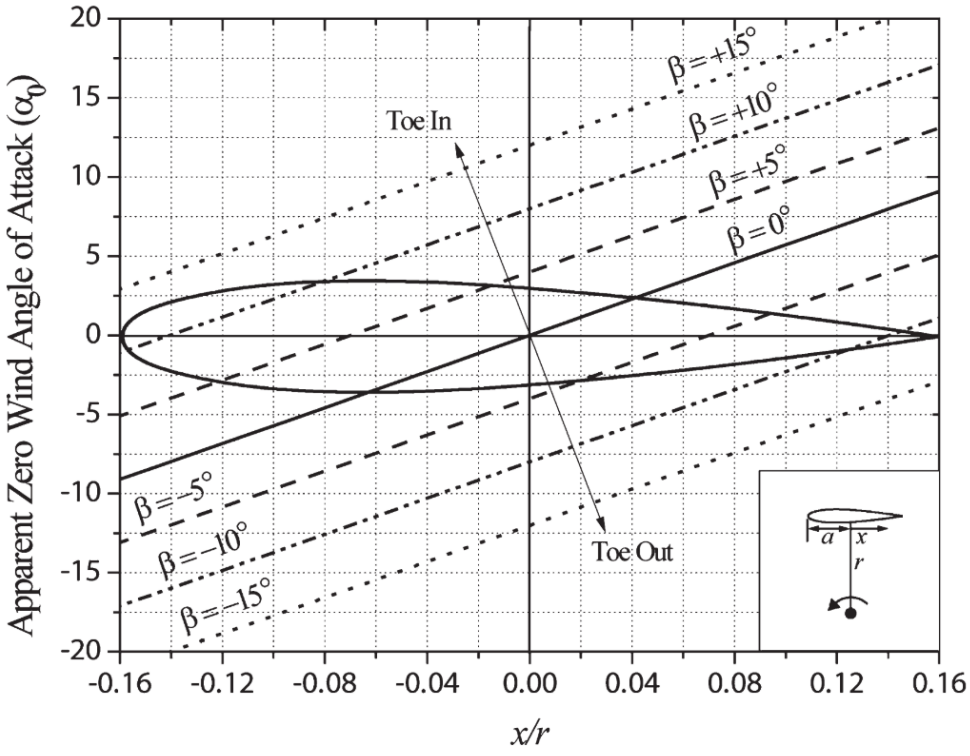

Figure 2.5: Diagram demonstrating impact of mounting point on effecive angle of attack [5]

used by Lee and Rezaeiha is that Fiedler's has a higher solidity, however this opposes Sagharichi et al.'s findings that fixed pitch ceases to improve C_p at higher solidities[58]. In context, Fiedler's results may be anomalous.

Asr et al. showed opposing results with a small positive pitch of +1.5 degrees giving the optimal performance, however a cambered aerofoil was used[44]. Meanwhile Mohamed et al. showed that for the LS(1)-0413, which is also cambered, a pitch of zero is ideal[51]. It can be concluded that the optimum fixed pitch angle is dependent on aerofoil choice.

The mounting point of the strut on the blade causes an inherent toe-in or toe-out pitch, and so altering the mounting point has similar effects to changing the pitch with a single mounting point. Fiedler[5] finds that moving the mounting point forward resulted in an inherent toe-in pitch and so reduced C_p. In 2D simulations, Ferreira[47] shows that moving the pitching axis towards the trailing edge of the blade significantly reduced torque ripple while reducing C_p by $<4\%$. In 3D however there was a 5% increase in C_p.

Variable pitch mechanisms add complexity to the system but can improve power output and provide aerodynamic braking. The possible performance improvements are dependent on the control scheme as shown in table 2.2.

Table 2.2: Comparison of Variable Pitch Control Schemes

Control Scheme	Fixed Pitch C_p or Annual Power (kJ)	% increase
Sinusoidal (Jain) [61]	0.25	44%
Sinusoidal (Elkhoury) [48]	0.18	39%
Eccentric (Sagharichi) [58]	0.33	33%
Target Angle (Gosselin, 2D) [30]	0.34	64.7%
Target Angle (Gosselin, 3D) [30]	0.19	63.2%
Genetic Algorithm (Paraschivoiu) [23]	-	30%
ANN (Abdalrahman) [66]	148kJ	39.8%
PID (Abdalrahman) [66]	148kJ	42.7%

The sinusoidal[61][48] and eccentric[58] schemes are the simplest methods and can be implemented passively. Jain[61] only compared pitch amplitudes from 20 to 35 degrees and found that 20 degrees offered the best performance, so a lower

amplitude may be more desirable. Jain and Abhishek also investigated a variable amplitude method which would cater to varying TSRs to maximise performance during start-up and above TSR_{opt}.

Sagharichi et al.[58] demonstrates that variable pitch has greater effects as solidity increases, particularly for turbines with more blades, and that torque ripple is reduced considerably using the eccentric scheme. Variable pitch also helps eliminate C_p dead-zones which will improve self-starting behaviour. Sagharichi also found a negative correlation between solidity and wake size using variable pitch.

Gosselin[30] uses a target angle of attack where the blades turn towards this angle during the upwind stroke and then towards the negative of this angle during the downwind stroke[30]. By using large angles of attack of 9 degrees the cost corrected C_p increased significantly while small angles of attack of 3 degrees resulted in a decrease of 26.4%. By using different target angles for upstream and downstream strokes, wake recovery can be improved at the cost of C_p decreasing by 0.03. Using a downstream angle of 18 degrees improved power ripple but caused worse wake velocity recovery.

Abdalrahman et al. found that the Artifical Neural Network control scheme (ANN) offered a small advantage over PID due to its ability to model non-linearities, while both increased power compared to the fixed pitch reference[66].

2.2.7 Performance Enhancing Modifications

The performance of a turbine can be altered in other ways which often have a smaller impact on the overall design and may even offer cost effective upgrade pathways for operational turbines.

Samsonov and Baklushin[67] added small airbrake flaps of 0.01-0.05*S which had a considerable impact on C_p. Jet brake flaps have the best braking ability and the potential to considerably increase max C_p, without considerable power loss like air brakes[67].

Gurney flaps have been evaluated in several forms. Yan et al. used a single edged Gurney flap at the trailing edge which reduced TSR_{opt} and increased $C_{p\text{-}max}$. The height of the Gurney flap affects performance with a height of 3% of chord

offering the highest $C_{p\text{-}max}$ until TSR>2.5. The relationship between height and performance between 2-4% of chord needs clarification[68]. Malael et al.[69] used double edged Gurney flaps at the trailing edge, finding significantly reduced TSR_{opt} with a wider, but lower operating range. Zhu et al. completed a comparison of two side, one side inboard and outboard, and equivalent dimple Gurney flaps[70]. The outboard and outboard dimple Gurney flaps offered the best performance with insignificant difference between them for lower solidity turbines. At higher solidities however, while $C_{p\text{-}max}$ is still higher than the clean aerofoil, high TSR>2.5 performance is often worse than the clean aerofoil. There is also a significant difference between the performance of the dimple and no dimple gurney flaps at higher solidity however the relationship is unclear.

The original Sandia tests investigated utilising Vortex generators to trip the boundary layer which would reduce the effects of dynamic stall, however no significant effect on efficiency was seen[1]. A leading edge rod design was proposed by Zhong et al.[71] as an alternative to vortex generators showing a 31.7% increase in lift-to-drag ratio, however this was not implemented for a full VAWT and would require significant investment into its structural design, particularly regarding the flexibility of the rod and its effects on aerodynamic performance.

Gosselin added end-plates to the blade-tips in order to reduce tip vortex effects, finding that a small aerofoil shaped end-plate resulted in a 10% increase in C_p while a large circular end-plate reduced performance due to increasing drag[30]. Jiang et al.[72] used a similar aerofoil end-plate design but found smaller improvements in power output of up to 5.2%, with larger end-plates increasing efficiency. This may be due to Jiang et al. using a turbine with a blade aspect ratio of 14.97 compared to Gosselin using a blade aspect ratio of 7, where tip effects are greater for a lower aspect ratio and therefore have greater scope to be reduced by the end-plate, resulting in a greater increase in C_p. Jiang also found that moving the struts towards the end-plate resulted in further increases up to 10.48%. In contrast, Villeneuve et al.[73] used circular and semi-annular end-plates which cover the circumference of the turbine, a design also proposed by Gosselin, finding 31.1% and 20.6% increases in

efficiency from initial C_p of 0.337 and 0.07 respectively. These are a simple device for improving performance however their increase in efficiency must be balanced against material costs, alongside effects on the turbine wake, particularly in a farm context. The circumference covering end-plates could also be used as struts which may further reduce cost of energy.

Winglets are a commonly utilised technology in modern aeroplanes due to the significant improvements in efficiency offered, and this has also been considered for VAWTs. Laín et al. tested two winglet designs, finding that a symmetric raked wingtip could improve efficiency by up to 20%[74], while Zhang et al. tested 25 different cases finding increases in C_p of up to 10.5%[75]. Zhang's testing found that a single blade case increased performance by up to 31%, demonstrating the importance of a full VAWT case for representative results. Designers and researchers will need to make a choice over whether to use winglets or end-plates, as the semi-annular and circular end-plates offer higher efficiency improvements, but their effects in an array context require analysis.

Leading edge suction slots were first investigated in VAWTs by Sasson and Greenblatt[76] finding that efficiency improvements up to 150% were possible with a double suction slot design. Sasson's research was built upon by Rezaeiha et al.[77], finding that a single suction slot could produce efficiency increases of up to 1134% by avoiding dynamic stall at low TSR and low turbulence intensity where C_p is very low, however this was highly dependent on turbulence intensity and TSR, with their testing using a higher turbulence intensity of 25% showing a more modest increase of up to 99%, occurring at TSR=2.5. Rezaeiha found that the performance improvements increase with TSR however their testing only goes down to TSR=2.5, so further testing is required for lower TSRs. If this trend continues at lower TSR then improvements in self-starting behaviour and low TSR performance would be seen, producing an overall more viable turbine design which allows self-starting and increased operating TSR performance.

Synthetic jet actuators serve a similar purpose to leading edge suction slots but allow for both suction and blowing. Zhu et al. completed a CFD analysis with

synthetic jet actuators showing a 15.2% increase in power coefficient compared to normal blades[78]. Given that synthetic jet actuators are placed closer to the trailing edge where there is still high vorticity in the leading edge suction slot blade testing by Rezaeiha, the combination of the two technologies may allow for a further combined increase in performance than each technology alone.

Mohamed et al.[79] proposes a passive leading edge slot design, finding increases in C_p at low TSR giving improved self-starting performance but a lower $C_{p\text{-}max}$ and worse high TSR performance. Torque ripple is reduced in the downwind section at low TSR too. This design involves a large cutout from the blade, which occurs where most blades would contain their major stress bearing components including the spar and spar cap, so there would be significant implications for the structural design. These could be mitigated by using the slot in limited regions across the length of the aerofoil, for example at the ends of blades where load bearing is lower, however the aerodynamic implications would need to be reconsidered.

Qin et al.[80] suggested that struts must be designed to minimise the high losses they caused. Elkhoury et al.[48] showed that including struts in their simulation significantly reduced $C_{p\text{-}max}$ and caused a lower TSR_{opt}, however it was also shown that effects were negligible at low TSR ($<$0.75). Goude et al. stated that Turbine Aspect Ratio should be balanced against the number of struts needed to meet structural design requirements because the introduction of an additional strut per blade would cause significant losses[81]. Hand and Cashman studied strut design and produced aerofoil-shaped struts with a variable thickness-to-chord ratio (t/c) which would improve high TSR C_p[32]. Significant differences were found between t/c=0.12 and t/c=0.21 aerofoils with $C_{p\text{-}max}$ reducing by 0.01, and a further decrease of 0.05 when moving up to t/c=0.30. Effects of changing thickness below TSR$<$1.7 were negligible. Mendoza[82] found that pitching the struts can reduce turbine wake effects which can be used to improve array performance.

Wang and Zhuang investigate a serrated leading edge design which is biomimetic of whale fins[83]. Using a serrated edge resulted in C_p increases up to 18.7% with most improvement towards lower TSR, however no performance

is lost at higher TSR. The wavelength of the serrations affects the TSR/C_p curve however no clear relationship was found with both wavelength=0.33c and 1.0c outperforming 0.67c, with the 0.33c condition having better performance below and around TSR_{opt}, while 1.0c has a higher $C_{p\text{-}max}$ and better performance around and above TSR_{opt}. This design would be more complex to manufacture, which would impact cost of energy. The effects of surface roughness due to debris collected over the turbine life cycle will also need to be considered.

Zamani et al. proposed J-blades to improve $C_{p\text{-}max}$ and self-starting behaviour, which was confirmed in their studies using 2D and 3D CFD[84][85]. However worse performance was found at high TSR (>2.5). It was also shown that wake velocity recovered sooner. Pan et al.[86] disputes these results, with overall reduced performance compared to conventional blades. J-blades also require investigation from a structural design viewpoint.

Howell et al. tested a turbine with rough and smooth blades, finding that the surface roughness had an impact on performance which varied with wind speed. At lower wind speeds performance reduced with smoothing while performance improved at higher wind speeds, particularly at high TSR[60]. Therefore regular cleaning or coatings which reduce deterioration of surface roughness are required to avoid performance losses with age.

An alternative take on aerofoil-based struts is the Cross Axis Wind Turbine (CAWT) design by Chong et al.[87] which attempts to create additional power from struts. Deflectors or tilting of the turbine are used to produce a more favourable flow direction for the design, showing very large C_p increases of up to 131.6% compared to an equivalent VAWT with no deflector[87][88]. Wang et al. showed that CAWT designs have reduced torque ripple and a higher TSR_{opt} compared to equivalent VAWTs[89]. This testing was conducted only at low TSR so further testing is required.

Guide vanes and stators offer a simple way to increase the swept area of a turbine and improve flow direction, thus improving power output significantly. Takao et al.'s[90] unidirectional guide vane increased power output by 80% while Nobile

et al.'s[91] omnidirectional stator showed an increase of 35%. Zanforlin and Letizia proposed a rooftop design with up to 50% power increase using a cowling, however they also found that raising the turbine by 1m to utilise boundary layer effects instead of using the cowling resulted in a 56.25% increase[92].

A hybrid Darrieus-Savonius VAWT proposed by Mohamed et al. showed improved starting behaviour but very poor C_p otherwise with significantly reduced $C_{p\text{-}max}$ and a rapid decrease in efficiency at high TSR[62].

Strom et al. proposed Variable TSR control, where the rotational speed of the turbine is varied with angular blade position, as an alternative method to Variable Pitch control. Compared to fixed TSR this resulted in a 59% performance increase using a semi-arbitrary control scheme and a 53% increase with a sinusoidal control scheme[93]. The scheme used results in very large, impractical changes in TSR across a rotation, with the TSR varying between 0.4-3.8.

2.3 Arrays

Wind turbines are often clustered to take advantage of high wind speeds in a small area so it is necessary to consider impacts of clustering for VAWTs. For HAWTs this involves minimising the distance between turbines while also minimising the effects of turbine wakes on following turbines[94]. Meyers and Meneveau[95] showed that a distance of 10D between HAWTs for utility scale wind farms results in a power reduction of 40% compared to a turbine in the freestream. In contrast, Chowdhury shows that 9D is sufficient for complete recovery to freestream velocity for a helical VAWT[96], and so power reductions will be much smaller. This study was conducted at a Reynolds number of $5.25\text{x}10^5$, which is sufficient for comparison to utility scale due to achieving Reynolds independence as discussed in 2.2.2. Additionally this flow may have higher turbulence intensity which could even improve performance compared to isolated turbines[97]. Hezaveh et al. finds that approximately 13D is sufficient for near complete recovery in some circumstances, with high solidity, high TSR, and intermediate to low turbine AR producing the fastest recoveries[64]. Other studies detailed in this section consider that VAWT farm de-

sign procedure could use other flow characteristics to increase power output. These studies are divided into those which consider small arrays, and large arrays which would be applicable to utility development.

2.3.1 Small Arrays

Zanforlin and Nishino's closely spaced turbine pairs show improved performance compared to isolated turbines, with staggered outward counter-rotating turbines performing better than parallel or inward counter-rotating turbines[98]. Zanforlin also showed in a separate study on Vertical Axis Tidal Turbines (VATTs) that a side-by-side configuration increases C_p by 0.09, and a triangular formation pointing against the stream also increases $C_{p\text{-}max}$ although only by 0.03[99]. However the triangular configuration was less susceptible to severe power drops from adverse current direction. Considering the wake, the forward turbine demonstrates much faster contraction as a result of the following turbines, whilst this contraction isn't demonstrated in the side-by-side results. The side-by-side results demonstrate much higher increases in velocity between the turbines, which is likely to be the cause of the increased power output. Ahmadi-Baloutaki et al. found opposing results for counter-rotating pairs with a slightly decreased performance in a low intensity wind tunnel, but the triangular configuration resulted in considerable power output increase for the downstream turbine compared to the isolated conditions[97]. They also found that the TSR/C_p curve was vastly different for the downstream turbine, even when adjusted for turbulence intensity, so experimental validation may be required for downstream turbines in arrays.

Lam and Peng conducted wind tunnel tests for turbine pairs, and provides lateral and vertical velocity profile graphs which are useful as an experimental validation of turbine pairs[100]. Counter-rotating turbines offered the best results and showed much better wake velocity recovery. The wakes of the two turbines begin to merge together downstream, with a high velocity maintained in the middle between the turbines which begins to dissipate cross-stream until the wake merger. Use of inwards or outwards rotation will depend on the context of the turbines, where inward rotation is advantageous for closely-packed farms due to a smaller lateral

wake, allowing for lateral spacing between pairs of 2.5-3D compared to 3-4D for outwards rotating pairs. Streamwise velocity reduction in the wake was greatest towards the mid-span of turbines, while the greatest cross-stream effects occurred towards rotation at the mid-span and against the rotation at the tips, with reduced effects at quarter-span. The greatest vertical velocity effects were at the tips with the velocity directed towards the mid-span on the outside of the turbine pair and away from the mid-span between the pair. De Tavernier et al.'s[101] pairs of co and counter-rotating VAWTs increased C_p from 0.55 to 0.58, with increasing solidity and TSR increasing C_p, confirming Lam and Peng's results[100]. De Tavernier et al.'s C_p predictions are very high to the point of approaching Betz' limit as a result of use of the Actuator Cylinder model which demonstrates higher C_p predictions, however the trend of increased C_p from arrays is still demonstrated and the results remain within Betz' limit[17].

Giorgetti et al. found an efficiency increase of up to 10% using rotating pairs compared to isolated turbines, and a 4.4% increase for a 4 turbine array[102]. They also showed that wake structures produced by VAWTs cannot be recreated using rotating cylinders via the Magnus effect.

Brownstein et al.[103] investigates the effects of wind direction on VAWT pair performance, finding that there is a region of approximately 50° where power output increases by an average of 14%, however the power output of the following turbine can decrease to zero when in the minimum velocity regions of the wake. The effects of wind direction reduce with greater spacing between the wind turbines. Given that the wind direction at most sites tends towards a given direction, arrays can be designed to maximise the time spent in a favourable direction and minimise time spent in an unfavourable direction. Further investigation is needed regarding larger spacing between turbines as Brownstein's largest spacing condition retained good performance while reducing the impact of unfavourable direction significantly.

Sahebzadeh et al.[104] investigates the optimal configuration for dual rotor configurations, using CFD in contrast to the experimental method used by Brownstein. They find a smaller increase in power output of 1.8% at an inter-turbine

distance of 1.25D and angle of 75°. The pattern for the increase for the downstream turbine is similar with both studies demonstrating an increase providing the downstream turbine is situated sufficiently off-centre. However for the upstream turbine the results differ with Sahebzadeh only finding power increases when the turbines are parallel, while Brownstein finds increases when the downstream turbine is placed on the downstroke side for both co- and counter-rotating conditions, and a significant decrease on the upstroke side for the co-rotating condition. This difference is likely due to the differences in solidity, with Sahebzadeh using a low solidity turbine of 0.06 compared to 1.13 for Brownstein, which has been demonstrated to reduce the impact of arrays on performance by De Tavernier et al.[101].

2.3.2 Larger Arrays

Due to the slower speed of simulating larger arrays there is less literature which can be applied to commercial scale farms. Whittlesey et al.[105] proposed the 'School of Fish' design which could offer up to 40% improvements in turbine efficiency while Dabiri[18] expected that power per land area could be improved by a magnitude by using VAWTs instead of HAWTs. However, Dabiri failed to consider that very small spacing can be undesirable as the land around turbines is often used for other purposes, particularly agriculture. In practice there will be a case-by-case trade off between minimising the area required and maximising the use of that area. This is even more relevant for VAWTs due to their typically greater footprint over the land. Hezaveh et al. found that clusters of 3 closely packed turbines provided the highest array efficiency in comparison to continuous aligned and staggered configurations with an increase of over 100%[106]. De Tavernier et al.'s results[101] showed that decreasing solidity may decrease the impact of array optimisation.

2.3.3 Mechanism of Improved Performance in Arrays

Several hypotheses for why VAWTs exhibit improved power output in arrays have been proposed. These mechanisms work together to create a combined effect. The virtual bluff-bodies of the turbines create an initial constriction[103][107] resulting in the Venturi effect[108][109][110] which increases the effective velocity on the

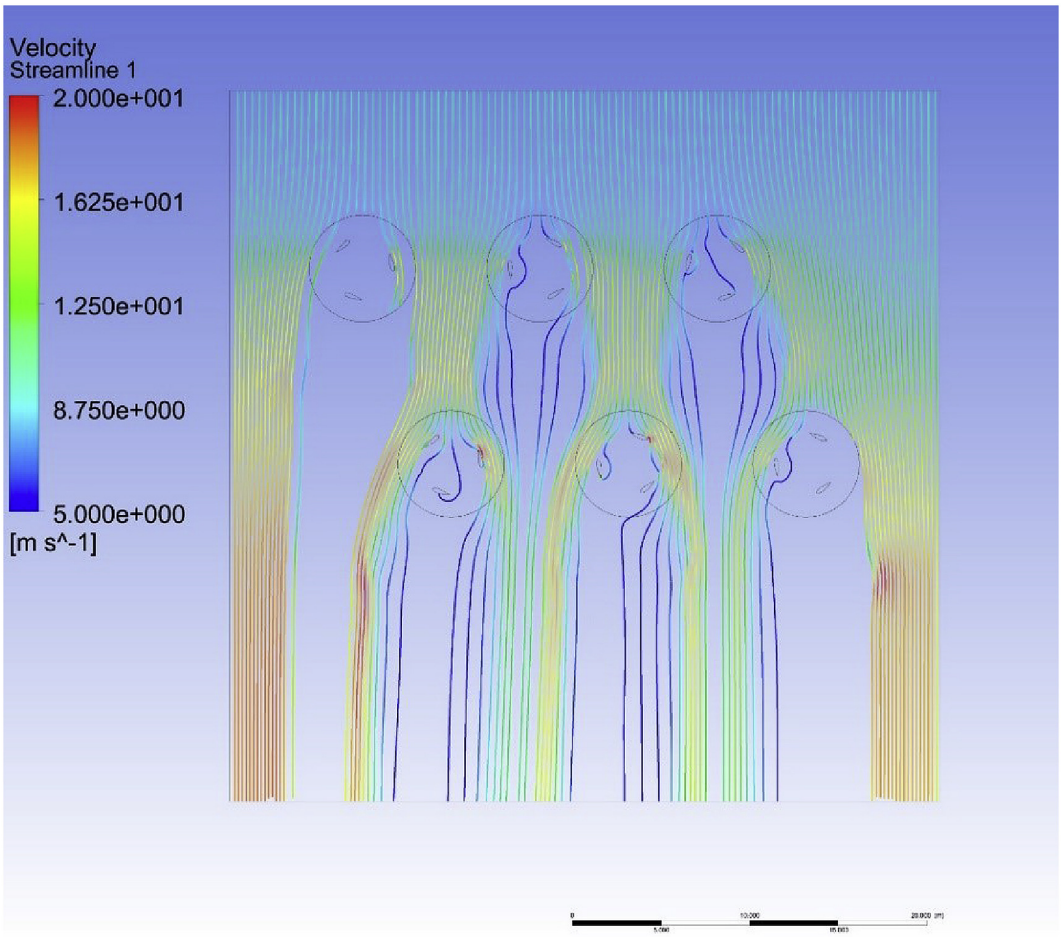

Figure 2.6: Diagram of velocity streamlines demonstrating increased velocity of flow between turbines and change in direction

blades and produces a more favourable wind direction upon the blades[98]. These are demonstrated in Figure 2.6 where the streamlines show increased velocity between turbines due to the flow constriction and consequent Venturi effect. It can also be seen that for the second layer of turbines, the streamlines more closely follow the circumference of rotation of the blades compared to the first layer of turbines, resulting in a more stable effective angle of attack throughout a rotation, and so greater efficiency. The vortical structures in the wake of the turbine then allow the constriction of the airflow and thus increased velocity to continue further downwind, hence resulting in increases in power output in a staggered configuration also[103][107]. The higher velocity in the constricted region as a result of the combined effect of two turbines also results in faster wake contraction[98][108][103].

2.4 Experimentation

In order to validate design choices, they must be tested to determine their impact on the performance characteristics and dynamics of the system. Testing can be conducted either via practical experiment or by simulation. Firstly experimental testing methods for VAWTs will be considered, where experiments offer an environment and results which should be more representative of usage in the field.

Experimental testing typically uses a wind tunnel, however there are examples of field testing[6][111][1]. The advantage of wind tunnel testing is to ensure a controlled environment which is more 'real' than modelling by simulation, and may allow for measurements to be taken which would not be possible in the field such as higher resolution wake measurements and greater capability for identification of vortical structures which currently require use of Particle Image Velocimetry (PIV) in a wind tunnel, as opposed to lower resolution LiDAR[112]. Field experiments ensure that results are realistic because they are being taken in a fully realistic scenario, however the lack of control over the system means that any associated variances must be accounted for. Both methods have issues in terms of planning and costs, where use of larger scale or cold wind tunnels to account for the high Reynolds number representative of utility scale turbines incurs a high financial cost, and field testing often requires planning permission and determining a suitable site for the experiment.

Both of these methods can use similar techniques for measuring power output, using either a generator to measure power output or a torque meter to measure torque combined with a measurement for rotational speed such as a tachometer[97] or laser displacement sensor[100].

Several experimental methods can be used for the flow analysis of VAWTs. Wake characteristics are analysed by carrying out PIV or Stereoscopic Particle Image Velocimetry (SPIV). With PIV, the fluid is seeded with particles which are assumed to follow the same fluid dynamics as the fluid, the particles are then tracked through the flow using a camera. This allows for instantaneous tracking of fluid velocity along a two-dimensional plane, which for VAWTs is typically recorded at

the mid-span of the blades. SPIV adds a second camera to track velocity in a third axis. Hot-wire anemometers can also be used which measure velocity in a single dimension and are typically used to measure the velocity across the horizontal axis of a wind tunnel. Laser and acoustic Doppler velocimetry or Cobra probes can also be used, however these only measure velocity at a single point, although they can measure velocity in all three spatial dimensions.

Buchner et al.[8] investigated the blade wake at the point when the blade is furthest upwind at three different TSRs using SPIV. Tescione et al.[12] used SPIV to measure the velocity field in the near-turbine wake up to 2 turbine diameters (D) downstream at TSR=4.5. A partner study by Castelein et al.[9] used the same experimental setup for the blade wake at several different rotational points at TSR=2.0 and TSR=4.5. Posa et al.[13] studied near turbine wake velocity using PIV up to 1D downstream at two TSRs (1.35 and 2.21).

Peng et al.[113] used hot-wire anemometers and a cobra probe to measure velocity downstream of the mid-span of the turbine. Peng et al. recorded results up to 10D, but at a lower resolution of only 1D. Lam and Peng[100] conducted a study using two turbines in co-rotating and counter-rotating formations with the same methodology as Peng, Lam, and Lee[113], where co-rotating has both turbines rotating in the same direction whilst counter-rotating has the turbines rotating in opposite directions. Tescione et al.[12] and Peng et al.[113] also recorded results in the vertical direction, which enables validation of 3D CFD models. Ferreira[47] also utilises hot-wire anemometry.

More modern methods also allow for studying the wake in field experiments, for example Li et al.[6] used ultrasonic anemometers to measure wake angle in both wind tunnels and the field, measuring along two lines placed 1 and 2 turbine diameters behind the turbine respectively. Sun et al.[114] conducts a review on measuring the wakes of turbines in the field, with many modern studies utilising Lidar. This method proves to be very cost effective compared to large wind tunnels, supporting a preference for field experiments by reducing its disadvantages compared to wind tunnel methodology.

It is necessary to consider how applicable available VAWT literature is to the field, with the aim of moving VAWT technology towards commercialisation where it may be deployed at utility scales of megawatts of power output. This is particularly important given that the literature demonstrates that VAWTs tend to have improved performance characteristics in situations more representative of the field as will be demonstrated in this section. The core guidelines for this are IEC64100[36] which, alongside its amendments, set out industrial standards for wind turbines, setting out the conditions that both HAWTs and VAWTs must be analysed for in order to determine their performance characteristics.

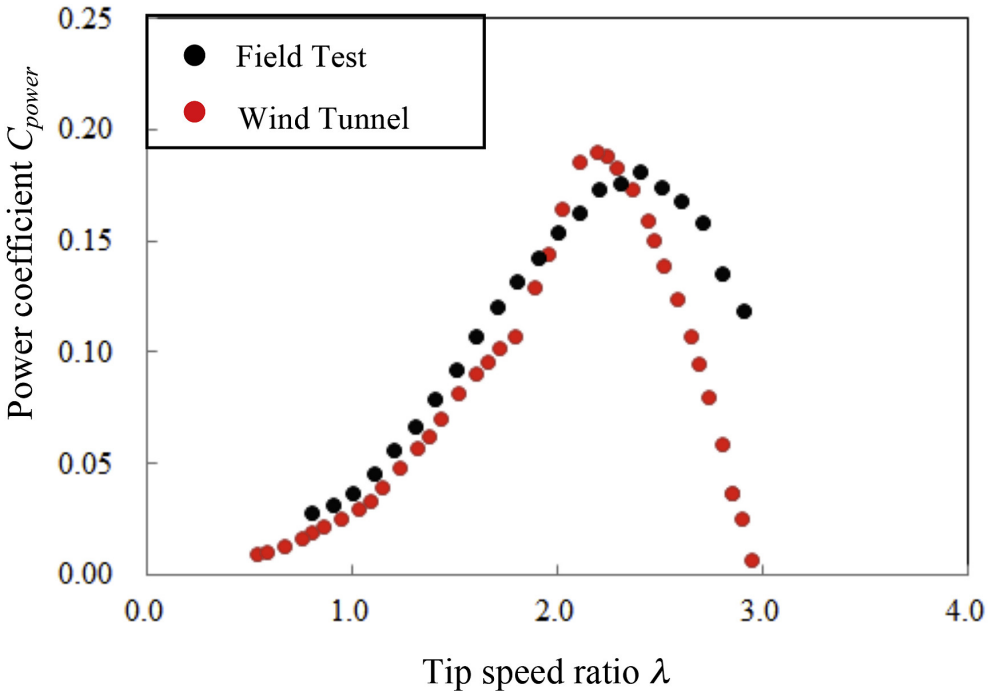

Figure 2.7: Comparison of TSR/ C_p curves for field and wind tunnel experiments [6]

The need for testing to IEC64100 specification is demonstrated by Li et al. who compared wind tunnel and field results with, as shown by figure 2.7, the wind tunnel TSR/C_p profile having a slightly higher $C_{p\text{-}max}$ and lower TSR_{opt} albeit with a smaller operating range[6]. Schito et al.[115] also showed very different results between an Open-Jet wind tunnel and field testing for their VAWT in simulation. This shows that wind tunnel results may not be representative of real conditions which has major implications for evaluating the performance of new VAWT designs, and

also for evaluating simulation techniques.

Further support for this hypothesis comes from other research on scale[116] and scale-related variables such as Reynolds Number as demonstrated in section 2.2.2, which show that the typical small wind tunnel experiments used for VAWTs, with scales of 1m diameter or less, often around 0.3m, are not valid for evaluating utility scale turbines which would have diameters at least one magnitude greater. Turbulence intensity in the field is also much greater than in typical wind tunnel at 12% or greater based on IEC64100 standards[36] compared to 0.5% which is used in most wind tunnel studies covered in this thesis, with the impact of this explored later in this section.

Here the wind condition aspect of IEC64100 will be focused on in order to evaluate the validity of previous VAWT testing regarding applicability to utility scale turbines, considering how or if a scenario has been tested in the literature to outline where further research is necessary to better illustrate VAWT performance. All equations are sourced from IEC64100[36].

2.4.1 Normal Wind Conditions

Normal wind conditions are described by the following equations 2.2-2.4. Equation 2.2 denotes the distribution of wind speed based upon the class of turbine.

$$P_R = 1 - exp(-\pi(V_{hub}/2V_{avg})^2) \tag{2.2}$$

Where $V_{avg} = 0.2V_{ref}$ and V_{ref} is found from the wind turbine class I, II, or III. For a Class I turbine V_{ref} is 50m/s [36]. The normal distribution is used to calculate average power output by testing at different wind speeds to find the power curve of the turbine then using the distribution to find the average power output.

Equation 2.3 denotes the wind profile showing the boundary layer effect

$$V(z) = V(z_{ref})(z/z_{ref})^a \tag{2.3}$$

where a=0.2. The scenario described by equation 2.3 has been tested by Rolin and Porté-Agel[117] which uses boundary layer flow. Two pairs of counter-rotating

vortices are produced by the VAWT and wake recovery is asymmetrical.

Equation 2.4 denotes the Normal Turbulence Model for estimation of the standard deviation of turbulence intensity, based on observational data collected for onshore wind turbine in Europe and America[118]

$$\sigma_1 = I_{ref}(0.75V_{hub} + b) \tag{2.4}$$

where in equation 2.4, b=5.6m/s. σ_1, shall be given by the 90% quantile for the given hub height wind speed and I_{ref} is given by the class of turbine, where classes A, B, and C have I_{ref} values of 0.16, 0.14, and 0.12 respectively. For VAWTs V_{hub} should be considered as the velocity at the turbine mid-span.

While the turbulence profile isn't investigated directly, the effect of turbulence intensity is. Ahmadi-Baloutaki et al.'s experimental study finds that increasing turbulence intensity from <0.2% to 4 to 6% for an isolated turbine results in increased power output[97]. Bianchini et al. finds that increasing turbulence intensity causes an increase in rotational speed, however this effect is insignificant between 0 to 10%[119]. However Untaroiu et al. shows that decreasing turbulence intensity from 5% to 1% leads to a decrease in start-up time[120]. Li et al. found that reducing turbulence intensity improves performance, however they used very high turbulence intensities with 25% being the lowest tested[6].

Molina et al.[121] and Belkacem and Paraschivoiu[116] demonstrate that turbulence intensity can alter the C_p/TSR curve with increasing turbulence intensity resulting in increased C_p. The impact of turbulence intensity on power coefficient reduces as Reynolds number increases, and combined with the reduction of impact of turbulence intensity with increasing TSR it can be inferred that this may be partially related to the effective Reynolds number of the blades. Notably this occurs after TSR_{opt} and so this information can only be applied to off-design performance. For the 35m diameter VAWT, this results in an insignificant change in the C_p/TSR curve as turbulence intensity changes, meaning that low turbulence intensity wind tunnel results would remain applicable to higher turbulence intensity scenarios demonstrated in IEC64100, however in practice most VAWTs and wind

tunnels aren't at sufficient scale to allow this. Kuang et al.[122] also disagrees with this finding, with C_p starting to decrease with turbulence intensity for higher Re. The cause of this disagreement is unclear due to the similar methods and conditions used between Kuang et al. and Belkacem and Paraschivoiu, with the main differences and therefore potential causes for disagreement being Kuang et al.'s turbine using a fixed pitch blade with a pitch of 6°, having a higher solidity (0.44 compared to 0.22), and using a different aerofoil (NACA0021 compared to NACA0018).

More commonly, VAWT experiments in wind tunnels are conducted at scales closer to the 0.5m diameter condition. Using CFD simulation, Belkacem and Paraschivoiu found an increase in $C_{p\text{-}max}$ of over 40% between turbulence intensities of 0.07% and 14.8%[116], where the former is more representative of typical VAWT wind tunnel experiments whilst the latter is representative of the field, lying between the IEC64100 ratings of 12 to 16%[36]. Further investigation is needed within this range however.

Lopez-Villalobos et al.[123] demonstrate that turbulence intensity can be higher at lower wind speeds, and that the IEC64100 ratings are often below the average turbulence intensity at a given wind speed, with a substantial proportion of readings at a given wind speed being significantly above the average. From these readings it may be necessary to test VAWT performance at turbulence intensities up to 25%, and this is particularly important for low wind speeds due to its potential to affect self-starting as shown by Untaroiu et al.[120]. The simulation results by Belkacem and Paraschivoiu[116] further reinforce the desirability of studying the 10 to 20% range, with nearly all of the change in C_p due to turbulence intensity occurring in this range for the smaller turbine studied (Re=333,000), with plateaus before and after this range. This is particularly emphasised by the contrasting results with Molina et al.[121] which show a more linear relationship from 0% to 14.8%.

2.4.2 Extreme Wind Conditions

Extreme wind conditions are described by the following equations and scenarios.

Equations 2.5 and 2.6 are the extreme wind speeds based upon likelihood of

occurrence for 50 years and 1 year respectively.

$$V_{e50} = 1.4V_{ref}(z/z_{hub})^{0.11} \tag{2.5}$$

$$V_{e1} = 0.8V_{e50} \tag{2.6}$$

Equation 2.7 denotes longitudinal turbulence standard deviation.

$$\sigma_1 = 0.11V_{hub} \tag{2.7}$$

Equations 2.5-2.7 are variations upon what has been covered under normal wind conditions and can be tested by using higher wind speeds or Reynolds number.

Equation 2.8 denotes the maximum velocity of a gust, with equation 2.10 describing a scenario to test reaction to gusts.

$$V_{gust} = MIN\{\begin{matrix} 1.35(\mathrm{V}_{e1} - V_{hub}) \\ 3.3(\sigma_1/(1+0.1(D/\lambda_1)) \end{matrix} \tag{2.8}$$

where D is rotor diameter and λ_1 is the turbulence intensity parameter, defined as:

$$V(z,t) = \{\begin{matrix} 0.7\mathrm{z} & \mathrm{z_{hub}}<60\mathrm{m} \\ 42\mathrm{m} & \mathrm{z_{hub}}>60\mathrm{m} \end{matrix} \tag{2.9}$$

$$V(z,t) = \{\begin{matrix} \mathrm{V(z)\text{-}0.37V}_{gust}sin(\frac{3\pi t}{T})(1-cos(\frac{2\pi t}{T})) & 0<\mathrm{t}<\mathrm{T} \\ \mathrm{V(z)} & \text{otherwise} \end{matrix} \tag{2.10}$$

where V(z) is defined by the power law of equation 2.3 and T=10.5s. Scheuric and Brown[31] and Danao et al.[124] both investigate unsteady wind speeds by using sinusoidal time-variant wind profiles, which while not the same as the scenario defined in equation 2.10, offer insight into VAWT behaviour under these conditions. Danao discovered that $\mathrm{TSR_{opt}}$ in unsteady conditions was slightly increased compared to steady conditions, and that ideally the fluctuations were small in amplitude ($<0.1\mathrm{V_{avg}}$) and high in frequency ($>$1Hz). Scheurich and Brown tested velocity

fluctuations of 10% and 30%, finding that fluctuations of <10% can be treated as quasi-steady-state[31].

Equation 2.11 denotes the standard deviation of extreme turbulence.

$$\sigma_1 = cI_{ref}(0.072((\frac{V_{avg}}{c})+3)(\frac{V_{hub}}{c}-4)+10) \tag{2.11}$$

where c=2m/s

Equations 2.12 and 2.13 describe the scenario of an extreme direction change

$$\theta_e = \pm 4tan^{-1}(\sigma_1/(V_{hub}(1+0.1(D/\lambda_1)))) \tag{2.12}$$

$$\theta(t) = \begin{cases} 0 & t<0 \\ \pm 0.5\theta_e(1-cos(\frac{\pi t}{T})) & 0<t<T \\ \theta_e & t>T. \end{cases} \tag{2.13}$$

where T=6s is the duration of the extreme direction change. θ_e denotes the direction change magnitude while $\theta(t)$ represents the transient process of the direction change.

Similarly vertically skewed flow should be considered, although this isn't included in IEC64100. Chowdhury et al. found that tilted turbines show a significant increase in C_p at high tilts[96], but worse wake recovery. This is likely due to the higher swept area and reduced effects of leading blade wakes.

Equations 2.14-2.17 describe the scenario of an extreme coherent gust with a direction change.

$$V(z,t) = \begin{cases} V(z) & t<0 \\ V(z)+0.5V_{cg}(1-cos(\frac{\pi t}{T}) & 0<t<T \\ V(z)+V_{cg} & t>T \end{cases} \tag{2.14}$$

$$V_{cg} = 15m/s \tag{2.15}$$

where T=10s

$$\theta_{\text{cg}} = \{ \begin{array}{cc} 180 \text{ degrees} & \text{V}_{\text{hub}}\text{<4m/s} \\ (720 \text{ degrees m/s}) / \text{V}_{hub} & \text{4m/s <V}_{hub}\text{<}V_{ref} \end{array} \tag{2.16}$$

$$\theta(t) = \{ \begin{array}{cc} 0 \text{ degrees} & \text{t<0} \\ \pm 0.5\theta_{cg}(1 - cos(\frac{\pi t}{T})) & \text{0<t<T} \\ \pm\theta_{cg} & \text{t} \end{array} \tag{2.17}$$

where T=10s

While researchers may consider that this scenario is unlikely to have any significant effect on VAWTs given their inherent omnidirectionality, Wu et al.[125] found otherwise, with lateral gusts causing significant changes in power output. The magnitude and direction of the change depended on aerofoil, TSR, gust magnitude, and number of blades. Reductions in performance were found at TSR=3 while small increases were seen at TSR=4, which is important as this is the common range for VAWTs. Further analysis is needed in this region in order to consider the transition through no performance impact. Symmetrical aerofoils had similar relationships between C_p change and TSR with small increases from TSR 4 to 7. At TSR=3, the NACA0018 aerofoil had a markedly smaller reduction in performance than the other symmetrical aerofoils (-2.92% compared to -8.92% and -11.43%). The tested cambered aerofoil had power decreases of up to 17% at higher TSR, which could risk poor off-design performance.

Equations 2.18 and 2.19 consider the extreme wind shear in horizontal and vertical directions respectively[36]. Regarding VAWTs, the vertical shear can affect performance due to the change in velocity along the blade, this is notable for helical VAWTs as it impacts their torque ripple. Horizontal shear may affect performance by changing the effective freestream velocity dependent on the position of the blade.

$$V(z,t) = \{ \begin{array}{cc} \text{V}_{hub}((\frac{z}{z_{hub}})^a) \pm (\frac{z-z_{hub}}{D})(2.5 + 0.2\beta\sigma_1(\frac{D}{\lambda_1})^{\frac{1}{4}})(1 - cos(\frac{2\pi t}{T})) & \text{0 <t} \\ \text{V}_{hub}(\frac{z}{z_{hub}})^a & \text{otherwise} \end{array} \tag{2.18}$$

$$V(y,z,t) = \{ \begin{array}{ll} \mathrm{V}_{hub}((\frac{z}{z_{hub}})^a \pm \frac{y}{D}(2.5+0.2\beta\sigma_1(\frac{D}{\lambda_1})^{\frac{1}{4}})(1-\frac{cos(2\pi t}{T})) & 0<\mathrm{t}<\mathrm{T} \\ \mathrm{V}_{hub}(\frac{z}{z_{hub}})^a & \text{otherwise} \end{array} \quad (2.19)$$

where a=0.2, β=6.4, T=12s.

The sign for the horizontal wind shear transient shall be chosen so that the worst transient loading occurs rather than both extreme shears being applied simultaneously.

2.5 CFD Simulation

Simulation offers a cheaper alternative to experimental testing including the ability to conduct tests which are otherwise impractical to complete in the real world. However, this can come at the cost of accuracy due to incomplete modelling hence it is necessary to validate simulation results against experimental baselines. The most popular method of simulation for VAWTs is Computational Fluid Dynamics (CFD) due to it being a general purpose solver, and the accuracy and efficiency of different CFD procedures will be considered in this section.

2.5.1 2D vs. 3D

The initial consideration in VAWT CFD is the use of a two- or three-dimensional domain, and this especially applies to H-VAWTs where the 3D design is an extrusion of a 2D design. A midway 2.5D approach is also available which uses a 3D model but only considers a section of the blades, with symmetry conditions applied to the walls at the ends of the section. Tip effects and struts, which can only be modelled in full 3D, have significant effects on VAWT simulation results however, with Castelli et al.[126] and Hand et al.[32] showing large decreases of up to 45% in C_p when these are accounted for.

Results overwhelmingly show that 3D offers better prediction than 2D, with very good predictions until high TSR and even then this is partly due to the simulated turbine lacking struts and shaft[60] as these have greater impact at higher TSR. An exception is Orlandi et al.[127] which shows worse prediction of C_l (de-

noted in Orlandi et al.'s study as C_n) and C_t compared to 2D, however this is likely due to the considerably reduced domain length and higher blockage ratio in their 3D simulation.

Li et al. tested using 2.5D, where tip effects and struts are neglected, and showed that the differences from 2D for Unsteady Reynolds Averaged Navier-Stokes (URANS) modelling were negligible but significant differences were seen for Large Eddy Simulation (LES) modelling[128]. He et al.[129] conducts a similar study but with a comparison to 3D simulations also. They show similar results with 2D and 2.5D URANS producing similar predictions while 3D URANS, 2.5D LES, and 3D LES produce similar results to each other and different to 2D and 2.5D URANS.

2.5.2 Turbulence Models

Turbulence models are used to solve the gross effect of turbulence on the flow at the appropriate scale, in order to avoid Direct Numerical Simulation which is extremely computationally intensive. Two forms of turbulence modelling are commonly used: LES, which directly solves large scale eddies and uses a sub-grid scale model for smaller scale processes, and Reynolds Averaged Navier-Stokes (RANS) which uses the model at all scales, although some RANS models change behaviour near walls. As LES uses a more direct solving procedure it is usually more accurate than RANS, but at the cost of significantly greater computational requirements, so in cases where RANS models can provide sufficient accuracy these are used instead. Detached Eddy Simulation (DES) is an alternative which can be described as either LES with a wall model or hybrid LES/RANS depending on the setup. DES enables accuracy similar to or better than LES in appropriate circumstances, albeit with reduced time commitments. Furthermore, there is also Scale Adaptive Simulation (SAS), which aims to perform between RANS and DES.

It should be noted that LES and DES models require 2.5D or 3D analysis for good performance while RANS models do not so many studies which use RANS turbulence models use 2D analysis to reduce computational resource requirements.

As stated in the previous section, the choice of 2D, 2.5D, or 3D has a significant impact on the predictions, so the best performing turbulence models in 2D may perform poorly in 3D. Relatively high accuracy in 2D could even be an indicator of poor accuracy in 3D because large decreases in C_p are to be expected at high TSR when including tip effects and struts.

Within LES models, Elkhoury et al.[48] uses LES with a Smagorinsky sub-grid-scale model to validate C_p prediction against an experiment within a TSR range of 0.25-1.5. $C_{p\text{-}max}$ and TSR_{opt} are predicted accurately for all inlet velocities and aerofoils where both experiments and LES simulations were conducted. However for the NACA63_4-221 there was a small overestimation around $C_{p\text{-}max}$ demonstrating a need for case-by-case validation for CFD simulation of VAWTs, especially given that the experimental setups were the same in this study so the difference cannot be due to unknown factors.

Posa et al.[13] considers wake prediction of an experiment by Howell et al.[60] at TSR=1.35 and 2.21. Wake recovery was overestimated however this may be due to the small domain volume relative to the turbine resulting in blockage effects, which is evidenced by the freestream velocity being 5-10% greater than the inlet velocity. It should be noted that the experimental model uses an even smaller domain however, so this difference may be due to reduced blockage effects enabling greater recovery of the wake. The blockage effects also impact the Spanwise vorticity results, with the outer wake lines converging in the simulations further downstream while they continue to diverge in the experiment.

Li et al. compares 2.5D LES against a URANS model, k-ω SST in 2.5D and 2D. 2.5D LES shows the most accurate prediction of C_p, C_l, C_d and C_m overall although there were some situations where 2.5D LES predicted less accurately [128]. Significant inaccuracies remained even with 2.5D LES however, which could be due to using the same mesh for LES and URANS simulations when typically a much higher cell count mesh is required for LES as this was not verified in the paper, or it could suggest that other methods such as 3D LES may be required for accurate analysis.

Different forms of DES are also used such as Delayed DES (DDES) and Improved Delayed DES (IDDES). An accompanying RANS model must also be chosen, with Spalart-Allmaras, k-ε, and k-ω being the most common.

Lei et al. uses 3D IDDES with k-ω SST and compares against k-ω SST by itself alongside an experiment[130]. The k-ω SST model, where SST is an acronym for Shear Stress Transport, switches between the k-ω turbulence model near the wall and k-ε away from the wall in order to combine their areas of strength into a single combined turbulence model. IDDES agrees very well with experimental C_p, overestimating by 2.89% at $C_{p\text{-}max}$ while k-ω SST underestimates C_p. At TSR=1.38 IDDES showed good prediction of wake velocity recovery while k-ω SST underestimates, however IDDES overestimates considerably at a higher TSR=2.478. Lei's study conducts a rudimentary mesh verification however with only two meshes considered, and the higher density mesh having only 25% more cells than the original mesh, but despite this a 1% increase in C_p was found, implying that there is a significant difference between the value found by Lei and the converged value. The geometry of the mesh also does not include the struts of the turbine which have significant effects on power coefficient[32][126]. The study does not include dimensions of the struts in the experimental turbine so it is difficult to determine whether the difference between the simulation and experimental results is within the expected range, although they appear to be cylindrical struts in the diagram which Hara et al.[131] finds to cause much larger decreases in C_p than aerofoil struts, as considered by Hand[32], or no struts.

Lam and Peng[11] compared 3D IDDES with 2D and 3D simulations using the RANS model Transition SST, and an experiment by Tescione et al.[12], finding that both 3D models had very good agreement with the experimental wake velocity while 2D estimated poorly. There was little overall difference in accuracy between the Transition SST 3D and IDDES 3D results, with Transition SST slightly more accurate for streamwise velocity and IDDES slightly more accurate for cross-stream velocity, however both demonstrate an offset from the experimental results on the upstream side of the turbine wake.

Dessoky et al.[132] compared DDES-WENO with URANS-JST and an experiment by Li et al.[6], finding that DDES-WENO predicted C_p well. Their URANS results overestimated C_p compared to DDES however it is unclear which turbulence model they used for URANS testing, so conclusions cannot be made that URANS approaches are overall less accurate. Their results also demonstrated that using a 3D simulation domain with matching dimensions to the wind tunnel domain was important to ensure comparability, as using a larger domain resulted in increases in C_p at higher TSRs.

Scale Adaptive Simulation for VAWTs has seen limited study, with Rezaeiha et al.[133] providing the reference for its performance. In the study, SAS was compared against the Transition SST RANS model and SBES, a hybrid LES/RANS model, using 2.5D CFD. They found that the prediction from SAS was closer to SBES than RANS. It should be noted that while SAS did allow for a reduction by nearly half in mesh cell count and time per revolution compared to the hybrid LES/RANS model, the time per revolution was over 23 times higher compared to Transition SST so computational resource requirements remain prohibitive. There were still significant differences between predictions from SAS compared to SBES in some circumstances such as C_l and C_d so an argument for using hybrid LES/RANS models remains.

RANS is a computationally cheaper approach than LES based models, and due to the complex flow around VAWTs involving dynamic stall it is necessary to use an unsteady approach when completing CFD analyses, often resulting in the use of Unsteady RANS (URANS) for CFD VAWT modelling. The flow shows a periodic nature which could allow for use of Periodic methods such as Periodic RANS which can enable significantly faster analysis for appropriate flows. Campobasso et al. found that simulating HAWTs with Periodic RANS had good accuracy and a time reduction factor of 6.5, but was unpromising for VAWTs due to a smaller time reduction factor and worse accuracy when compared to URANS[134]. It also highlights that incorrect selection of complex harmonics can result in very poor accuracy or slower analysis, meaning there is an additional layer to the verification

process.

Amongst RANS models, the turbulence models commonly used in VAWT simulation are variants of k-ε, k-ω SST, and Transition SST. Several other models will also be covered.

A comprehensive comparison of RANS models was carried out by Rezaeiha et al.[10], which considers 7 turbulence models: Laminar, Spalart-Allmaras, k-ε RNG, k-ε Realizable, k-ω SST, k-ω SSTI, Transition SST, and k-k_l-ω. Rezaeiha compares these turbulence models using a 2D CFD simulation against 3 experimental baselines covering leading edge circulation, turbine wake velocity, and C_p against TSR. The k-ω SST variants and Transition SST show the only good predictions with Transition SST performing best. No verification was shown for the meshes and a different meshing technique is used compared to Rezaeiha's previous VAWT papers where verification is shown[59][65][135][136] so it is indeterminable whether these results are representative of the converged results from these turbulence models. In some of the comparisons, only single rotation phase averaging is used due to computational resources required however this is unusual given the proportionately small additional resources needed for longer averaging.

A similar study was conducted by Daróczy et al.[137] which tested 8 turbulence models covering the same models as Rezaeiha, with the exception of Laminar and k-ω SSTI, and addition of SAS and k-ε Realizable with standard wall treatment. SAS, k-ε Realizable with standard wall treatment, and k-k_l-ω were not used in the later testing however due to issues with convergence and stability. 2D CFD was used and the results are compared against 4 experimental baselines of C_p. It was found that Spalart-Allmaras, k-ε Realizable, and k-ω SST were the most accurate around TSR_{opt} while all models were inaccurate at low TSR and overestimated at high TSR. In each of the comparisons, Transition SST overestimated TSR_{opt} which was also seen in Rezaeiha's results[10] amongst other studies[58][41][43][124]. This study demonstrates a rigorous verification process, considering 5 different meshes, all of the turbulence models, two different CFD software, and two TSRs in the verification. However there are deficiencies in their verification process, for example the

lack of using Grid Convergence Index for determining mesh convergence[138] and a potential false plateau in domain size verification.

From these two comparison studies, k-ω SST is the only model which performs well in both. Further research is needed, including the use of more transparent and rigorous verification processes. Daróczy's study also does not consider wake prediction so can only be applied to C_p. Both studies use 2D simulation meaning their results cannot be applied to 3D simulations. They also utilise meshes with target y+ values of 1 in all scenarios, when Spalart-Allmaras and k-ε models allow for wall modelling which enables much higher y+ values of $30<y+<300$ to be used which can reduce computational resource requirements. In order to address some of these issues and consider other aspects of the CFD results, more research must be considered and produced.

Almohammadi et al. produced a similarly wide-ranging study including Spalart-Allmaras, k-ε RNG, k-ω SST, Transition SST, and Transition SST with Curvature Correction, however without comparing to an experimental baseline[139], although the setup is based upon an experiment by Bravo et al.[140]. Instead of C_p which was investigated by the experiment, Almohammadi considered the separation bubble on the blades at 3 different angles of rotation. Blade position 1 inner and outer, alongside position 3 inner, represent an absence of separation bubble, and show recovery towards freestream velocity and beyond occurs at a shorter distance from the aerofoil surface with Transition SST models, followed k-ω SST, then k-ε RNG, and Spalart-Allmaras in that order. Positions 2 inner and outer, and 3 outer, show significant separation. Position 2 outer shows a similar relationship to above however the different turbulence models converge towards different velocities, and with k-ε RNG showing the greatest difference from the Transition SST results. For position 2 inner, the Transition SST models show much higher velocity. The other models show a reduction in velocity after reaching a peak while Transition SST models show a very slow recovery, with the curvature corrected version showing no clear recovery within the distance measured. Transition SST, k-ω SST, and k-ε RNG all converge to the same velocity with each showing an overshoot. For posi-

tion 3 outer, k-ε RNG demonstrates the largest overshoot, followed by k-ω SST, then Transition SST. S-A and Transition SST with curvature correction show very different results with S-A appearing to converge to a lower velocity, while the curvature corrected model shows no signs of convergence within the distance measured.

The lack of an experimental baseline prevents a conclusion being made about the overall accuracy of each model, although it can be determined that for situations where separation is limited or does not occur that there is little difference in accuracy between the models. However, the study can indicate the accuracy of a given turbulence model when used in conjunction with results from a sufficiently high resolution PIV experiment alongside a verified CFD simulation using one of the turbulence models used by Almohammadi. The very small distance of velocity measurement of 2.5% of chord used in the graphed data makes it difficult to compare results to most published experimental results which report separation bubble results using an image rather than comparable data points. While data could be extracted from these images, the accuracy of the extraction itself may be an issue, particularly at the distances used by Almohammadi which would often be sub-pixel scale. A suitable distance for measurement would be $>$30% of chord which would capture the full separation bubble under some circumstances, and potentially $>$150% of chord as shown by Buchner et al.'s experimental results[8].

2.5.3 Pressure-Velocity Coupling

In most studies the SIMPLE Pressure-Velocity coupler is used as it is regarded as having the best performance for most applications. Lam and Peng[11] uses SIMPLEC alongside Li et al.[128] with the justification that it offers faster convergence than SIMPLE and higher stability than PISO. Chowdhury et al. uses PIMPLE which is a combination of PISO and SIMPLE that is available in OpenFOAM[96]. Several authors have done comparisons though they each leave out SIMPLEC and PIMPLE so these need further investigation.

Lanzafame et al. found that PISO offered quicker convergence than SIMPLE and unlike Coupled predicted the wake accurately[141]. Contrastingly Balduzzi et al. found that PISO had poor accuracy for torque coefficient while SIMPLE

and Coupled were accurate, however Coupled allowed for the same performance at larger time steps than SIMPLE[7]. Daroczy et al. showed that the Coupled solver produces identical results with 24 iterations per time step while PISO required 100 iterations[137].

Coupled should be the default option due to much faster convergence but if investigating wakes it's necessary to conduct a verification of both SIMPLE and Coupled.

2.5.4 Spatial Discretisation

For the Spatial Discretisation, Almohammadi et al. compared k-ε RNG and Transition SST using first and second order models[142]. They found a significant difference when using Transition SST with up to 1% change in C_p but a negligible difference for k-ε RNG, so individual verification is required.

2.5.5 Domain Size

Rezaeiha et al.[135][136][143] found that for 2D simulations a blockage ratio of 5%, or a domain width of 20D, is necessary for good prediction of C_p. Daroczy et al.[137] supports this as although they stated that 50D was necessary, their results show that as low as 15D is sufficient. Balduzzi et al.[7] however did find that a width of $>$40D was necessary, these changes can be visualised in figure 2.8. The reason for these differences is unclear as the magnitude of Reynolds number is similar for these studies, it may be due to Balduzzi's turbine design which wasn't published.

For inlet distance Rezaeiha found that 10D was adequate however 12.5D was a safer choice, but Balduzzi and Daroczy found that 20D was necessary. For outlet distance Rezaeiha showed that 10D is adequate for converged C_p prediction while 25D may be necessary if investigating wakes due to the asymmetrical outlet pressure experienced with smaller outlet distances. Balduzzi and Daroczy suggested higher requirements again with both suggesting $>$40D.

Rezaeiha demonstrated that the rotational domain diameter had a negligible effect. Dessoky showed that increasing TSR results in larger domain size require-

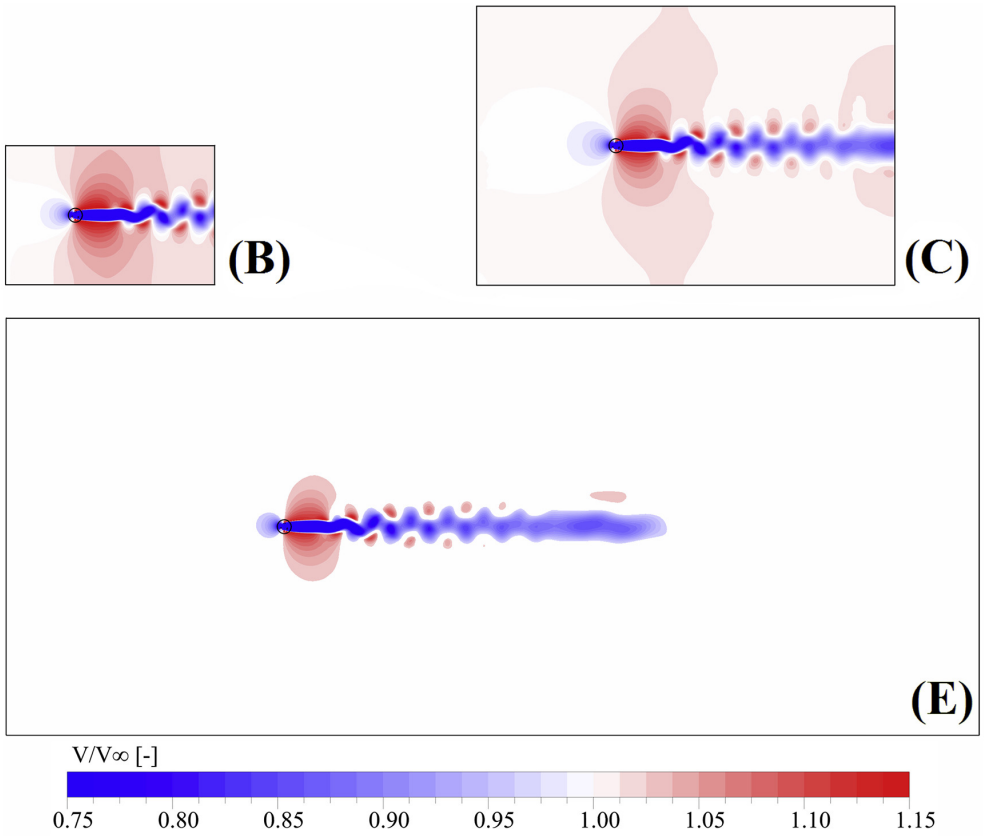

Figure 2.8: Velocity contours dependent on domain size, where B, C, and E refer to domains of increasing length and width relative to the turbine diameter [7]

ments.

Given the relatively few additional elements needed to increase domain size it is advisable to opt for a larger domain, giving an inlet length of 20D, outlet length of 40D, domain width of 40D or blockage ratio of 2.5%. Increasing the rotational domain size increases the element count considerably but has negligible effects, so a diameter of 1.25D is acceptable as demonstrated by Rezaeiha et al.[135].

2.5.6 Time-step

Significant variation between time step recommendations for both 2D and 3D is presented, with 2D being the most documented and most using rotational steps rather than time domain. Rezaeiha et al.[143], Danao et al.[124], and Rossetti and Pavesi[144] all suggest that 0.5° increments are sufficient, with Rezaeiha and Danao clarifying it is only sufficient for high TSR>4.5 and 4 respectively, and the former

finding that 1 degree is acceptable. Smaller increments must be used at lower TSR with Danao suggesting 0.25° and Rezaeiha 0.1°.

Balduzzi et al. shows that the increment is dependent on the pressure-velocity coupling with Coupled allowing for larger steps than SIMPLE, recommending 0.9 and 0.27° respectively[7]. Balduzzi also finds that smaller time-steps are needed for coarser meshes, and that time-step size has a significant effect on blade wake prediction. Trivellato and Castelli take a Courant number (CFL) oriented approach which is suited to free-spinning turbines by adapting time-steps to the variable rotational speed[145]. They find that CFL$<$0.15 is necessary for converged results, however it is recommended that this should be a maximum and smaller steps are ideal. Like Rezeaiha and Danao, Gosselin also demonstrated different increments for different TSRs, with 0.36° being adequate at high TSR and 0.072° necessary at lower TSR[30]. Based upon these studies it would be recommended for researchers to use time steps of 0.25° as a starting point and then verify themselves according to TSR used.

In 3D larger time steps are acceptable with Alaimo et al.[2] showing near-convergence with 3.6° at TSR=0.89 and Elkhoury et al.[48] showing convergence for both 1.2 and 0.6° at TSR=1, meaning the convergence point likely lies between 1.2 and 3.6°, even at low TSR. Belkacem and Paraschivoiu[116] demonstrate a convergence time step of 0.5°for 3D simulations however also find that 1 and 2 degree time steps result in a 1.2% and 2.2% error respectively which can be considered within a reasonable margin of error, particularly if computational requirements are significantly reduced.

2.5.7 Mesh coarseness

A wide range of element counts is found amongst the literature, with some authors advising that as low as 65,000 is sufficient for accurate results[51]. There is also evidence that the necessary coarseness relates to turbulence model, with Transition SST requiring a finer mesh[137].

For 2D k-ω SST a reasonable starting point to test convergence is 450,000 cells

with 50 inflation layers on the blades however it is possible that much lower values will be acceptable so verification would be advised[7][144][11]. For Transition SST this should be increased to 550,000 cells[137]. With 3D simulations a starting point of 2,500,000 cells should be used for both LES/DES and URANS models[130][11]. Little discussion of cell height is available outside of Balduzzi's study[7], except for the use of Y+$<$1 necessary in SST models. Bedon[49] found that a finer mesh with a thicker inflation region is necessary as inlet velocity is increased, and Almohammadi showed that high resolution aerofoil profiles are necessary for good performance with 7552 nodes necessary for convergence[142]. Almohammadi also found that areas of false convergence presented with the k-ε RNG model, where a researcher would believe that the results had converged or plateaued, showing that it's necessary to design stringent convergence criteria. Bangga[146] demonstrates that the overall meshing design may also have a significant impact on results. While they are comparing several different CFD software to determine consistency when using the same settings, they also use very different mesh designs, with the meshes used for the FLOWer simulation having a much higher cell count due to a very high density ring connecting the blades, which is not seen in the FLUENT mesh. Different turbines are also used for the grid studies, suggesting that a verification for one turbine may not be applicable to different turbines.

2.6 Non-CFD and Hybrid Simulation Methods

Alongside CFD, there are a number of other methods available including some hybrid models with a CFD component. The desire for other models stems from the very high computational resources necessary for accurate CFD modelling of VAWTs due to VAWTs being a particularly complex flow problem. In recent years, computational capability has caught up to the needs of VAWT flow problems and so the use of other models is starting to diminish.

Bangga et al.[146] conducted a study comparing the accuracy of several CFD software with several low order models. Low order models, particularly Improved Double Multiple Streamtube, often provided similar accuracy to the CFD models

and sometimes were more accurate, however they performed worse in the high solidity condition. The comparable accuracy between CFD and low order models shown in this study may be due to lack of consensus on how to model VAWTs in CFD, and also the use of 2D CFD, as other studies have shown greater accuracy using CFD. The simpler modelling can result in lower accuracy, or only be valid in limited circumstances. As these are widely covered by Islam et al.[147], Jin et al.[148], and Mohammed[149], they are summarised in table 2.3. Several other models have not been covered in previous reviews however so details are included below.

Table 2.3: Summary of Low Order Models

Model	Notes
Streamtube	Wind speed dependent[119][61][23][144][150]
Actuator Line Model	Closest model to full CFD[64][106][151]
Vortex	[152][153]
Cascade	[154]
Vorticity Transport Model	[155]
LLFVW	Includes Turbine Wake Modelling[156]
Hand Low Order	[32]
Tingey Reduced Order	[157]

2.6.1 Vorticity Transport Models (VTMs)

VTMs were developed originally for helicopters by Brown[158] then adapted for VAWTs by Scheurich and Brown[155]. VTM uses the Navier-Stokes equations in vorticity-velocity form to predict the wake, then uses aerofoil data to predict lift and drag, and thus power coefficient. Combining VTM with a dynamic stall model and strut corrections produces good predictions[155].

2.6.2 Lifting Line-Free Vortex Wake (LLFVW)

LLFWV is a more general method which can be utilised for both HAWTs and VAWTs with minimal adaptation required. Turbine wakes can be predicted using this model which can also enable modelling farms with LLFWV. It is utilised by the open source application QBlade, where a validation by Marten et al. found good agreement with CFD results[156].

2.6.3 Other Low/Reduced Order Models

Hand and Cashman developed a Low Order Model in both 2D and 3D forms, where the 2D model shows reduced error of normal and tangential force coefficients (C_N and C_T) compared to Spalart-Allmaras CFD and DMST models[159]. Very good prediction of C_p is shown using the 2D model until TSR_{opt}, while the 3D model continues to predict accurately until TSR>4.5. Tingey and Ning produced a Reduced Order Model which predicts wake velocity within 5-6% accuracy in milliseconds [157].

2.7 Impact of Aerodynamic Design and Simulation Procedure on Arrays

Both aerodynamic design and accuracy of simulation procedures will impact array design, and the potential effects of these must be considered.

2.7.1 Aerodynamic Design

Array design is inherently impacted by the wake produced by each turbine because this will affect the flow downstream of the turbine and therefore the flow within an array. These adjustments will affect the efficiency of a given array design meaning that optimisation procedures will give different results as the VAWT's wake changes. Aerodynamic design factors which affect the wake and therefore array design will be considered here.

The shape of the turbine will impact array design due to the three-dimensional nature of wake contraction, with Φ turbines demonstrating a different contraction pattern compared to H-turbines.

Turbine dimensions have a significant impact on array wake as demonstrated by Belkacem and Paraschivoiu[116] with the 35m turbine showing significantly higher velocities in the turbine wake compared to the 0.5m model.

Active pitching allows turbine wakes to be manipulated as demonstrated by Sagharichi et al.[160], which could be used to improve the performance of the array as a whole. The reduction in size of vorticies will improve the steadiness of flow

within the array.

Zou et al.[161] find that solidity impacts the behaviour of the wake, with increasing solidity resulting in tendency towards bluff body wake behaviour. The solidity required to achieve this is very high however at 1.08 and so unlikely to be seen in utility-scale arrays. Similarly, De Tavernier et al.[162] finds that solidity impacts array power coefficient.

De Tavernier et al.[101][162] also show that aerofoil choice affects performance of arrays in a double rotor layout.

Beyond these, the impact of other technologies on VAWT wakes must be considered where they have not previously been analysed in the literature, including winglets, end plates, and Variable TSR.

2.7.2 Accuracy of Simulations

Designing arrays using simulations requires high accuracy in several aspects of their predictions, namely changes in power output and the near and far turbine wake velocity components. The wake velocity components must be predicted accurately in order to evaluate the flow within the array and therefore the impact on power output. Theoretically, absolute power output does not need to be accurate for simulating an array, only the relative change in power output between conditions must be accurate, with the absolute power output then being inferred based upon another method which accurately evaluates the power output of an isolated VAWT. In practice, a turbulence model which can accurately predict relative power output in an array will also accurately predict the power output of an isolated VAWT.

Simulation procedure has been evaluated in section 2.5 but the consequences for array design have not been directly considered. The literature has considered simulation of arrays and prediction of VAWT wakes, however has not considered whether numerical studies can accurately predict VAWT wakes and relative power output in the array context, leaving a research gap.

Current simulation studies have focused on the wakes of isolated VAWTs and demonstrated mixed results.

A major factor in the accuracy of CFD simulation is the turbulence model used,

so careful consideration is required to ensure the most suitable choice of turbulence model. Large or detached eddy simulation (LES/DES)-based turbulence models offer supreme accuracy but require higher resolution meshes and a 3D approach, therefore, needing much higher computational resources[133]. In this regard, a need for using LES-based models is very undesirable for array simulation due to both of these aspects being highly computationally intensive.

Alternatively, RANS models can be used, which allow for faster analysis, including in 2D which further reduces the resources required. Within RANS there are several popular models for the analysis of VAWTs, the most common option being k–ω SST[163][7][39][164][165], followed by k–ε [60][166][29][86][79] and Transition SST[136][10][44]. Previous studies have also used other models including Spalart–Allmaras which has shown to be inadequate[137][45], k–kl–ω [137][167] , and corrections of k–ω SST[45] and Transition SST[139] such as the low Reynolds number and curvature corrected versions. There is also uncertainty regarding which RANS model provides the most accurate results, with some articles making opposing conclusions, particularly regarding k–ω SST and Transition SST[124][41][137][10]. A contrast also exists amongst the literature between which models better predict the power output of VAWTs and which better predict the wake characteristics, which is problematic given that accurate prediction of both is necessary for analysing arrays.

The 2D approach has some limitations which are demonstrated by Jiang et al.[72], with the flow at the tips being significantly distorted, an effect which cannot be modelled in 2D and so requires a 3D approach. However, it can be seen that this has limited effect on velocity at the midplane for sufficiently high aspect ratio blades, so 2D results remain a valid estimation for wake velocity downstream at the midplane up to a certain point downstream providing the VAWT design does not use struts at or near the midplane as per Bachant and Wosnik[168]. Boudreau and Dumas[169] find this point to be approximately 2 diameters downstream whilst Jiang et al.'s results and the results from Lam and Peng[11] imply that this point occurs beyond 5 diameters downstream. The discrepancy is likely to be the result

of diferences in tip speed ratio which result in Boudreau and Dumas' setup having greater vortex shedding due to the higher effective angle of attack of the blades as a result of the lower tip speed ratio compared to Jiang et al.'s experiment.

Alongside these are two experiments by Tescione et al.[12] and Rolin and Porté-Agel[117], where Tescione et al.'s experiment does not show an impact from tip effects on the midplane wake within the sampled region downstream, whilst Rolin and Porté-Agel shows an impact at the earliest sampled distance downstream, 2 diameters. Both Tescione et al. and Rolin and Porté-Agel show increased wake enlargement at the midplane which may be due to 3D effects, however, given that many 3D CFD results in the literature using both URANS and LES models alongside experiments do not demonstrate this wake enlargement it is inconclusive whether using 3D CFD is currently a solution[11][13][169][130].

Results are found by Posa et al.[13] and Lei et al.[130] for turbines with no tip devices, showing that both the experiments and 3D CFD using LES, DDES, and k-ω SST had insignificant shift of the wake velocity minima position, so not all VAWTs will demonstrate this behaviour. In the study by Posa et al., the shift, and failure for CFD to predict the shift, was seen in the low TSR condition but not the high TSR condition, although this was not seen between the low and high TSR conditions in Lei et al.

The difference between Posa et al. and Lei et al. is that the latter uses significantly higher Reynolds numbers, so the shift could be related to Reynolds independence which is a well-documented phenomena for prediction of power coefficient of VAWTs[42][5][24], and may be a phenomena which CFD struggles with[43]. However the chord Reynolds number (Re_c) which is being experienced by the VAWT in both low and high TSR conditions is far below that expected for Reynolds independence for power coefficient, approximately $2x10^5$, whereas Posa et al.'s results would indicate that Reynolds independence for the wake can occur at approximately $3x10^4$. The difference between the results for the low and high TSR conditions implies that the simplified chord Reynolds number which does not take rotational speed into account is not sufficient for predicting whether a shift will

occur.

The shift could be due to the blade reaching low effective Reynolds numbers as a result of the rotation, where the crossover point would occur at TSR=1 representing the point at which a blade positioned at the 90° position will have an effective Reynolds number of zero. Although this logic can be applied to any point in the downstroke where the streamwise velocity of the blade minus the streamwise velocity of the airflow is greater than zero. It would then be expected that CFD estimates would be incorrect for TSRs above 1 if the effective Reynolds number remained sufficiently low and the turbulence model was inaccurate for low Reynolds number scenarios. For Posa et al. the change in Re_c between TSR=1 and TSR=1.35, where the shift still occurred in the experiment, is approximately 10,531 whilst for TSR 2.21, where the shift was no longer seen, this is approximately 66,821. The range for wake Reynolds independence can be further narrowed down using Lei et al.'s results, where the change in Re_c between TSR=1 and TSR=1.38, where no shift is found in their results, is 54,014.

Tescione et al.'s experiment[12] demonstrates a shift towards the upstroke side which is the opposite direction to expected. It also uses a TSR of 4.5, a Re_c change of 132,691, and a low turbulence intensity of 0.5%, all of which appear to be indicators of reduced shift based upon results and considerations so far. So Tescione's study is evidence against these hypotheses although it may have confounding factors which affect the results. For example, the cross-stream velocity profiles found by Tescione et al. indicate that the inlet cross-stream velocity does not have a uniform profile and so this will affect how the blades interact with the airflow in comparison to other turbines due to the blades experiencing a different effective velocity and direction compared to a uniform inlet profile.

Lam and Peng[170] find that 3D CFD using k-ω SST and DES turbulence models still fail to predict the shift in the minima position found in their experimental baseline, reinforcing that the issue may be unrelated to the number of dimensions used.

Further research is needed to gather evidence specifically on these hypotheses,

focusing on how the accuracy of CFD is affected by turbulence intensity and low or negative effective Reynolds number during the downstroke. Beyond this, the impact on predicting array flow and power output must be considered.

2.8 Summary

The main findings of the literature review are summarised below:

- The current best progress towards a standard utility scale VAWT design is a slender H-bladed turbine using aerofoil-shaped struts, with a solidity of 0.2-0.4 where the higher end of this range is more likely to enable self-starting behaviour[3][32]. For smaller turbines, higher solidities are acceptable.

- Other modifications to VAWT design such as blade pitching have the potential to significantly increase the efficiency of VAWTs[30][5] alongside other performance characteristics such as self-starting behaviour.

- Arrays offer strong potential for increases in power output, however further research is required for determining best design practice, particularly for larger farms, realistic conditions, and how VAWT design affects array design[18].

- Field testing larger VAWTs in the chord Re$>$250,000 range, dependent on solidity, using Lidar to capture the wake, offers significant advantages in terms of applicability of research to utility scale turbines[42][5][24][114].

- Gaps remain in the evaluation of VAWTs in general against the industrial standard for wind turbines IEC64100.

- VAWT simulation procedures require further improvements to the accuracy versus efficiency balance to allow rapid and reliable general purpose testing via simulation[133]. High accuracy is currently possible using LES-based models however these are prohibitively computationally expensive, whilst cheaper RANS models are not sufficiently accurate[128][130]. The recommended procedure based upon the literature is stated in Table 2.4 below

- Some of the error between simulation and experimental results may be due to the conditions used in wind tunnel testing with low Reynolds number and turbulence intensities which pose a more complex problem for CFD solvers and are less representative of utility scale turbines[6].

- Changes to VAWT design have the potential to significantly affect array design, with factors such as active blade pitching allowing manipulation of wakes and aerofoil choice demonstrably changing array power output[58][101].

- No research was found which considers the accuracy of simulation methods for analysing arrays when validated against an experimental baseline array. There is also no direct study on how most VAWT design parameters affect array design.

Table 2.4: Recommended Settings for VAWT CFD

Turbulence Model	IDDES or k-ω SST
Pressure-Velocity Coupling	Coupled
2D or 3D Analysis	3D
Inlet Length	20D
Outlet Length	40D
Blockage Ratio	2.5%
Rotational Domain Diameter	1.25D
Rotational Step (2D)	0.25°
Rotational Step (3D)	1.2°

2.9 Research Gap

From the literature review several research gaps are established. There is a need for further comparison on array designs, including optimisation procedure and how turbine design such as solidity will affect array performance. The applicability of typical VAWT experimental procedure for evaluating utility scale wind turbines needs improvement, including greater adherence to IEC64100, in order to ensure that results are a reasonable representation of utility scale VAWT performance. Previous

literature has not fully examined the impact of Reynolds number on VAWTs which is another aspect of ensuring that VAWT research at small scales and wind speeds is applicable to larger scales and higher wind speeds. Further progress can be made on evaluating the accuracy of CFD methods to optimise the balance between accuracy and efficiency so that VAWT development can move more quickly compared to the current slow pace which limits the ability to optimise VAWT design. There is also no validation of the accuracy of CFD methods for predicting VAWT array performance, where the validation compares accuracy to an experimental array baseline.

2.10 Aim

Section 2.9 established a series of research gaps to be addressed in this thesis, demonstrating the incompleteness of the fields of VAWT arrays and VAWT simulation. The research in this thesis therefore investigates how to increase the power efficiency of VAWT arrays and to understand the factors involved in determining array efficiency, alongside considering the accuracy of different CFD procedures based upon several different experimental baselines.

Using CFD, array designs were evaluated and optimised for power output, and different CFD procedures were evaluated to reduce prediction error. The literature was also reviewed and analysed to identify trends regarding the applicability of VAWT research to utility scale turbines, including comparisons between field and wind tunnel testing, and the impact of Reynolds number.

Therefore the aim of this thesis is as follows: *"To improve the design procedure for Vertical Axis Wind Turbine arrays through analysis of array layout to determine potential improvement in power output and to evaluate the procedure for numerical analysis."*

2.11 Objectives

These objectives were satisfied in order to achieve the research aim:

1. Conduct a critical review of the literature to determine any research gaps and provide a direction for the research in this thesis

2. Investigate VAWT array layout design choices by conducting Computational Fluid Dynamics modelling to determine array power coefficient

3. Determine the change in power coefficient possible for VAWT arrays compared to isolated turbines after an optimisation procedure has been completed

4. Determine whether the solidity of VAWTs in an array affects the array power coefficient

5. Examine the applicability of wind tunnel experiments for determining power output curves and wakes of utility scale VAWTs in the field

6. Investigate the impact of Turbulence Intensity dependence on the accuracy of Computational Fluid Dynamics modelling for VAWTs

Chapter 3

Methodology

This chapter discusses the methodologies used in the studies conducted. In order to investigate the research gap, the design of arrays will first be investigated to determine how different parameters affect power output. A comparison of CFD methodology in 2D and 3D will then be conducted in order to determine guidelines for accurate and efficient CFD simulation to improve upon the literature-guided methodology used in the optimisation. The impact of Reynolds Number on CFD results will then be considered.

3.1 Array Design

This section discusses the methodology used to assess potential array designs, including the choice of experiment or simulation, seeder designs, optimisation procedure, impact of turbine design on array design, and verification and validation procedure and results.

3.1.1 CFD justification

CFD was chosen to complete this study because of the significant difficulties involved with using other methods. CFD has low setup costs and this was particularly important given the size and number of turbines required to study arrays. Good accuracy for using CFD to predict VAWT performance has been demonstrated in the literature review 2.5.

In contrast, wind tunnel and field testing methods have high costs for setup due to the need for manufacturing turbines alongside use of measurement tools

and either the wind tunnel or field space. In the case of wind tunnel testing, size limitations would have either significantly increased costs or restricted the possible experiments which could have been conducted.

Similarly, 2D CFD was used due to the high costs of 3D simulation, particularly for the desired experiments which involve numerous turbines where computational requirements are proportional to the number of turbines.

The software ANSYS Workbench 18.2 was used because this is one of the industry standard softwares used for CFD and offered a complete suite within which geometry and meshing could also be completed. Using ANSYS also aids in easy replicability. The main alternative softwares are STAR-CCM+ and OpenFOAM.

The CFD model was setup as per the results of Lanzafame[141] which fits with the results of the literature review 2.5. A Transition SST model was used, with a PISO pressure-velocity coupling scheme. Second order Upwind spatial discretisation algorithms were used for all equations and a Least Cell Based algorithm was used for gradients. For the transient algorithm the Second Order Implicit Formulation was applied.

3.1.2 Geometry

The turbine used was based upon Carrigan et al.[56] because this offered an already optimised baseline to compare results to. This incorporates the NACA 0023.7 aerofoil shown in figure 3.1 with a solidity of 0.883. Using a blade chord of 1m, this results in a turbine with a diameter of 3.4m. This size was used because it offers a good compromise between larger turbines which would be used for commercial sized farms, and smaller turbines used in urban settings, and resultantly ensures that results are less affected by Reynolds dependence.

The 2D turbine was created in ANSYS DesignModeler using an imported aerofoil from the Airfoil Tools NACA 4 Digit Airfoil Generator, the aerofoil was then patterned to create a 3 bladed turbine.

A rotating domain was placed around the turbine to allow for rotation in the dynamic mesh, and so the VAWT will spin as a result of the airflow. The rotating core was chosen to have a 5m diameter, or 1.5D.

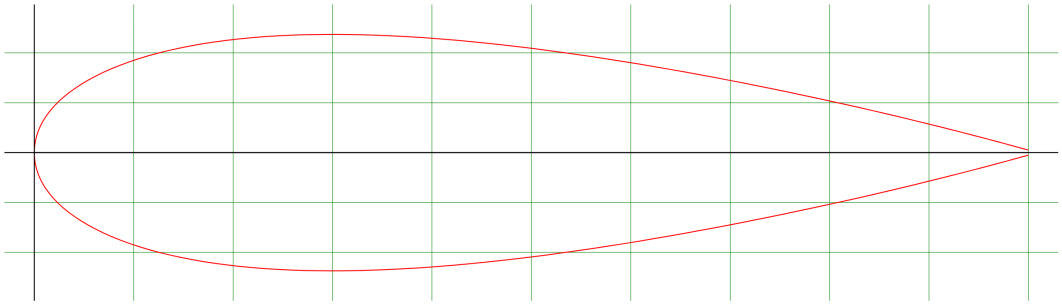

Figure 3.1: Diagram of NACA 0023.7 aerofoil

The literature review suggested distances to inlet, outlet, and width of 20D, 40D, and 40D respectively however a verification for inlet and outlet distance was carried out for this in the results chapter, resulting in dimensions of 3D and 6D respectively. A width of 6D was used, implemented for arrays as width between the furthest turbines plus 6D, with symmetry used for the side walls which has been demonstrated to allow smaller widths down to 4D by Lanzafame et al.[141].

3.1.3 Farm Configurations

A series of array configurations were chosen from the literature to be tested and to act as seeders for optimisation. These were the grid, truss/offset grid/triangular/hexagonal, pairs, and the ”school of fish”/biomimetic configurations. Both the grid and truss designs were considered with alternating rotation directions as well as single rotation directions. Alongside this, two hybrid configurations were produced, the first used the truss configuration but with the intra-line spacing recommended for the biomimetic configuration, whilst the other used the biomimetic configuration with reduced spacing between the lines. These were chosen in order to consider the value of the biomimetic spacing recommendations. The grid, truss, and biomimetic layouts are shown in figure 3.2.

The initial spacings chosen are described in Table 3.1, where a represents vertical spacing between rows, b represents the horizontal spacing between the column line and the turbine in the second row of that column, and c represents the horizontal spacing between columns. For the Pairs formation, the value b represents the horizontal distance between turbines within a pair. These are demonstrated in figure 3.3

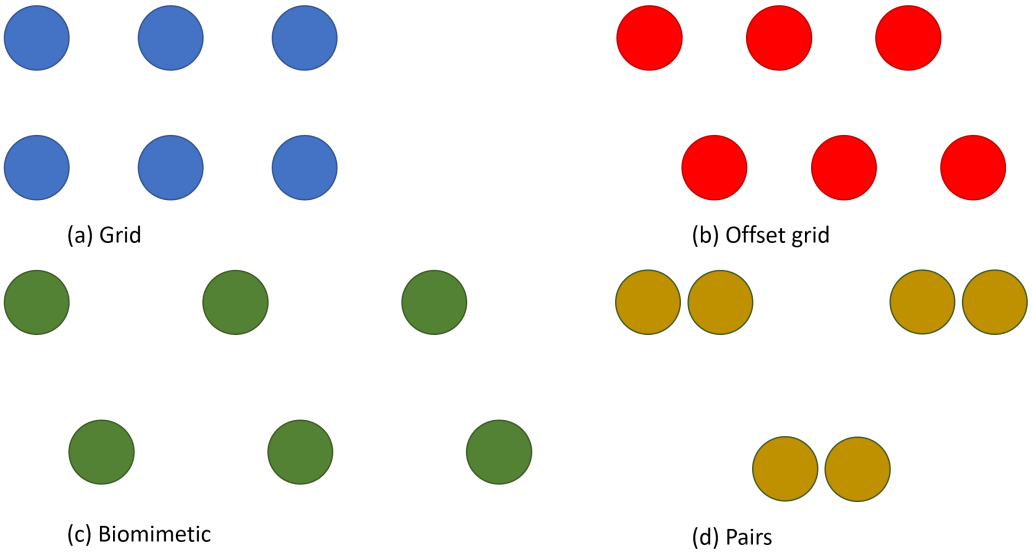

Figure 3.2: Diagram of the main array layouts

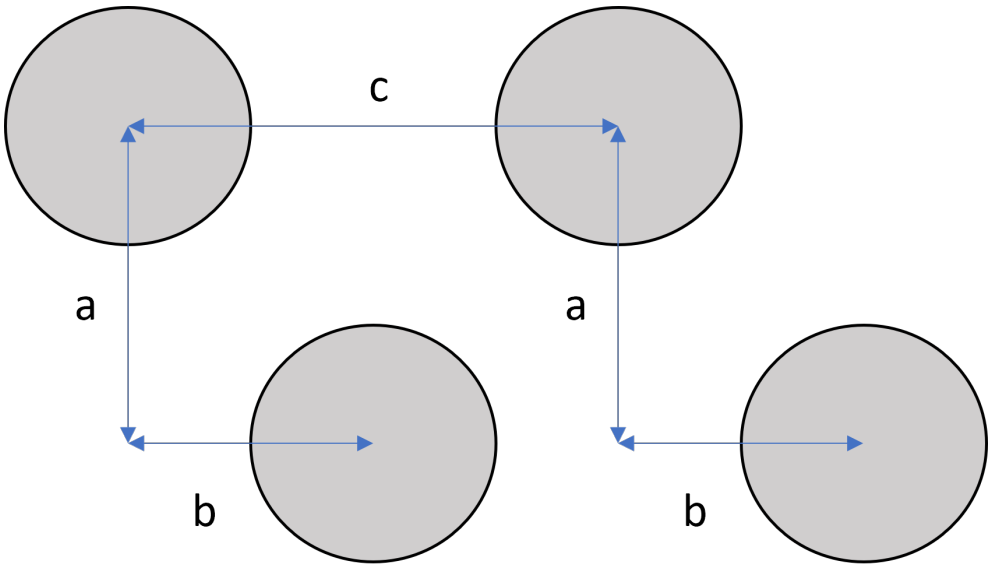

Figure 3.3: Diagram illustrating the spacing definitions for table 3.1

Table 3.1: Spacings used for seeder configurations

Configuration	Spacing (m)		
	a	b	c
Grid	10	0	10
Truss	10	5	10
Biomimetic	11.33	3.4	13.6
Pairs	10	5.1	15.4

From these seeder configurations, additional arrays were chosen for investigation. The first arrays were to verify the number of turbines necessary to achieve representative results. These included 4x4 and 3x3 arrays, and from consideration of the results it was chosen to use arrays which consisted of 3 columns and 2 rows of turbines because addition of rows and columns did not add additional flow features for investigation and so would not add value to the simulations, especially considering the additional computational resources required which would delay investigation of more valuable studies including array optimisation and effect of solidity on array performance. The use of 3 columns provided insight into the main possible positions within an array and so additional rows were not necessary to extrapolate results also.

In addition, a 3 layer V-shaped configuration was chosen to investigate hypotheses regarding the mechanism of action for increased power coefficients of turbines within the array.

After the seeder designs were investigated, a gradient-based optimisation was completed for the truss-configuration to maximise power output. Once completed, the turbine was then substituted with a low solidity version of the same turbine modified by reducing the chord length to result in solidity=0.12 which represents the opposite extreme end of typical solidity used for VAWTs, in order to determine if solidity impacts the power output of the optimised array.

A single wind direction was initially assumed because optimisation for multiple wind directions can be added to extend the study, and the design of the optimisation procedure mimics a crude implementation of small variations in wind directions due to both being inherently linked to changes in the relative angles be-

tween the turbines. Using small variations is more representative of a typical wind farm where the wind rose for the location will tend towards a specific direction. Whilst it is not as representative as implementing directions according to a complete wind rose or higher resolution time-domain data, this implementation requires no additional simulations to complete so is more efficient at the cost of accuracy.

3.1.4 Meshing

A mesh is required for CFD simulation in order to split the domain into smaller subdomains called cells. The governing equations are then solved for each of these cells. Production of a good mesh is essential for an accurate and functional simulation as a coarse mesh can provide inaccurate results and a mesh with highly skewed cells can cause the results to become divergent. The meshing was completed in the Meshing tool of ANSYS Workbench 18.2.

The 'Proximity and Curvature' size function was chosen in order to ensure a high mesh density around the blades of the turbine. Relevance centre was set to medium, and 'Faces and Edges' was chosen as the Proximity Size Function Sources. Global maximum face size was chosen to be 0.10m and an additional maximum face sizing of 0.04m was applied to the rotating core regions. Inflation was applied to the turbine blades with a maximum of 12 layers allowed with first layer height set to ensure that y+$\leq$ 1 as required by SST turbulence models. This provides a finer, more structured mesh around the blades, which is necessary as flow in these regions will have the greatest effect on the system.

This method resulted in some poor characteristics in the mesh with a max Aspect Ratio (AR) of 55.2, which occurred in the boundary layer so is expected and as the long direction is along the direction of flow it is not problematic. Outside of the boundary layer the maximum AR was in the single digits as shown by the mesh metrics available in ANSYS Meshing. The maximum skewness produced was 0.77824 however when the mesh was imported to fluent and the "Improve quality" function was run it enabled a reduction to 0.248 which is excellent. The average skewness was 0.06 and y+ values were $\leq$1 as expected by definition, both of which are also excellent. Orthogonal quality was a minimum of 0.27 which is acceptable

and an average of 0.988.

3.1.5 Computer Specifications and Impact on FLUENT setup

The simulations were completed on a computer with a 4 core/8 thread Intel i7 6700T CPU, 24GB of memory, and an Nvidia GTX 1070 8GB GPU. Simulations were run on 7 threads to ensure quick completion, with the last thread left for other system usage including the Operating System and internet browsing. During the simulations with up to 16 turbines up to 21GB of memory was used, as such for larger farms it would be necessary to use a computer with a greater memory capacity. As GPU acceleration can often offer little performance increase, or even a decrease in performance, a 6 turbine simulation was tested with and without GPU acceleration. It was found that the average time per iteration with the GPU was 0.567 seconds compared to 0.623 seconds without, a 9% reduction in time taken.

For the first 40 seconds of simulation time, the amount of time required to ensure the turbines had reached steady state, the convergence criteria required residuals to be set to 10^{-3} for $\geq$6 turbine simulations and 10^{-4} for smaller farms to ensure good accuracy while allowing for reasonable compute times. After this, the size of the time steps were reduced in order to ensure greater accuracy and the residual requirement for convergence was reduced to 10^{-4} for simulations of 6 turbines and above, and 10^{-5} for any simulations with fewer than 6 turbines.

3.1.6 Simulation Conditions

Table 3.2 describes the boundary conditions for the control volume.

Table 3.2: Boundary Conditions

Inlet Velocity	10 m/s
Turbulent Intensity	5%
Turbulent Viscosity Ratio	10
Outlet Pressure	0 Pa
Symmetry	On side walls
Fluid	Air
Walls	Rigid Bodies

These conditions were selected to meet requirements set out in the literature

review chapter 2 or section 3.1 in order to better represent average field conditions, or were left at default if no guidance was provided for the setting.

A dynamic mesh was also implemented in order to allow the turbines to rotate freely instead of at a set speed as used in most other VAWT simulations. This is more representative of a practical scenario where the turbine is driven by the free wind.

The walls between the rotating cores and the rest of the control domain were set as interfaces to allow the fluid to flow through them and thus rotate the turbine and produce a wake downstream.

The Dynamic Mesh methods of Smoothing, Layering, and Remeshing were enabled, where the Smoothing method was set to Diffusion, Layering was left at default, and for Remeshing the maximum length scale was set to the original value and maximum skewness was set to 0.7.

The rotating cores were then setup using the 6DOF (6 Degrees of Freedom) solver in Fluent where only one degree of freedom was allowed: rotation around the Z axis.

3.1.7 Power Calculations

The power output of a VAWT is defined by equation 3.1, where τ is torque and ω is rotational speed in radians/second.

$$Power = \tau\omega \tag{3.1}$$

Carrigan et al.[56] established a method for calculating average torque from the data collected in FLUENT, shown in equation 3.2 where t_0 is the beginning of the rotation with minimum torque, and t_n. t_i is the data point before the next point of minimum torque, the end of the revolution.

$$\tau_{avg} = \frac{\Delta t}{2(t_n - t_0)} \left[\tau(t_0) + 2 \sum_{i=1}^{n-1} \tau(t_i) + \tau(t_n) \right] \tag{3.2}$$

This was then modified to account for the free rotation resulting in equation 3.3

$$\tau_{\text{avg}} = \frac{\Delta t}{2(t_{\text{n}} - t_0)} \left[2 \sum_{i=1}^{n-1} \tau(t_{\text{i}}) - \tau(t_0) \right] \tag{3.3}$$

The individual torque values $\tau(t_i)$ were recorded using the moment report function in FLUENT, this produced a list of the torque values at each interval which was then input into MATLAB to calculate the average power. A time step of 0.005 seconds was set during this data collection stage and this was run for 120 steps in order to capture a full revolution of the slowest rotating turbines. The ω values were output by FLUENT's dynamic mesh utility. The rotational speed is sufficient for finding the plateaued power value in the verification process because it has been shown by Cuesta et al. that for at a specific wind speed, a given rotational speed will correspond to a specific torque[171].

Mechanical power only on the turbine was used and losses due to friction and windup were not considered, hence the rotational speed of the turbine is restricted by the average torque from drag over a revolution matching the average torque from lift.

The power values for all turbines in the farm were then averaged to produce P_{avg}. This was then divided by the power of the airflow available to an isolated turbine (equation 3.4) as calculated using equation 3.5 to produce the Array Power Coefficient:

$$P_{\text{Wind}} = \frac{1}{2} \rho V_{\infty}^3 S \tag{3.4}$$

$$C_{\text{AP}} = \frac{P_{\text{avg}}}{P_{\text{Wind}}} \tag{3.5}$$

It was important to use the array power coefficient with P_{Wind} rather than localising to each turbine in order to ensure comparability, as the local velocity varies for following turbines due to wake effects of leading turbines, and so averaging the local C_P would provide incomparable results.

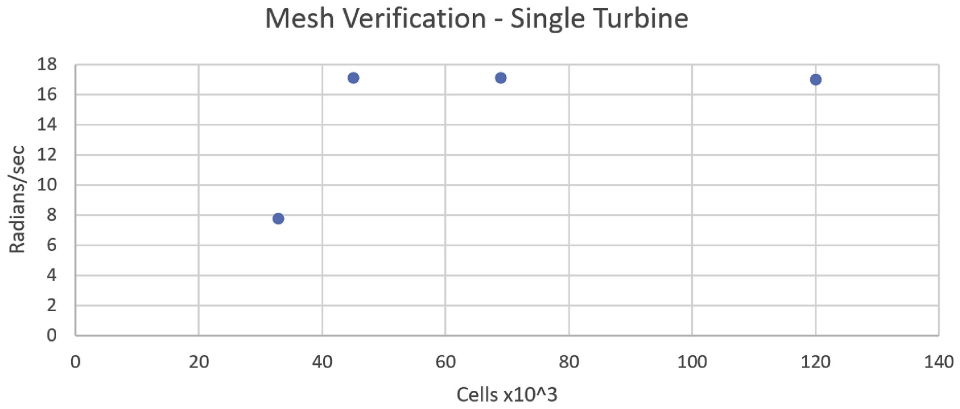

Figure 3.4: Effect of Cell Count for Single Turbine on Rotational Speed

3.1.8 Verification

A verification was first completed on the mesh to determine the impact of cell count and domain dimensions on the results. The verification was conducted against the rotational speed of the flow-driven turbines for the cell count because these were conducted before the method for calculating torque was implemented, whilst the domain geometry was conducted against C_p. Using only rotational speed remains a valid measurement because a peak in rotational speed corresponds to a peak in torque and therefore C_p based upon the relationship between power, torque, and rotational speed, where any further increase in torque must correspond with a decrease in rotational speed. Whilst the methodology for calculating torque was not yet finalised, the moment coefficient in Fluent was used as an indicator of torque, showing that torque plateaued at the same time.

The cell count verification was conducted first for a single turbine then for a 4 turbine grid shaped array to verify that the methodology would also work for arrays.

In figure 3.4 it was seen that rotational speed plateaus after approximately 45,000 cells, whilst in 3.5 the plateau begins at 160,000 cells or approximately 40,000 per turbine. This discrepancy using the same meshing methodology is caused by the lower average mesh density in the larger static domain used by the 4 turbine domain. Figure 3.4 also demonstrates that a false plateau is unlikely, with the plateau continuing to 120,000 cells for the single turbine.

Figure 3.6 and 3.7 demonstrate the impact of domain dimensions on power

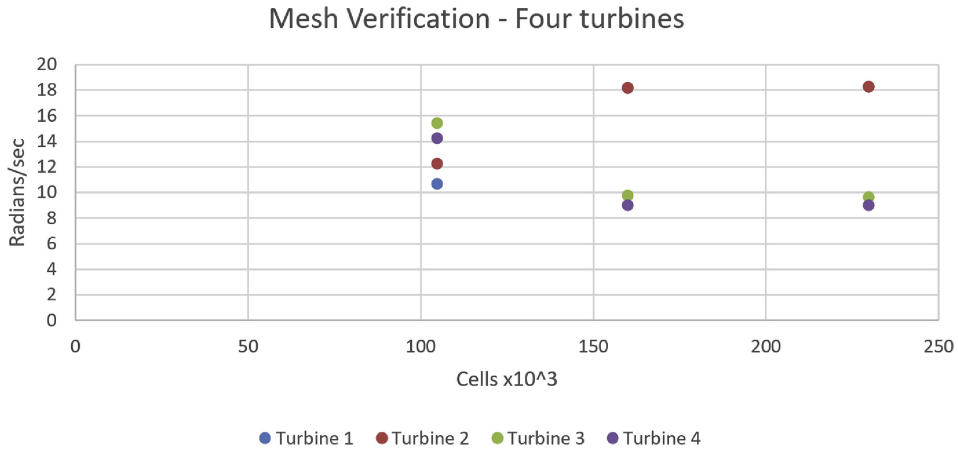

Figure 3.5: Effect of Cell Count for 4 Turbine Array on Rotational Speed

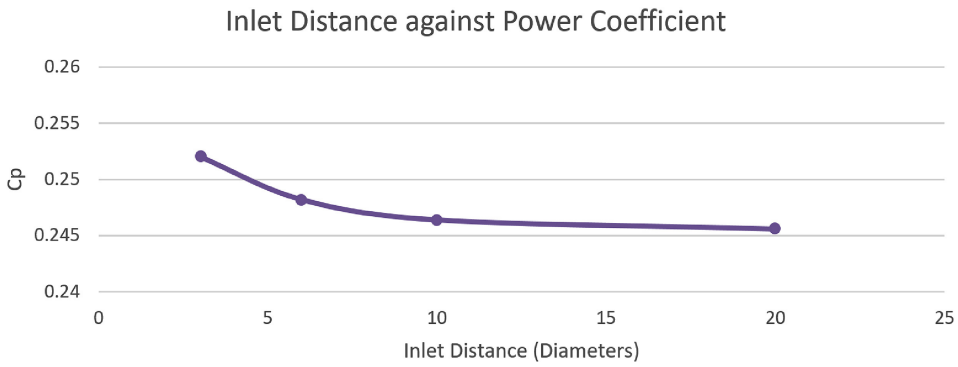

Figure 3.6: Effect of Inlet Distance from centre of turbine on Power Coefficient

coefficient for a single turbine. For inlet distance, whilst a plateau occurs from an inlet distance of 10D, the testing showed that for the test bed a distance of 3D was sufficient with a 2.6% overestimate of C_p compared to the 20D condition as shown in figure 3.6. Similarly it was found that 6D was sufficient for the outlet distance, an overestimate of 0.4% compared to the 20D condition, shown in figure 3.7.

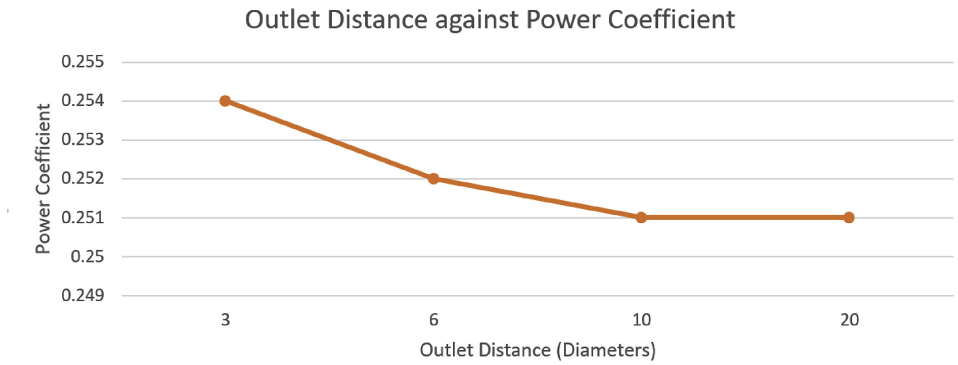

Figure 3.7: Effect of Outlet Distance from centre of turbine on Power Coefficient

A verification was also conducted for the number of turbines needed in order to produce representative results for an array.

An initial grid of 16 turbines in a 4x4 configuration was run for the grid condition and found that the first row of turbines performed on par with the isolated turbine ($C_p \approx 0.252$) but severe performance reductions were seen in each following layer of turbines, with the second layer demonstrating $C_p \approx 0.01$. Whilst it's clear that the performance losses become less severe with each following layer, it was also seen that there is a severe detriment to performance after the first layer. Interactions between columns were negligible with similar performance in each turbine within a row.

This was repeated for the offset grid/hexagonal with the same number of turbines in a 4x4 configuration, and Biomimetic configurations albeit using a 9 turbine farm in a 3x3 configuration. The first layer in both configurations again showed performance on par with the isolated turbines, however it was found that the second layer had a substantial increase in power compared to the first layer. This effect was more prominent in the offset grid design with turbines producing an average of 12.5kW compared to 10kW in the Biomimetic configuration, 5.25kW for the isolated turbine, and 2.7kW for the grid configuration. In the third layer it was found that turbines which were exposed to a more open flow of air, e.g. the leftmost turbine in the offset grid configuration produced up to 49.7% more power than those which were more closed off. These results were replicated in the Biomimetic design with similar performance across the layer albeit a smaller 18.8% power production advantage for the leftmost turbine, suggesting the spacing between each column pair should be larger than the guidelines provided by Whittlesey et al.[105]. It should be noted that the third layer in the offset grid design still retained a 16.9% performance advantage over the equivalent Biomimetic row, and the lowest power turbines in the offset grid third row produced 8% more power than the equivalent in the Biomimetic design.

This performance difference was equivalent to 3.3% of the baseline isolated turbine performance for a 3x3 farm which can be considered negligible compared

to the 21–30% seen in the second row. This is due to the combination of the blockage caused by both the first and second rows of turbines and the mechanism through which increased power output is seen for certain array configurations. It can be extrapolated that this would be even lower for any further following rows as a result of additional rows contributing a smaller proportion to the overall array power output, and so it can be concluded that a double row farm is sufficient in order to compare performance of the configurations.

From inspection of the offset grid and Biomimetic designs, it was decided that a width of 3 turbine columns or column pairs would provide a good representation of the performance of larger farms by providing a higher weighting to second row turbines which were preceded by leading turbines on both sides, these can be considered to be inner turbines as they are situated towards the inside of the farm. This size was sufficient to capture the interactions between parallel turbines and between the first and second rows. The mechanisms for reduced performance in later rows were already understood and would not differ between array layouts for any reasons other than what would be found in the first two rows or from the initial larger array testing. A width of 2 would provide equal weighting to inner and outer turbines so would provide a poor representation of a larger farm, whereas a width of 4 would result in a large increase in computational cost. As a result it was decided that farms with a 3x2 configuration, for 6 turbines in total, would be used.

Overall this resulted in a design for the arrays of a 3D inlet distance, 6D outlet distance, and 3x2 layout of turbines.

All cases were also analysed for their compliance with Betz' Limit due to the nature of the work in trying to increase the farm power coefficients to very high levels, where Betz's limit states that a Wind Turbine cannot remove more than 59.26% of the power from an airflow[17].

This was measured by placing a horizontal line, of equal length to the diameter of the turbine, 5m ahead of the centre of each wind turbine to measure V1, and another line 5m behind for V2, then measuring the velocities along these lines. The velocity was then used to calculate the power input and output from the turbine and

it was found that all cases were compliant with Betz's limit with a maximum value of 0.5923. Note that this does not describe the efficiency of the turbine itself, only the power lost from the airflow as a result of the turbine's interference. Whilst this doesn't account for streamwise expansion, the areas being ignored are towards the outside of the wake where the velocity deficit and therefore the measurable power lost to the airflow is significantly reduced. Accounting for the expansion would also require more complicated analysis techniques due to the varying expansion and sometimes constriction of streamtubes due to the flow mechanisms involved.

3.1.9 Validation

As found in the literature review and explained in the methodology, the H-Bladed VAWT design allows for 2D models to be used instead of full 3D models without compromising the model, for example blade rotation is still retained alongside consequent wake effects, and the H-bladed design lacks variable geometry which would require a 3D approach.

This study used a turbine design which has not been tested experimentally, however it is possible to estimate the expected performance of the turbine based upon the accuracy of the testing methodologies previously used by Carrigan et al.[56]. Using the results of Lanzafame et al.[141] and Chowdhury et al.[96] it was then possible to estimate the expected performance of the methodology used in this study.

Some difference was expected as shown by Chowdhury[96] due to Carrigan's use of the Spalart-Allmaras model in contrast to the use of Transition SST for this study which has been demonstrated as more accurate by the literature review. In order to maximise comparability, the accuracy of TSR=0.75-1.5 was compared using a fixed rotational speed and adjusting the freestream velocity from the baseline of TSR=1.0 using 10m/s, with this range covering TSR_{Opt}. Under Carrigan's study, at TSR=1 it was expected that Cp=0.4, and when adjusting for this using the results from Chowdhury et al. and Lanzafame et al., it was found that the Spalart-Allmaras model produced approximately a 34% overestimate in C_p compared to Transition SST, and so C_p=0.299 was expected. During testing a value of 0.289 was found

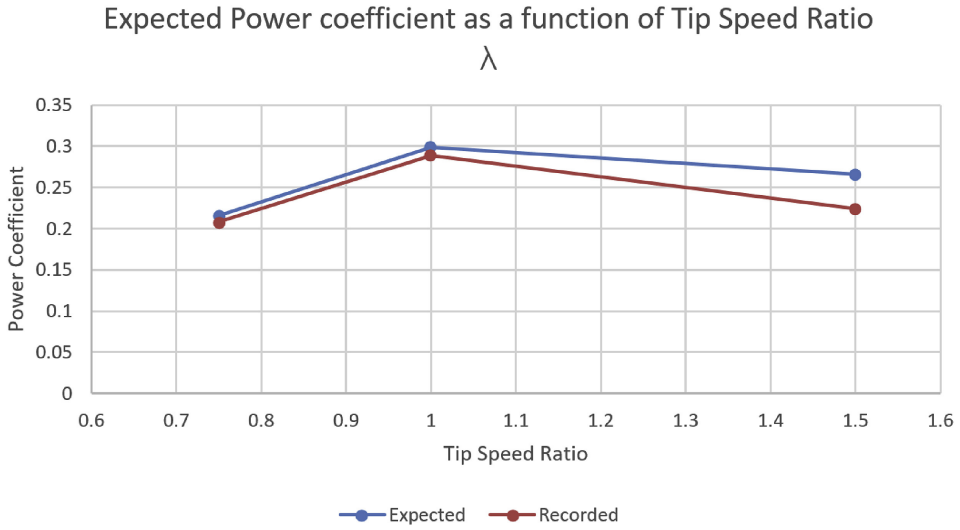

Figure 3.8: Validation against expected results from Carrigan et al. adjusted by Lanzafame et al.

showing good agreement as shown in figure 3.8.

It can be seen that there was good agreement at lower tip speed ratios, however at higher tip speed ratios they began to diverge. As Lanzafame's study showed a greater overestimate between the Transition SST model and the experimental results at higher tip ratios, this was a good result as this demonstrates that the expected overestimate would be reduced compared to expectations.

3.2 CFD Validation

This section discusses the methodology and conditions used in order to investigate the impact of simulation and CFD procedural design on the accuracy of simulations. The focus is on two main aspects, 2D versus 3D, and comparison of Turbulence models.

3.2.1 CFD justification

CFD was chosen to complete these studies because they are a common, accessible, and general purpose tool for fluid dynamics simulation, with the latter two being especially valuable for VAWT arrays due to a lack of other tools available for their design. Where this is possible there is a very high labour and skill cost to implementation, such as Actuator Line Models or other custom code. As per section

3.1, ANSYS Workbench was used to conduct the CFD however this was updated to version 2019 R2.

A notable potential exception exists to this rule in the form of QBlade which uses the Lifting-Line Free Vortex Wake method which analyses both power output and wake at the same time. Whilst it is not fully general purpose like CFD, it is largely sufficient for the purposes of the current state of the art of VAWT research and comes in the form of a simple Graphical User Interface, alongside offering much faster analyses than CFD. The available versions currently do not allow for users to simulate arrays however the creators have demonstrated proof of concepts and intend to allow for array simulation in commercial versions of the software.

Given the potential of QBlade in the future, it is also considered in this study when validating against single turbine experiments because the results will give some indication of future results for array simulation.

3.2.2 2D and 3D

The large increases in time requirements for 3D CFD have resulted in many VAWT researchers using 2D CFD for research purposes however there are questions regarding whether this can provide adequate accuracy for the scenarios studied, or whether the degree of loss of accuracy is acceptable in the context of the computational resource advantage of 2D CFD.

In order to consider the impact of this procedural choice, these two methods will be evaluated on comparable terms using turbine designs where the three-dimensional aspect of the VAWT flow problem is expected to be minimised. This design choice is valid and reasonable because it follows the results of the literature review for best practice on aerodynamic design and so such a comparison would be most applicable to expected utility scale VAWT designs. This includes high Reynolds number, high turbine Aspect Ratio, and maximising the distance between the struts and the plane used to analyse the wake.

This study will also investigate best procedure in both the 2D and 3D conditions in order to determine whether this differs between the two conditions, which will be detailed in the upcoming subsections. This also aids in determining where

inaccuracies emerge in the 2D condition compared to 3D and the experimental baseline.

3.2.3 Turbulence Models

A series of turbulence models have been chosen from the literature based upon their popularity and potential, these included: k-ε Realizable, k-ω SST with combinations of additional Low Reynolds Number and Intermittency Transition models, k-k_l-ω, and Transition SST. k-ε Realizable was only used for 3D simulations due to poor results in the literature for 2D but good results for 3D.

When comparing turbulence models, several different baseline experiments were considered in 2D in order to analyse where inaccuracies arise from each model which will aid with development of models suited to VAWT problems.

3.2.4 Baseline Experiments

Several experiments were chosen as baselines based upon the amount of data they provide, their ability to represent different conditions, replicability, and applicability.

The core baseline experiment was conducted by Tescione et al.[12] because this experiment used a high Reynolds number and low solidity turbine operating at a high TSR which was most likely to demonstrate Reynolds Independence. Tescione et al. provides a largely complete design of a custom turbine with measurements of the turbine used which allows good replication in CFD, with the exception of surface roughness which is rarely measured for VAWT experimental studies, with the exception of Howell et al.[60] which investigates this as a variable. Tescione et al. provides SPIV results for velocity in the turbine wake up to 2 diameters for the horizontal plane and 3 diameters for the vertical plane. It is also accompanied by another study using the same turbine and similar conditions by Castelein et al.[9] which focuses on the blade wake at different rotational positions. As a result it meets all 4 requirements. Tescione's study also demonstrates what appears to be a quirk for an experiment which should meet Reynolds independence in that it has significant wake asymmetry. This asymmetry has proven to be difficult for CFD to

predict in the literature so it is of particular value to find methods which are better able to predict this asymmetry.

Experiments by Lam and Peng[100] and Peng et al.[113] are used due to providing baselines for an array scenario using two turbines, and a single turbine to verify procedure respectively. The turbine used for these experiments was a high solidity turbine using a low Reynolds number and TSR so provides a contrast of conditions to the turbine using by Tescione et al. and Castelein et al. The experiments provide SPIV results for velocity and turbulence intensity up to 10D for the single turbine and 8D for the pair of turbines. The same turbine design is also used by Ahmadi-Baloutaki et al.[97] and Brownstein et al.[103], with Brownstein et al.'s being modified to use a smaller diameter and having end plates attached to the blades. This turbine is commercially sold as the Aleko WGV15 and Shanghai Aeolus Windpower Technology VAWT. This level of comparability allows for further validation with the conditions used by Ahmadi-Baloutaki et al. and Brownstein et al. Whilst this turbine isn't at a large enough scale to fully represent utility-scale turbines due to the Reynolds number being insufficient for Reynolds independence, it is comparable with many other turbines used in other wind tunnel testing of VAWTs. Its smaller scale is offset by the relatively high wind speeds used meaning it is approaching Reynolds independence so results are still applicable to utility-scale turbines.

Buchner et al.[8] was chosen to consider the accuracy of CFD predictions for the blade wake across different Tip Speed Ratios (1.0, 2.0, and 3.0) which a typical VAWT would experience. The Buchner et al. experiment notably focuses on PIV results for vorticity and turbulence intensity when the blade is in the rotational position closest to the windward direction, where it will receive the least amount of interference from previous blade wakes or the turbine wake. The turbine used is low solidity with varying Reynolds number and TSR. The turbine design used in the experiment uses struts located at the end of the blades and so maximises clearance between the midplane where measurements are taken and potential interference from the struts. This validation will help to determine the extent to which

inaccuracies in VAWT CFD may be due to certain characteristics of VAWT designs.

Each of these experimental baselines uses forms of PIV imaging, with the exceptions of Peng et al. and Lam and Peng. Their statistical certainty has been ensured through their own statistical checks. For images at a certain rotational angle, the images were taken using phase-locking between the shaft and PIV system, resulting in the photo being taken at the same position, within a margin of error, for example 0.04 degrees for Tescione et al.. The images are then averaged across a number of samples, corresponding to an equal number of rotations. The minimum number of samples used across the studies is 100, which is sufficient to smooth out anomalies. Peng et al. and Lam and Peng use cobra probes instead of PIV, with a sampling frequency of 3000Hz and sampling time of 30 seconds, equivalent to a minimum of 270 rotations which is again sufficient to smooth out anomalies.

3.2.5 Geometry

Details for recreating the geometry of the simulation domains are shown in Table 3.3, and the geometry of the turbines in Table 3.4 below:

Table 3.3: Domain Geometry

Experiment	Tescione\Castelein		Lam\Peng	Buchner
	2D	3D		
Domain Shape	Rectangle (Semi-circle inlet)	Cuboid	Rectangle	Circle
Inlet Length	5D	4.57D	10D	10D
Outlet Length	20D	9.13D	10D	20D
Width	10D	6.6D	20D	20D
Domain Height	N/A	4.1D (Symmetry)	N/A	N/A
Blockage Ratio	10%	1.85%	1.8\3.6%	5%
Rot. Dom. Shape	Circle	Cylinder	Circle	Ring
Rot. Dom. Diameter	1.25D	1.25D	1.5D	2D\0.75D
Rot. Dom. Height	N/A	1D	N/A	N/A

The turbine positions used for the two-turbine array for the Lam and Peng validation were $\pm$1D of the centre line, forming a line parallel to the inlet at 10D from the inlet as stated above.

Table 3.4: Turbine Geometry

Experiment	Tescione\Castelein	Lam\Peng	Buchner
Aerofoil	NACA0018	NACA6415	NACA0015
Blades	2	5	2
Chord	0.06D	0.15D	0.15D
Radius (m)	0.5	0.15	0.25
Pitch	0	-10	0
Height (m)	0.5	N/A	N/A
Shaft Radius	0.02D	0.02D	N/A
Shaft Height (m)	0.3	N/A	N/A

The domain dimensions were chosen based upon combination of results of the literature review, comparability with other studies, and matching the dimensions and blockage ratio of the baseline experiments. Circular rotating domains were chosen for the 2D Tescione/Castelein and Lam/Peng simulations because these involved replicating the shaft in the experiment which was assumed to be rotating in both cases, so the rotation and high resolution of the rotating domain was maintained within the centre of the circle in case this had a significant impact on the flow. In the case of the Buchner simulation this was unnecessary because the blade wake was analysed at the foremost position where the impact of the shaft on flow can be assumed to be negligible. The shaft radius for the Lam/Peng turbine was assumed to be 0.02D because this information was not publicly available in either study or from publicly available information about the turbine.

In the 3D Tescione/Castelein simulations, a cylindrical domain was chosen for the same reason as the circular domain in the respective 2D simulation. Spherical, ovoid, and capsular rotational domains were considered, with the spherical and ovoid domains chosen against due to resulting in varying distances between the blade and domain edge which would result in a larger high density region and therefore require greater computational resources than necessary. The capsular domain was chosen against due to meshing issues when this was attempted. The height of the domain was chosen as 1D due to the size of Z direction wakes in the Tescione et al. experiment.

In order to reduce computational resource requirements for the 3D simulations,

it was decided to divide the domain along the midplane and apply a symmetry condition to this wall based on the assumption that flow in the wind tunnel was largely symmetrical in this direction and asymmetries caused by, for example, the shaft protuding towards the floor, could be considered insignificant. This results in the domain height being 4.1D rather than 8.2D in the original experiment.

The 3D domain was initially run with blades only to reduce computational requirements during the verification process. Due to the resultant very high cell count this was continued for the comparison of turbulence models on the assumption that this was the dominant determinant of flow as found in 2D simulations. The struts and shaft were then reintroduced together to compare results for two turbulence models, k-ε Realizable and Transition SST.

3.2.6 Boundary Conditions

The boundary conditions for the simulations are detailed below in Table 3.5 as described by the original experiments. It was assumed that the change in inlet velocity from 9.3m/s to 9.1m/s and corresponding change in rotational speed due to the constant TSR between the Tescione and Castelein experiments was negligible and so simulations were only completed for the 9.3m/s used by Tescione et al. in order to minimise the number of simulations which needed to be completed. The varying velocities used for the Buchner experiment represent the different TSRs, with a single rotational speed being used, so 15m/s produces TSR=1.0, 7.5m/s gives TSR=2.0, and 5m/s gives TSR=3.0.

Table 3.5: Boundary Conditions

Experiment	Tescione\Castelein	Lam\Peng	Buchner
Inlet Velocity (m/s)	9.3	11.3/12.8	5/7.5/15
Pressure Outlet (Pa)	0	0	0
Turbulence Intensity (%)	0.5	1.11/2.5	1
Rotational Speed (rpm)	800	841(L) 809(R)/540	572.95
TSR	4.5	1.12-1.16/0.66	1/2/3

3.2.7 Pressure-Velocity Coupling, Spatial Discretisation, and Time Steps

The selected Pressure-Velocity Coupling Schemes and Spatial Discretisation settings are detailed in Tables 3.6-3.8.

Table 3.6: Pressure Velocity Coupling Scheme and Spatial Discretisation for 2D Tescione\Castelein\Buchner

Pressure Velocity Coupling Scheme	Coupled
Gradient	Least Squares Cell Based
Pressure	Second Order
Momentum	Second Order Upwind
Turbulent Kinetic Energy	Second Order Upwind
Specific Dissipation Rate	Second order Upwind
Transient Formulation	Bounded Second Order Implicit

The settings for 2D Tescione\Castelein\Buchner simulations were chosen based upon the literature review combined with a verification between the results of Coupled and SIMPLE which found insignificant differences between the results. The Transient Formulation was set to Bounded Second Order Implicit because this was a requirement of the LES turbulence model and so this was chosen to be used for all testing, however the LES model was ultimately not tested. Time steps were set to 0.5° as found in the literature review.

Table 3.7: Pressure Velocity Coupling Scheme and Spatial Discretisation for 3D Tescione\Castelein

Pressure Velocity Coupling Scheme	SIMPLE
Gradient	Least Squares Cell Based
Pressure	Standard
Momentum	First Order Upwind
Turbulent Kinetic Energy	First Order Upwind
Specific Dissipation Rate	First Order Upwind
Transient Formulation	First Order Implicit

For the 3D simulations the Pressure-Velocity Coupling scheme was changed to SIMPLE as a result of stability issues using the Coupled method. First order spatial discretisations were also chosen due to persistent stability issues. The time step was chosen as 1° based upon the literature review and a verification.

Table 3.8: Pressure Velocity Coupling Scheme and Spatial Discretisation for Lam\Peng

Pressure Velocity Coupling Scheme	Coupled
Gradient	Least Squares Cell Based
Pressure	Second Order
Momentum	Second Order Upwind
Turbulent Kinetic Energy	Second Order Upwind
Specific Dissipation Rate	Second order Upwind
Transient Formulation	First Order Implicit

The settings for Lam\Peng used the original determined settings from the literature review and Pressure-Velocity Coupling verification, with Transient Formulation set to First Order Implicit because Bounded Second Order Implicit was no longer necessary after the decision was made to not evaluate LES. The time step was set to 0.02° as the result of a verification process, this is expected to be lower than the other experiments as a result of the low TSR (0.66) used in the Peng validation. Whilst this could have been increased for the Lam validation which uses a higher TSR (1.12-1.16), this would have required a further verification procedure which was deemed unnecessary given the limited computational cost of the smaller time step in comparison to conducting further simulations to verify the optimal time step size.

3.2.8 Verification

Verifications were conducted for Length of Simulation, Averaging Period, Cell Count, Time Step, and Domain Size where appropriate. The results of these are outlined in the results section.

3.2.9 Meshing

A verification process was conducted for the cell count of the simulations, with the resultant meshing methods for Buchner also being used for 2D Tescione/Castelein due to using a similar turbine design, Peng's single turbine was used as a low computational resource equivalent for Lam due to using the same turbine, and 3D Tescione was verified alone.

The resultant meshing technique for 2D Buchner/Tescione/Castelein, using the Buchner experiment, involved using 50 inflation layers with a growth rate of 1.09

and a first layer height set to y^+=1. The domain was comprised of a higher cell density rotational domain in the form of a circle for Tescione/Castelein or ring for Buchner, and a stationary domain with lower cell density, with the dimensions of these outlined in section 3.3. The number of divisions on each blade edge was set to 400. The element size for the rotating domain was set to 0.001m with growth rate set to 1.01, and proximity functions enabled with a minimum local size of 0.000001m, with the proximity size function source set to edges. For the Tescione/Castelein mesh, an additional stationary high density region with a width equivalent to the diameter of the rotating region and length continuing from the rotating region to the outlet was added downstream of the turbine in order to ensure good capture of the downstream wake from the turbine which is the subject of interest of the study. Contact regions and mesh interfaces were implemented between the domains. This resulted in cell counts of 220,081 for the Buchner mesh and 1,351,811 cells for the 2D Tescione/Castelein mesh, with the discrepancy due to the high density cells in the middle of the rotational domain combined with the shaft in the middle which further engages proximity sizing functions in the meshing, and the large high density downstream wake region for the Tescione/Castelein.

For Lam/Peng, the verification process used the Peng experiment. The final mesh used 30 inflation layers on the blades with the first layer set to y^+=1, which is required for good performance with SST turbulence models, and a growth rate of 1.1. The size of elements on the blades was set to 0.0003m, except for the trailing edge which is treated by trimming and given an element size of 0.00005m. The rotating domain region has an element size of 0.0015m. The static domain has an element size set to 0.024m with a growth rate of 1.05 and Proximity and Curvature functions, each with a minimum size set to 0.0002m. A contact sizing of 0.001m is applied to the contact between the static and rotating region. This resulted in a Peng mesh of 526,000 cells, with the Lam mesh using corresponding settings being 810,000 cells due to containing two turbines.

For the 3D Tescione mesh, the verification process was completed using k-ε Realizable due to its allowance for lower computational requirements due to the

ability to use $y^+ \geq 30$ for the first inflation layer height. The mesh was then adapted to SST models by changing the inflation layers so that the first layer height was $y^+=1$, with the number of inflation layers also adjusted to ensure that the height of the inflation layers was similar. For the k-ε Realizable mesh, the face size of elements on the blades was set to 0.005m, with 18 inflation layers used with a first layer height to give $y^+=30$, and a growth rate of 1.1. Curvature was captured with a local minimum size of 0.0003m. These were also applied to the struts and shaft when added. The rotational domain was set to a body size of 0.02m with a growth rate of 1.2, curvature and proximity captured with a minimum size of 0.0005m, with both faces and edges used as proximity size function sources. The static domain was set to a body size of 0.04m, with edge biases set on the inlet and outlet edges to increase cell density through the midline of the domain. A Multizone method was applied to the static domain with the mapped mesh set to Hexa and Mesh Based Defeaturing turned off. For the SST turbulence model meshes, 32 inflation layers were used on the blades, struts, and shaft with a growth rate of 1.15. The resultant meshes had cell counts of: k-ε Realizable Blades Only 19.5M, SST Models Blades Only 29.1M, k-ε Realizable Full Turbine 23.7M.

All mesh quality metrics were acceptable for the meshes created.

3.2.10 QBlade

QBlade offers a potential alternative to CFD in that it can simulate VAWT wakes much more rapidly than 3D CFD by using the Lifting Line-Free Vortex Wake method, so it is included in this study for comparison of accuracy. The Tescione/Castelein turbine geometry described in section 3.2.5 and boundary conditions in 3.2.6 was recreated in QBlade with the polars being analysed between -25° and 25°, and then extrapolated using the Viterna method. The LLFVW settings were left at default except for the panel method being set to sinusoidal with 20 panels, the tower being included with appropriate width and height, and turbulent wake convection being turned on.

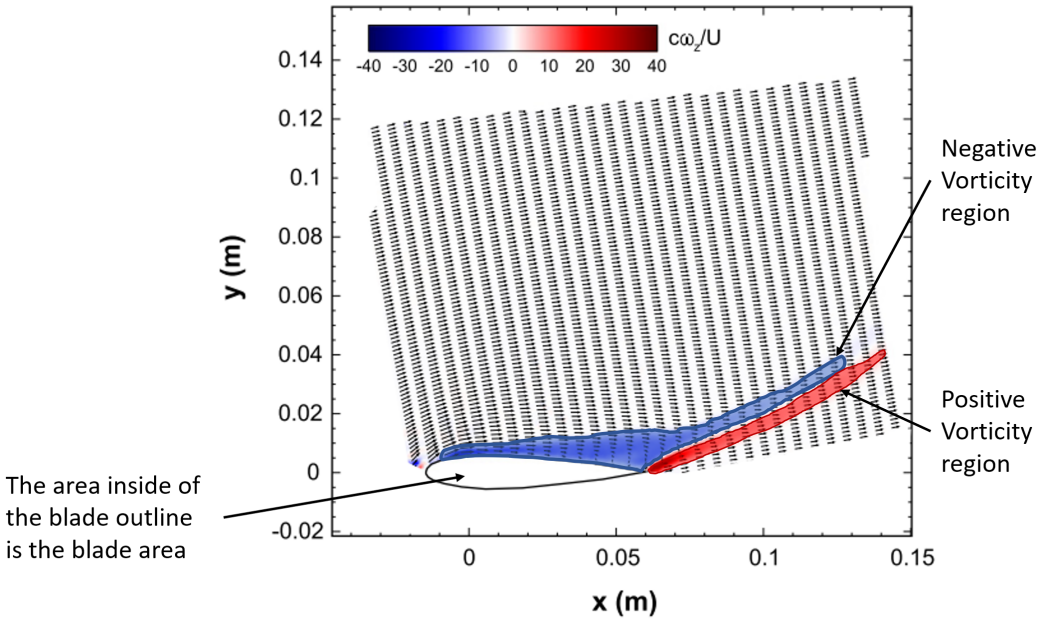

Figure 3.9: Example of the regions analysed when comparing contour areas

3.2.11 Evaluation Criteria

For the Buchner et al. experiment, the accuracy of the turbulence models was considered both quantitatively and qualitatively, assessing the turbulent kinetic energy and positive and negative vorticity in the near-blade wake. These were measured quantitatively by comparing the area of the matched contours between the simulation results and the experiments, with this area normalised to the area of the blade to ensure comparability (Blade area normalised wake area), as demonstrated in Figure 3.9. It was qualitatively assessed by comparing the shapes of the contours, considering the position and size of circulations and vortices.

Tescione et al. was evaluated against the streamwise and cross-stream velocity in the wakes along the horizontal midplane, with the 3D simulations also compared against the vertical midplane. These were measured by setting up a line from $\pm$0.75D horizontally or vertically at points downstream of the centre of the turbine staggered by 0.25D down the centre line of the domain up to 2D downstream from the turbine, as illustrated in Figure 3.10. The errors between the simulation results and the experiment were then calculated in terms of absolute deviation and as a ratio of the freestream velocity. The Castelein et al. experiment was evaluated using

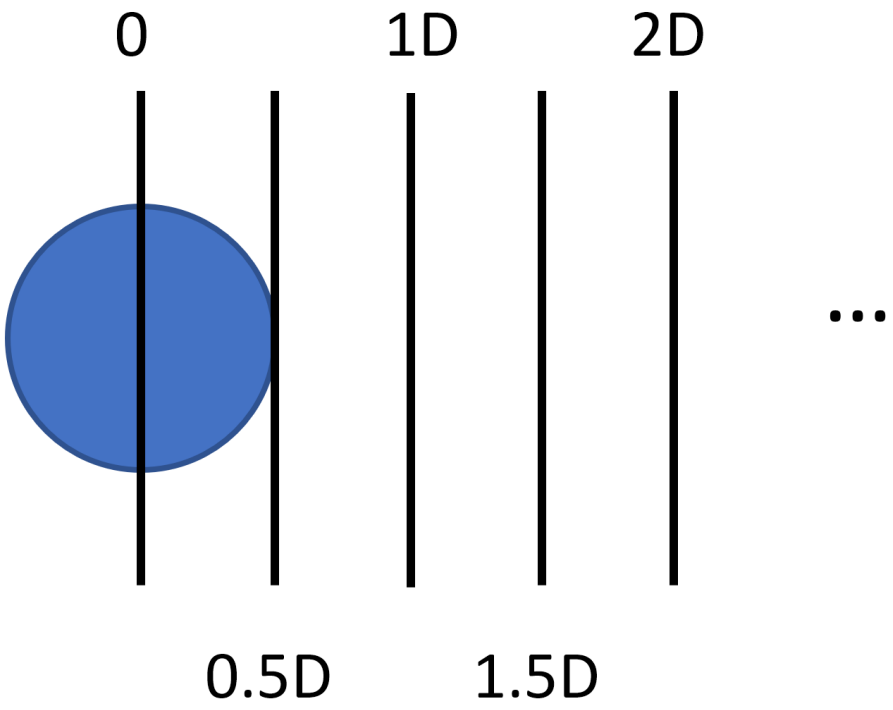

Figure 3.10: Diagram of downstream measurement locations compared to origin at centre of turbine

velocity along the horizontal midplane for the different rotational positions and was measured quantitatively by comparing the areas of the comparable contours as per the Buchner et al. validation, with contours being divided into high velocity regions (>6.5m/s) and low velocity regions (<6.5m/s).

Peng et al. and Lam and Peng were evaluated in the same way as Tescione et al.

3.2.12 Computer Specifications and Impact on FLUENT setup

Simulations were conducted across two computers, with 2D simulations being run on a computer with a 6 core/12 thread Intel i7 8700 CPU using 32GB of memory, and 3D simulations being run on a computer with a 32 core/64 thread AMD Threadripper 2990WX using 128GB of memory which was necessary for the larger cell count models.

In the highest cell count models, with 29.1M cells, the maximum amount of memory used was 126GB, so there is a need for very high memory capacity for

3D simulations for VAWTs and even more so for array simulation. It would be recommended to use at least 256GB of memory for future research.

GPU acceleration was not attempted because the method FLUENT uses to implement this would have required several high-end professional grade GPUs, which was not viable to acquire or setup, and was unlikely to provide good value in terms of time savings.

Residuals were set to 10^{-5} for the 2D setups and 10^{-3} for 3D setups.

3.2.13 Verifications

Verifying CFD procedure is necessary to ensure that the results of simulations are representative of the procedure's performance rather than due to errors caused by insufficient resolution due to low mesh cell counts, large time steps, short simulation lengths and more. The verification allows for simulations to be optimised by ensuring that the least amount of computational resources are used to reach the desired degree of accuracy. This subsection conducts verifications for each of these characteristics.

Cell count was verified for both the Buchner et al. and Peng et al. setups, where the meshing procedure for Buchner et al. was also used for Tescione et al. simulations with the addition of a high resolution wake region, and the procedure for Peng et al. was used for Lam and Peng simulations. In the case of Buchner et al., the cell count and simulation length were evaluated concurrently to consider whether this had an impact on the verification, as shown in figure 3.11, and was verified against the skin friction coefficient along the blade which was considered to be a quantitative metric to measure the blade wake. Three meshes were created: Low (47,679 cells), Medium (220,081 cells), and High (782,263 cells). The results found that the medium mesh with a simulation length of 10 rotations produced the same skin friction coefficient distribution as the high mesh with a simulation length of 5 rotations. Given the higher computational cost of the latter configuration, it was chosen to use the medium mesh with 10 rotations. For the 2D Tescione et al. simulations it was chosen to instead run the simulations until the average velocity across the measured regions had plateaued because this was possible in FLUENT,

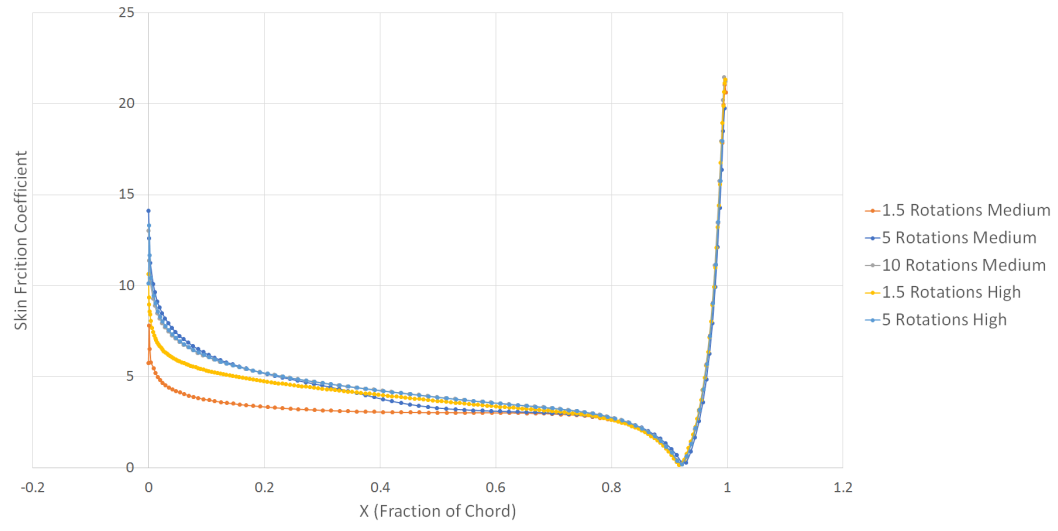

Figure 3.11: Buchner et al. Verification of Cell Count and Simulation Length

whereas the different measurements required for Buchner et al. would have required continuous export to CFD-Post to evaluate the results which would have taken more total time than running the simulations for longer.

For Peng et al. the simulation length was evaluated first using the medium mesh of 526k cells, using the reasoning developed under the Buchner testing that if the resultant mesh was a higher resolution then the simulation time would be an overestimate and so still produce acceptable accuracy. This verification also included consideration for the averaging period.

Per figure 3.12, a simulation length of 50 rotations followed by a 20 rotation averaging period was deemed the minimum required, with low error compared to the 70 rotations then 30 rotations averaging period condition. The 45 rotations then 15 rotations averaging demonstrated a shift towards the negative x direction so was deemed unsuitable. The 30 rotations then 10 rotations averaging condition also produced similar results to the converged results for much of the distribution however given that the 30,15 and 45,15 conditions were deemed unsuitable it was considered that this result was likely to be unconverged and so the higher 50,20 condition was chosen for further simulations instead given this better demonstrated convergence.

The meshes were then verified for cell count as demonstrated in figure 3.13,

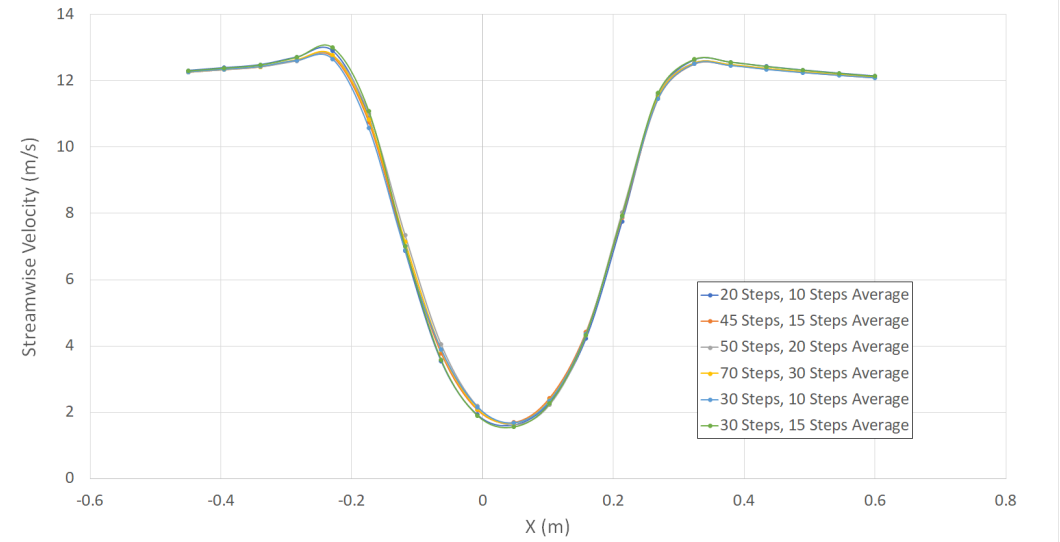

Figure 3.12: Peng et al. Verification of Simulation Length and Averaging Period

with low, medium, and high cell counts of 363k, 526k, and 1.7M cells respectively. A further mesh of 810k cells was run however an incorrect turbulence intensity was used resulting in anomalous results. As shown in the figure 3.13, there was limited change from 363k cells to 526k cells, but a larger change from 526k to 1.7M cells. A 223% increase in cells is required when moving from 526k to 1.7M, whilst only a 45% increase is required for 526k cells, so the 526k mesh was chosen to optimise resources. This choice is backed up by literature demonstrating that smaller time steps can be a substitute for higher cell counts[7]. The 1.7M model also resulted in a lower and further leftward trough, which opposed the experimental baseline results.

Time step was then verified in figure 3.14 with significant changes shown as the size decreased from 0.5°, until 0.02°. Whilst there were still some differences between 0.02 and 0.004°, these were minimal and occurred in regions which were less important to the study, with replicating the wake asymmetry being the main goal. The low time step required compared to previous studies is likely to be the combination of the low TSR which has been demonstrated to require smaller time steps, and the large jumps used between time steps in the verification.

One verification was completed using the Tescione et al. simulation setup which was for the Pressure-Velocity Coupler, comparing the results of SIMPLE

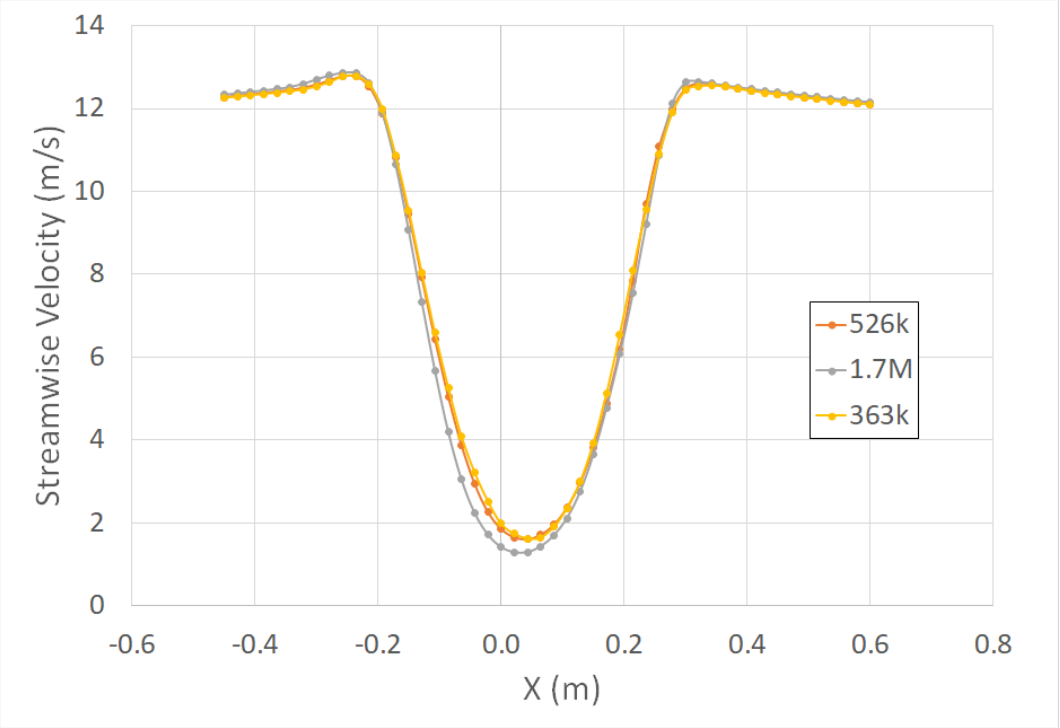

Figure 3.13: Peng et al. Verification of Cell Count

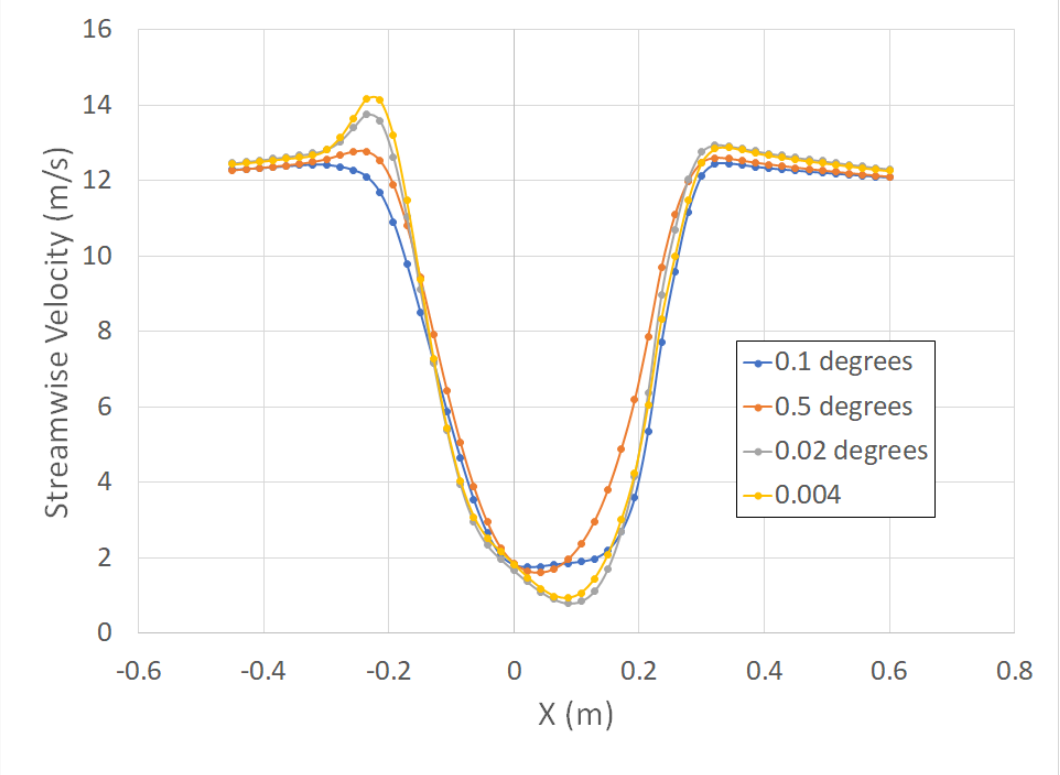

Figure 3.14: Peng et al. Verification of Time Step

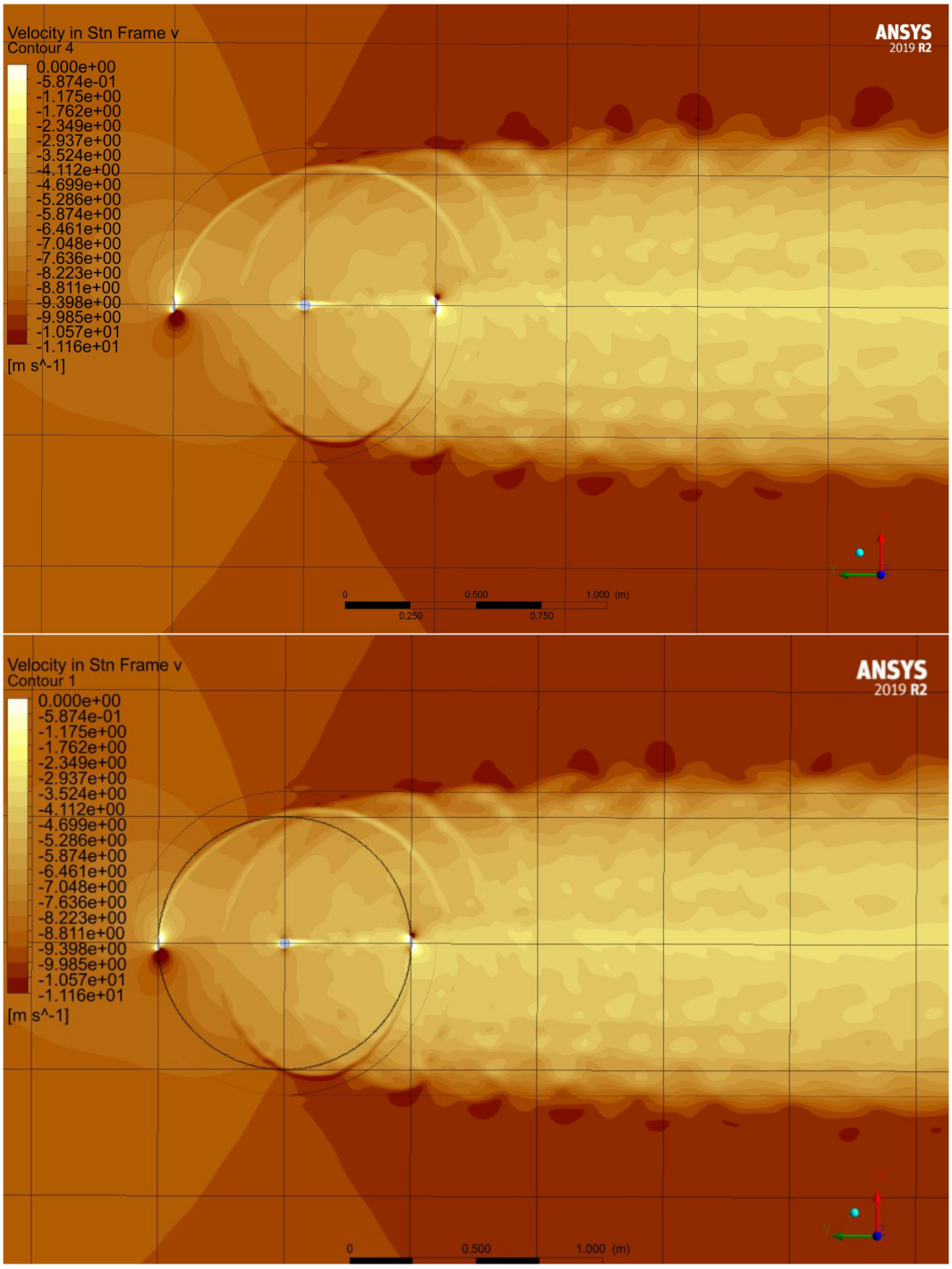

Figure 3.15: Verification of Pressure-Velocity Coupler using the Tescione et al. setup with upper: SIMPLE, lower: Coupled

and Coupled. As shown in figure 3.15, there is negligible difference between the two results.

For the 3D Tescione et al. verification, Cell Count was verified against both

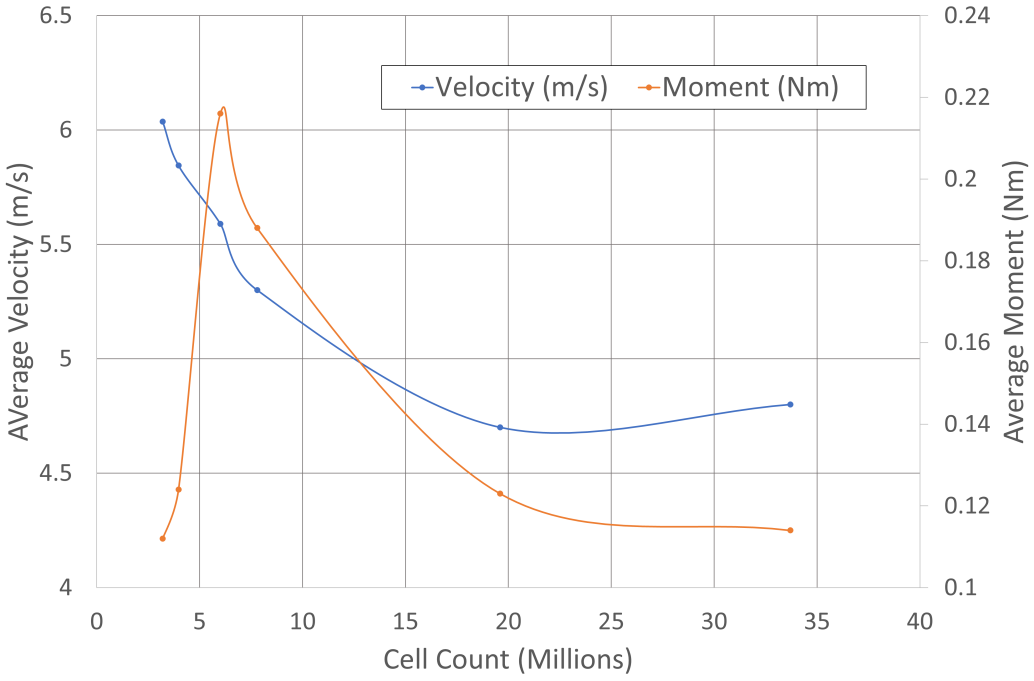

Figure 3.16: 3D Tescione Verification of Cell Count

average velocity 2 diameters downstream of the turbine and torque, with greater emphasis on convergence for velocity because this measures the wake which is the main focus of this validation. These verifications were conducted using k-ε Realizable, then the mesh was adapted using the resultant procedure for SST models by modifying the inflation layers appropriately.

As shown in figure 3.16, the velocity and torque have plateaued by the 19.7M cell count mesh with a 2.1% difference between the velocity estimated using the 19.7M cell mesh and the 33.7M cell mesh. When transformed into the SST mesh, this resulted in a cell count of 26.4M.

A further mesh was also attempted using polyhedra, derived from the 33.7M cell mesh and resulting in a 9.01M cell mesh, however this had a velocity of 6.54m/s and torque of 0.0475Nm so this methodology was deemed unfit for purpose.

The time step was also verified, considering time steps of 2° and 0.5° alongside the original 1°. In this scenario, using a 7.8M cell mesh, the 2° condition failed to complete whilst the 0.5° condition resulted in an average velocity of 5.23m/s and torque of 0.170Nm, compared to 5.30m/s and 0.188Nm for the 1° condition. Given

that the difference in velocity estimate was just 1.3% it was decided that decreases in time step below 1° were unnecessary given the implied computational cost, particularly given previous demonstrations in the literature review and Buchner et al. validation which found that increasing cell count can offset the need for other settings to be as stringent, so it is expected that this difference in results would reduce for the 19.7M cell mesh which was eventually used.

3.3 Impact of Field-representative values on VAWT simulation

This section considers the impact of turbulence intensity on VAWT wakes and the accuracy of CFD.

3.3.1 Baseline Experiments

Two experiments were used as baselines, Peng et al.[113] and Posa et al.[13]. Peng et al. was used to consider the impact of small turbulence intensity values typical of wind tunnels and so to validate the need for correct recreation of inlet flow turbulence intensity in CFD models to ensure accuracy, whilst Posa et al. was used to compare the wake using turbulence intensity typical of a wind tunnel to turbulence intensity in the IEC64100 range.

The Peng et al. experiment was chosen due to being used previously and so having previously been verified and validated, whilst Posa et al. was chosen due to its complex wake which demonstrated a change from asymmetric to symmetric with increasing TSR, potentially demonstrating a form of Reynolds independence for wake symmetry, and availability of LES simulation results to compare URANS results to. Both experiments show SPIV and PIV results for wake velocity respectively.

The geometry of the Posa et al. turbine is detailed in table 3.9 with the turbine replicated as per the study[13], with the shaft diameter estimated at 0.02m because this was not provided. Inlet velocity was estimated at 8.9m/s based upon the Re_D given of 180,000, and this subsequently allowed a rotational speed of 1252rpm for

Aerofoil	NACA0022
Chord	0.05m
Strut Position	0.025m
Turbine Diameter	0.3m
Shaft Diameter	0.02m

Table 3.9: Description of the Geometry of the Turbine used by Posa et al.[13]

the TSR=2.21 condition to be calculated.

3.3.2 Meshing and CFD Procedure

The methodology used for the previous Peng et al. and Lam and Peng[100] simulations for meshing and FLUENT as outlined in section 3.2 was also used for these simulations given that this procedure has already been verified. The turbulence model chosen for both was k-ω SST due to its popularity which allows comparability, and fair results in previous studies. The meshing procedure for Posa et al. was modified to match the turbine scale, for the rotational domain the following were used: the rotational domain face sizing set to 0.0015m, 20 inflation layers used on the blades with a growth rate of 1.1 and first layer height of y^+=1, blade and shaft edge size of 0.0003m with a bias factor of 1.5, trailing edge trim edge size of 0.00006m. For the static domain the following were used: face sizing of 0.024m with a growth rate of 1.05, capture curvature and proximity with a minimum size of 0.0002m for both. The walls shared between the rotational and static domains were given an edge sizing of 0.001m, and symmetry was applied to the side walls.

3.3.3 Conditions

For the Peng et al. simulations, results were compared between otherwise equal simulation run at turbulence intensities of 0% and 2.5% with the latter being the baseline from Peng et al.'s experiment. For the Posa et al. simulations the baseline % was estimated at 2.5% for Posa et al.'s experiment and this was compared to a turbulence intensity of 12.0% as used in the IEC64100 standard[36].

3.3.4 Evaluation Criteria

Both experiments were compared quantitatively using the position and depth of the velocity trough, with the width also measured where relevant. Qualitatively, they

were evaluated on the shape of the trough such as any oscillations and asymmetry.

Chapter 4

Results

4.1 Array Design

This section outlines the results of simulations run to determine the highest power output array designs, including results of an optimisation procedure for spacing between turbines and the effect of solidity on array performance.

4.1.1 Single Turbine

A single turbine scenario was run using flow-driven rotation and found a power output of 5247.9W at a TSR of 2.9, corresponding to C_p=0.252. This acts as one of two baseline values to compare results to, where the other was performance in the grid condition.

4.1.2 Six Turbine Arrays

The array power coefficients and performances relative to the baseline conditions are shown in table 4.1 below, with diagrams of the designs and their spacings previously described in Figures 3.2, 3.3, and Table 3.1.

An initial 3x2 grid configuration was run to provide a second directly comparable performance baseline to the other array designs, allowing for a comparison in the array context which isolated turbine power coefficient does not provide. This produced C_{AP}=0.131 when all turbines rotated in the same direction. A confirmatory simulation was run with turbines operating in alternating directions however this did not significantly change C_{AP} which was 0.133 under this condition.

The truss design had the highest C_{AP} at 0.425 which was significantly higher

Table 4.1: C_{AP} of different array designs

Configuration	C_{AP}	% Single	% Grid
Isolated	0.252	100	192
Grid	0.131	52	100
Truss	0.425	169	324
Biomimetic	0.356	141	272
Pairs (2-row)	0.383	152	292
Pairs (3-row)	0.323	128	257

than the Biomimetic, Pair, Grid, and Isolated conditions. The pair condition was run as 2-row, 4 turbine and 3-row, 6 turbine sets with the latter showing decreased performance as expected due to the wake of the leading row affecting the incoming flow for the third row.

Two additional farms which used hybrid designs were implemented. The first was based upon the offset grid design albeit with the horizontal distance b=3.4m as used in the Biomimetic design. This produced a reduced C_{AP} of 0.314. The second hybrid design used the Biomimetic design as the foundation, but used the distance between rows that had been used for the Grid and Truss, a=10m. This resulted in C_{AP}=0.380 which is significantly higher than the original Biomimetic school design as recommended by Whittlesey[105], however still considerably lower than the Truss design.

From these results it is clear that the Truss design would become the dominant basis of any design produced by a guided optimisation procedure as it offers a considerable advantage over the guidelines for other established designs.

4.1.3 Flow Visualisation

By inspecting the dynamic pressure and velocity contour maps of the arrays it is possible to visualise how these results have come to occur, a 15 turbine array with 5 rows and 3 columns was run in order to demonstrate the flow patterns. As shown in figure 4.1, to the sides of the turbine wakes are regions of increased wind speed. This allows for the following turbines which are placed inside these regions of high dynamic pressure to have a much greater power output whilst not breaking Betz's limit.

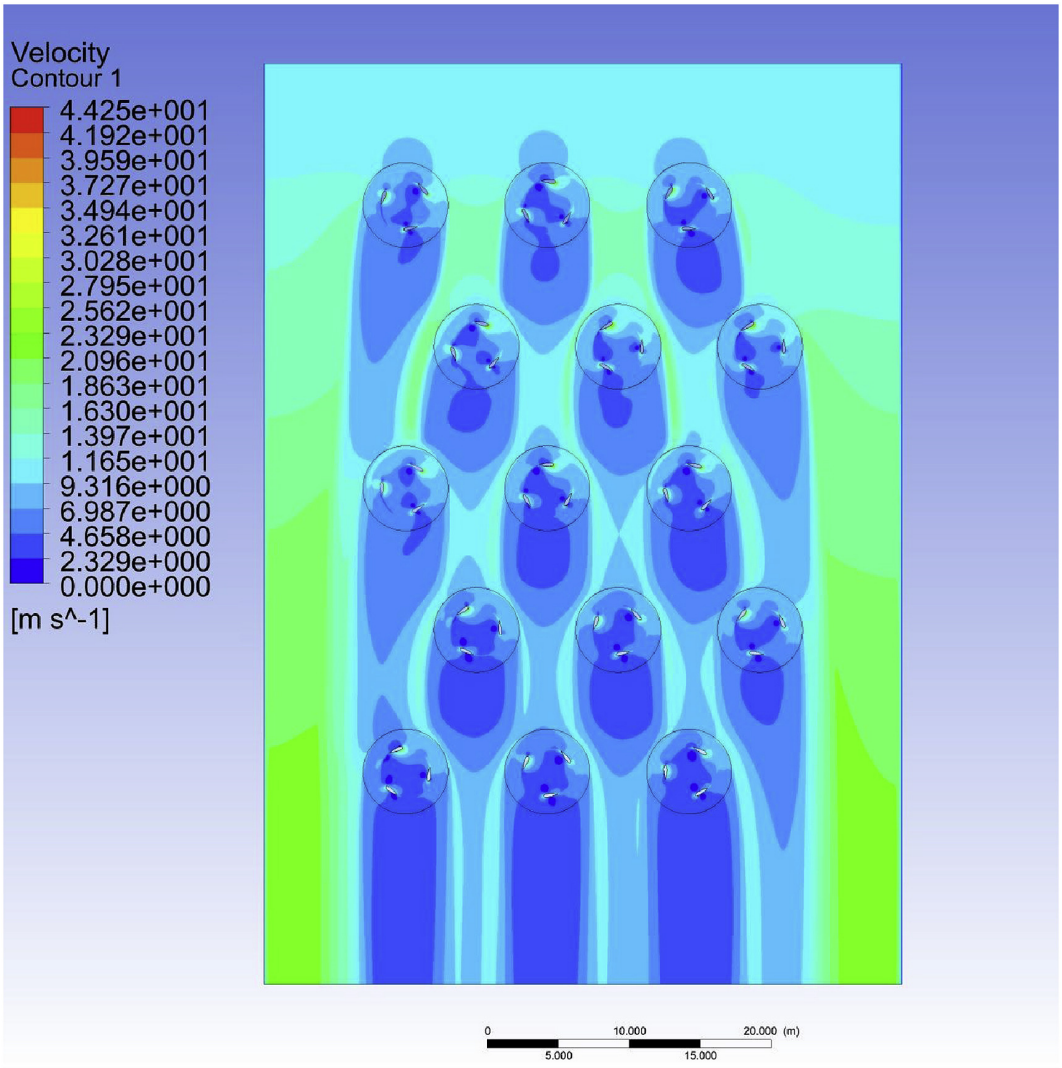

Figure 4.1: Velocity Contour Map for a 3x5 Array

In the simulation run to produce figure 4.1 it was found that the absolute wind speed in these regions between the first and second rows of turbines was 14.5m/s on average across a 1D long line compared to the 10m/s inlet condition. Due to the cubic relationship between velocity and power this results in a 205% increase in power in the airflow in the path of the turbine, hence why for the optimised farm design it was possible to find turbines in the second row with as much as a 181% increase in power output over the baseline isolated turbine. It can also be seen in figure 4.1 that these elevated velocity regions exist in following rows, allowing for further following turbines to receive a power boost also. Whilst the third row and beyond has reduced wind speed compared to the second row, the wind speed

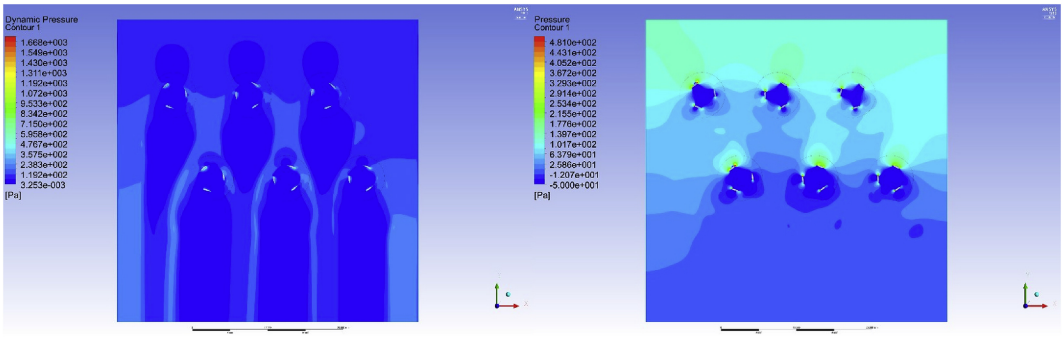

Figure 4.2: Dynamic Pressure (L) and Static Pressure (R) Contour Maps for a 3x2 Array

approaching the turbines remains elevated due to flow constriction, for example the velocity of the flow approaching the left and centre turbines in the fourth row is in the same contour band as the freestream velocity, when it would be expected to be much lower without the flow constriction due to the blockages of the preceding layers of turbines.

The increased flow around the outside of the array causes some flow constriction due to the nearby walls, however this is minimal as shown by inspection of the rightmost first row turbine, which experiences the least flow constriction, compared to the leftmost last row turbine which experiences the most flow constriction. The net effect also reduces for analysing fewer rows of arrays, again indicating that minimising the number of rows is the correct choice from both resource and scientific analysis aspects.

The high velocity flow occurs due to the Venturi effect which results from the conversion of static pressure into dynamic pressure when flow is constricted, in this case between the turbines. Figure 4.2 shows the increase in dynamic pressure between the wakes of each turbine, and the corresponding decrease in static pressure occur in the same regions as expected with the Venturi effect.

In practice due to the three-dimensionality of flow compared to the 2D simulation, increased dynamic pressure would cause some dispersion of the flow into the vertical direction resulting in a slightly lower flow velocity, however this would be partly compensated by the lower blockage ratio of a 3D domain which would provide freestream flow to the turbine.

The mechanisms discovered by Zanforlin et al.[98] were also confirmed as

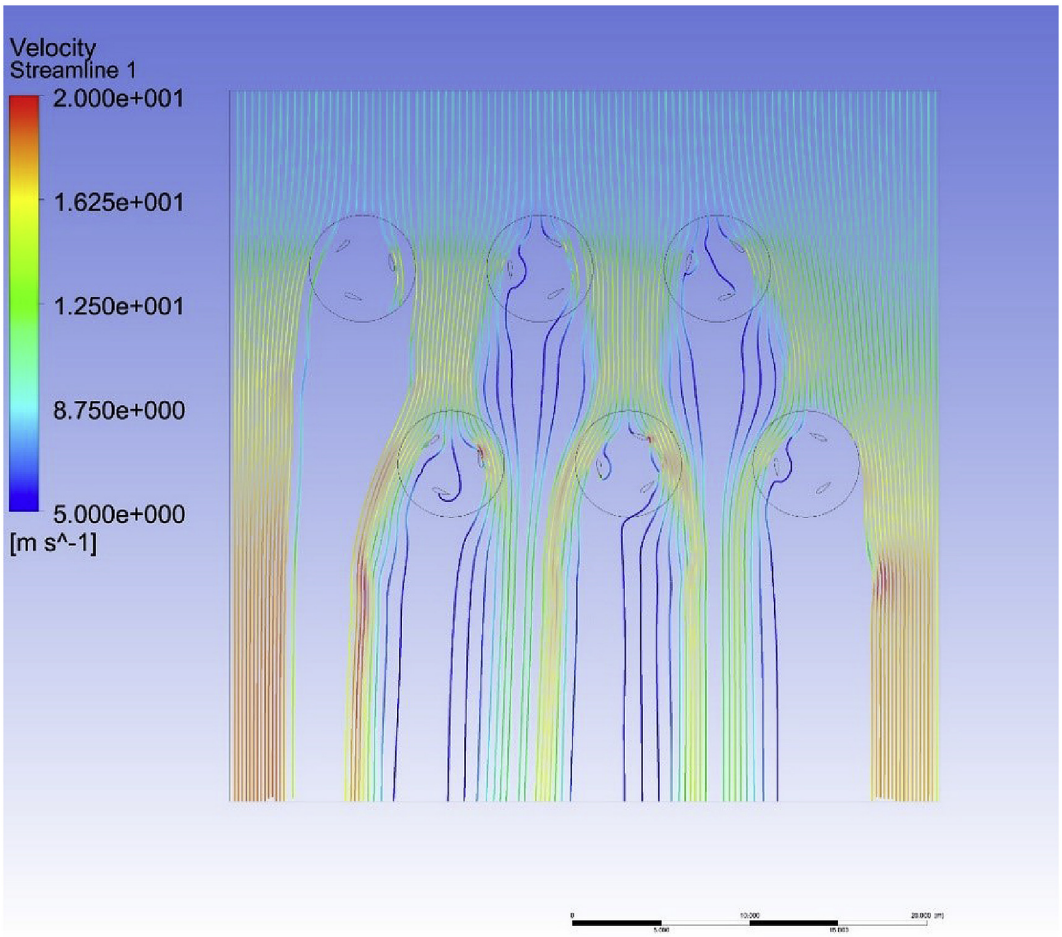

Figure 4.3: Velocity Streamlines for a 3x2 Array

seen in figure 4.3 which demonstrates the velocity streamlines, with clear wake contraction and cross-stream velocity suppression relative to the blade. The wake contraction can also be seen in figure 4.1.

To test this a V shaped farm comprised of 5 turbines was created and simulated as shown in figure 4.4. From the results it was found that the middle layer of turbines, which were only subject to this action from a leading turbine on one side, produced significantly less power than the final turbine and hence two leading turbines are required, one on either side of the turbine of interest, in order to get the greatest performance increase from the effect.

4.1.4 Gradient-based Optimisation

The Truss design was chosen as a basis to run a Gradient-based optimisation due to it providing the highest C_{AP} of the tested designs. There are two variables which

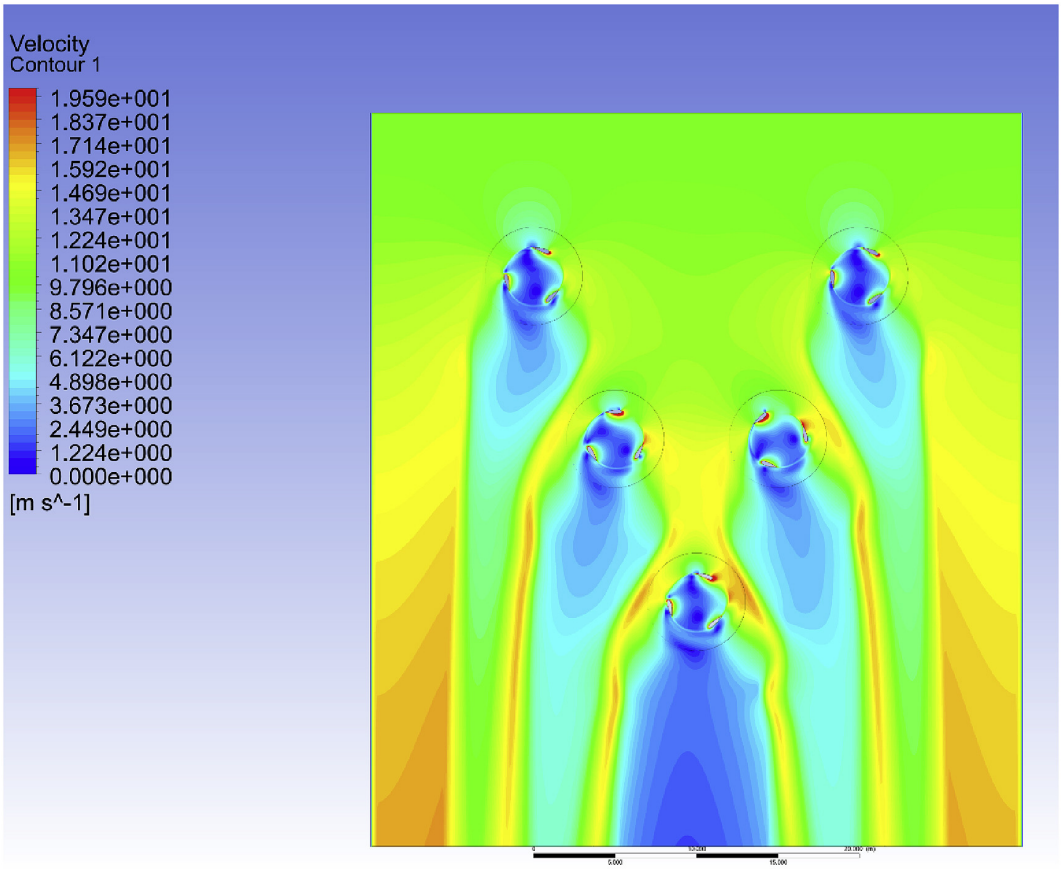

Figure 4.4: V-shaped array velocity contour

were optimised by iterating simulations using different distances to find the peak value, firstly Streamwise spacing followed by Cross-stream spacing using the previous results, previously referred to as a and b. The results of this are shown in figures 4.5 and 4.6, where the optimum Streamwise spacing occurs at 3.24D (11m) and the optimum Cross-stream spacing occurs at 1.47D (5m) with an array power coefficient C_{AP}=0.453. This represents an 80% increase over the baseline isolated turbine, and a 246% increase over the baseline grid layout.

The use of gradient-based optimisation may limit the achieved benefit compared to more global and comprehensive optimisation techniques, however it resulted in significantly reduced resource requirements because fewer data samples and therefore simulations were required. Using more comprehensive optimisation techniques could help understand the potential for multiple peaks which would mean that gradient-based optimisation via searching for the nearest peak would

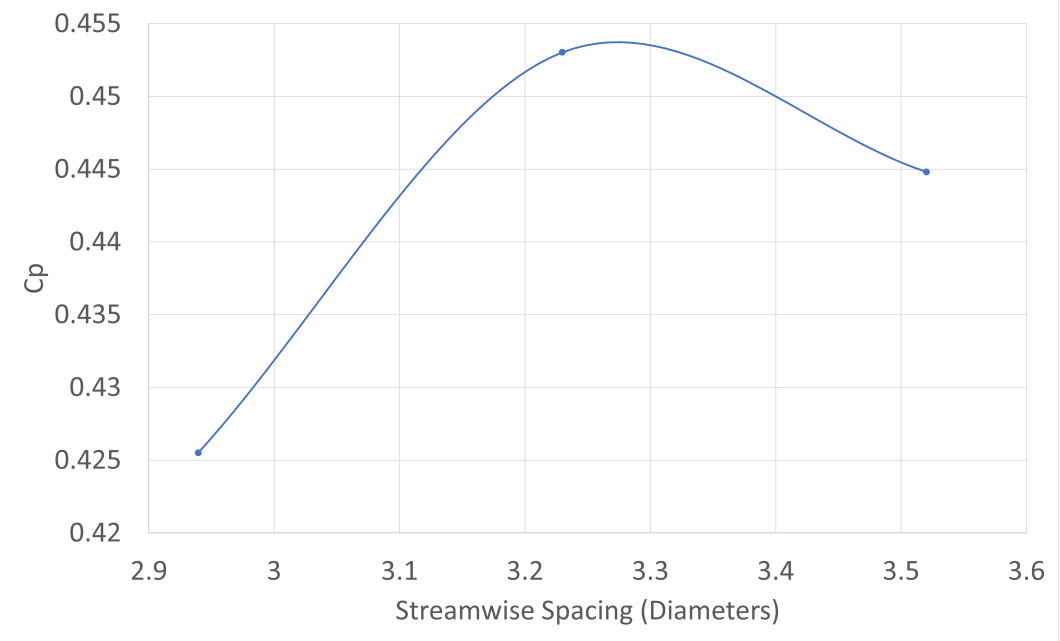

Figure 4.5: Streamwise Spacing Optimisation

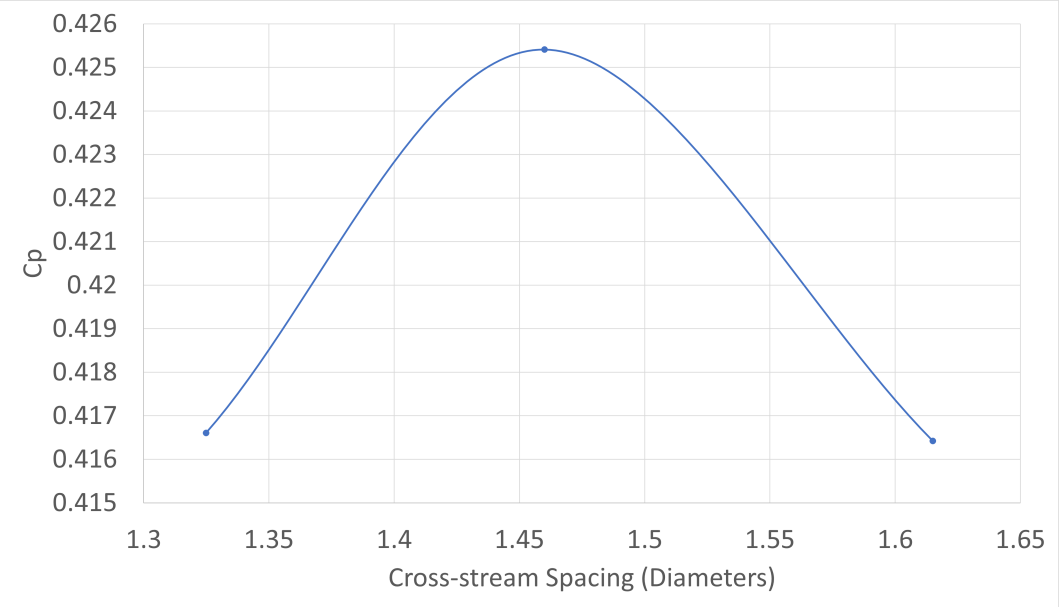

Figure 4.6: Cross-stream Spacing Optimisation

produce a suboptimal result. It would also help determine whether simultaneously optimising both variables would be beneficial for further increasing C_{AP}.

4.1.5 Low Solidity Turbines

A simulation was run where the turbines in the optimised condition were replaced with the σ=0.12 turbine. From the results, an array power coefficient of 0.355 was

found for a 17.2% increase over the isolated Low Solidity Turbine. However this is also a 21.6% reduction compared to the High Solidity case.

4.1.6 Discussion

From the results it is clear to see that cases of the Truss formation offer the best performance under the tested conditions. The optimised design resulted in an 80% increase in C_{AP} over the isolated turbine condition and 246% over a high density grid condition. Whilst the guideline Biomimetic and Pair Cluster designs, alongside Hybrid designs, also show significant improvements over the isolated and grid conditions, they still underperform compared to both the optimised and unoptimised Truss designs.

By comparing to the Genetic Algorithm optimised configurations by Bons[172] we can see that there are some similarities in that they also take advantage of staggering, albeit in a less organised way. As stated earlier, the 3 Turbine clusters of Hezaveh et al.[106] are also a special case of staggering.

Comparing to HAWTs, Bartl and Saetran[173] found that for a set of three identical in-line HAWTs using a spacing of 3D which is equivalent to that used in this study, with $C_{p\text{-}max}$=0.462, the leading turbine had a ratio of $C_p/C_{p\text{-}max}$ of 1 whilst the second and third turbines had ratios of 0.262 and 0.190, providing C_p values of 0.121 and 0.088 respectively. This clearly shows a large drop-off in power output when using such small spacing between HAWTs, however this is a worst case scenario and in practice farms will be designed to minimise the time spent in this situation. In contrast, the equivalent VAWT layout tested in this thesis with the grid and 3D spacing showed a $C_p/C_{p\text{-}max}$ ratio of 0.52 for the second row, so there is already an advantage for VAWTs using small spacings, even in the worst case scenario.

For more realistic scenarios it is necessary to consider Beland et al.[174] which investigates larger spacings between turbines, finding spacings of 12D still carry a highly reduced $C_p/C_{p\text{-}max}$ ratio of 0.6 for HAWTs. Given Beland et al.'s results, it is highly likely in a large wind farm that there will be a turbine directly downwind within 12D for any wind direction, meaning that even in a best case scenario there

are likely to be considerable performance losses in following turbines. As a result of this it is highly recommended against HAWT farms having such small spacing when in a grid configuration.

Mosetti et al.[94] has shown that for a single wind direction it was possible to achieve an overall farm efficiency of 95% of $C_{p\text{-}max}$ using Genetic Algorithm optimisation, corresponding to an array coefficient of 0.418 assuming $C_{p\text{-}max}$=0.44, as per the LW 8MW reference turbine based upon the Vestas V164-8MW, is typical for HAWTs[175]. For comparison, adjusted for mechanical and generator losses as determined by Ragheb and Adam[176], the optimised VAWT farm would have an array coefficient of 0.417. However Mosetti's configuration required a density of 1 turbine per $104D^2$. In comparison the optimised VAWT solution had a density of 1 turbine per $18.1D^2$. These can then be converted into power coefficient density = C_p*Turbine density, resulting in $0.00402D^{-2}$ for Mosetti's HAWT farm and $0.0230D^{-2}$ for the VAWT farm. Whilst this doesn't meet the magnitude increase in power density suggested by Dabiri[18], it has implications for development of wind farms on space limited sites.

In practice there will be a trade-off between turbine density and Levelised Cost of Energy with the latter being the main consideration. It is also necessary to consider that the land below turbines can still have value in other uses such as farming which may make high density arrays less desirable in some scenarios if they affect the ability to conduct such activities.

4.2 CFD Validation

This section will outline the results of simulations run to determine the best practice for CFD simulation of VAWTs, covering choice of turbulence model and use of 2D or 3D simulation.

4.2.1 Turbulence Model Validation - Near Blade

Firstly, the Buchner et al. experiment was analysed, representing the near blade wake, considering Turbulent Kinetic Energy (TKE) and Vorticity as Positive Vorticity (+Vort.) and Negative Vorticity (-Vort.). The quantitative results for the nor-

malised wake areas for these are shown in table 4.2, with results given to 3 significant figures, followed by the average absolute deviations from the experiment in table 4.3.

Table 4.2: Comparing the normalised area of the wake of different turbulence models against the Buchner et al. experiment

Condition	TKE	% Dev.	+ Vort.	% Dev	-Vort.	% Dev
Tip Speed Ratio = 1						
k-ω SST	8.10	-48.0	3.96	-17.0	5.60	-57.2
k-ω SST LRN	8.28	-46.8	3.85	-19.3	5.72	-56.3
Transition SST	7.20	-53.8	3.29	-31.0	6.28	-52.0
k-k_l-ω	15.6	0.415	2.67	-44.0	7.00	-46.5
Experiment	15.6	N/A	4.77	N/A	13.1	N/A
Tip Speed Ratio = 2						
k-ω SST	1.47	-43.2	1.90	153	1.21	-44.1
k-ω SST LRN	2.04	-21.2	1.85	147	1.36	-37.7
Transition SST	1.87	-27.8	1.05	40.3	1.26	-42.2
k-k_l-ω	3.22	24.2	1.81	142	1.33	-38.9
Experiment	2.59	N/A	0.749	N/A	2.17	N/A
Tip Speed Ratio = 3						
k-ω SST	1.04	-58.0	1.05	30.7	0.829	-50.6
k-ω SST LRN	0.608	-75.3	1.09	34.8	0.858	-48.9
Transition SST	1.19	-51.8	0.977	21.0	0.848	-49.4
k-k_l-ω	3.71	50.4	0.727	-9.91	0.826	-50.8
Experiment	2.46	N/A	0.807	N/A	1.68	N/A

Table 4.3: Average of the absolute deviation from experimental results for each turbulence model

Turbulence Model	Average Absolute Deviation %
k-ω SST	55.8
k-ω SST LRN	54.2
Transition SST	41.0
k-k_l-ω	45.2

Large deviations can be seen between nearly all simulations and the experiment, with significant variation between the different measures of wake size also. The largest deviations occur for positive vorticity at TSR=2.0 with overestimations greater than 140% for most models, with the exception of Transition SST which demonstrates its improved performance in the laminar-to-turbulent transition re-

gion. The normalised wake area for the turbulence models for negative vorticity is relatively consistent, with the percentage difference between the models decreasing as TSR increases. Compared to the other turbulence models and the experiment, k-kl-ω tends to overestimate the Turbulent Kinetic Energy wake area whilst producing lower estimates of Positive Vorticity.

In terms of the average absolute deviation shown in Table 4.3, Transition SST offers the lowest absolute deviation, followed by k-k_l-ω. Both of these models have lower average deviation due to improved performance in a number of circumstances compared to other models rather than consistently improved accuracy.

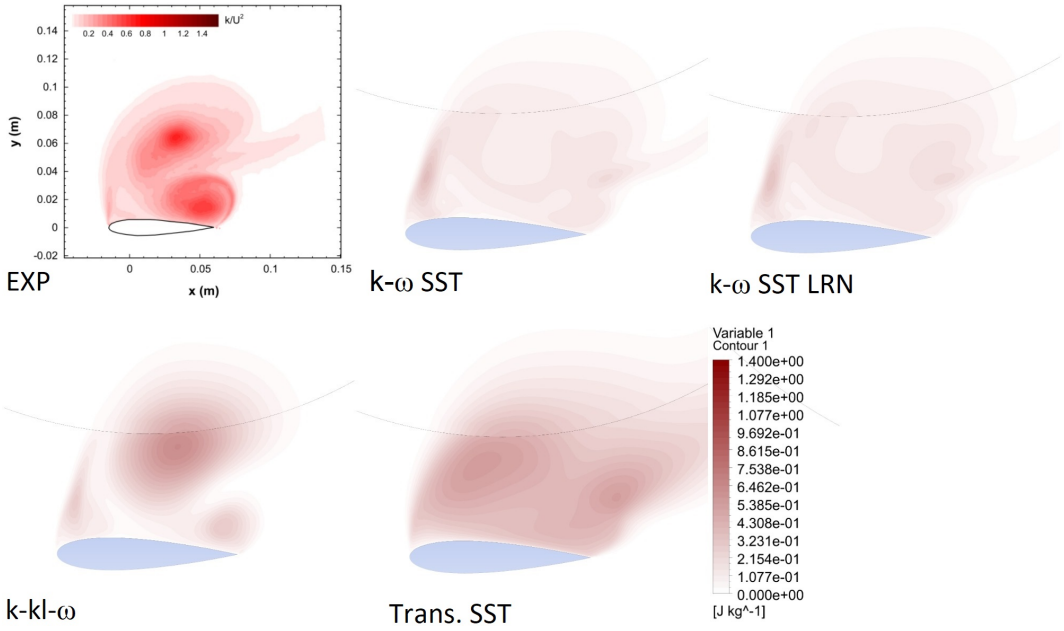

Figure 4.7: Upper left: Buchner's experimental result for Turbulent Kinetic Energy at TSR=1.0 [8], Upper centre: k-ω SST, Upper right: k-ω SST LRN, Lower left: Transition SST, Lower middle: k-k_l-ω

The results can then be considered qualitatively to understand some of the causes of these deviations. The upper left image in figure 4.7 shows Buchner's PIV results for Turbulent Kinetic Energy at TSR=1.0, showing a wake with a height of 0.11m, a circulation at the leading edge which was approximately at a right angle to the chord, one vortex at the trailing edge and one vortex above the three-quarter chord position, and a tail which extends from between the two vortices.

The other images in figure 4.7 show the CFD results for the 4 turbulence mod-

els at TSR=1.0. Transition SST produces the closest representation of the wake with vortices at the trailing edge and above the three-quarter chord position. A faint tail was also found alongside the leading edge circulation. However, it failed to predict the angle between the leading edge circulation and chord, and underestimated the size of the wake and TKE. The other models failed to predict the position of the vortices but predict a stronger tail. The k-k_l-ω model also produced a better prediction of the leading edge circulation.

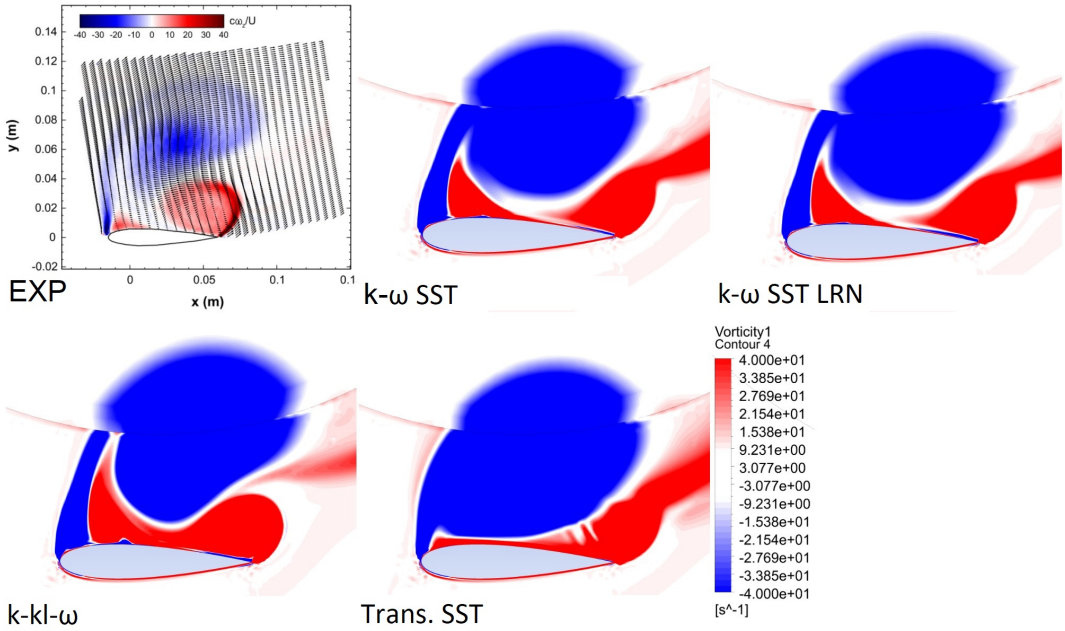

Figure 4.8: Upper left: Buchner's experimental result for Vorticity at TSR=1.0 [8], Upper centre: k-ω SST, Upper right: k-ω SST LRN, Lower left: Transition SST, Lower middle: k-k_l-ω

For vorticity at TSR=1.0 in figure 4.8, two vortices are seen with a leading edge circulation and trailing edge circulation. The upper vortex had negative vorticity while the trailing edge vortex had positive vorticity. A small triangle of positive vorticity was also seen behind the leading edge circulation.

As shown in the other images in Figure 4.8, vorticity was overestimated significantly. The k-ω SST models produced the most similar shape of the wake overall. K-k_l-ω produced a more accurate prediction at the leading edge with a thinner leading edge circulation and a smaller triangle of positive vorticity, but underestimated the size and impact of the trailing edge vortex as shown in the quantitative results.

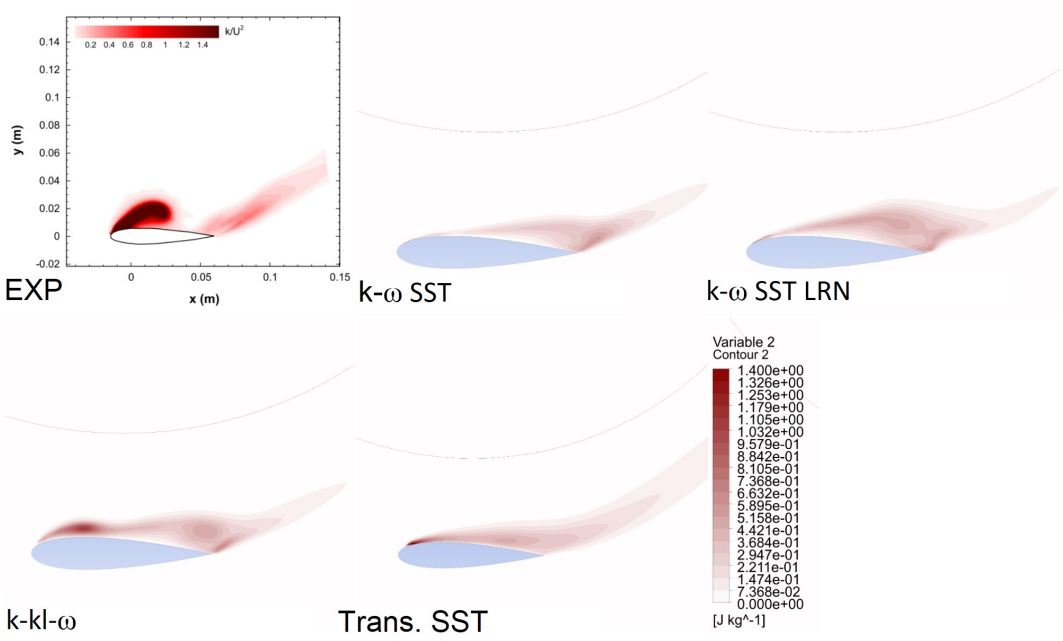

Figure 4.9: Upper left: Buchner's experimental result for Turbulent Kinetic Energy at TSR=2.0 [8], Upper centre: k-ω SST, Upper right: k-ω SST LRN, Lower left: Transition SST, Lower middle: k-k_l-ω

Figure 4.9 shows the TKE experimental result at TSR=2.0, with a separation of very high TKE stemming from the leading edge, followed by reattachment, then a tail originating at the trailing edge.

Transition SST was the best predictor of the leading edge separation amongst the models shown in figure 4.9 but significantly underestimated the size of the separation and did not predict the reattachment. The size of the tail was also underestimated significantly.

The experimental vorticity result in the top left of figure 4.10 shows the same pattern as the Turbulent Kinetic Energy result, with a negative vorticity leading edge separation followed by reattachment. At the trailing edge the tail was split into an upper negative vorticity region and a lower positive vorticity region.

Vorticity was again significantly overestimated in the CFD shown in the other images in Figure 4.10 compared to the experimental results and the overall prediction was poor. All models predicted the negative vorticity upper tail and positive vorticity lower tail, although k-ω SST LRN and k-k_l-ω predicted shorter but wider tails.

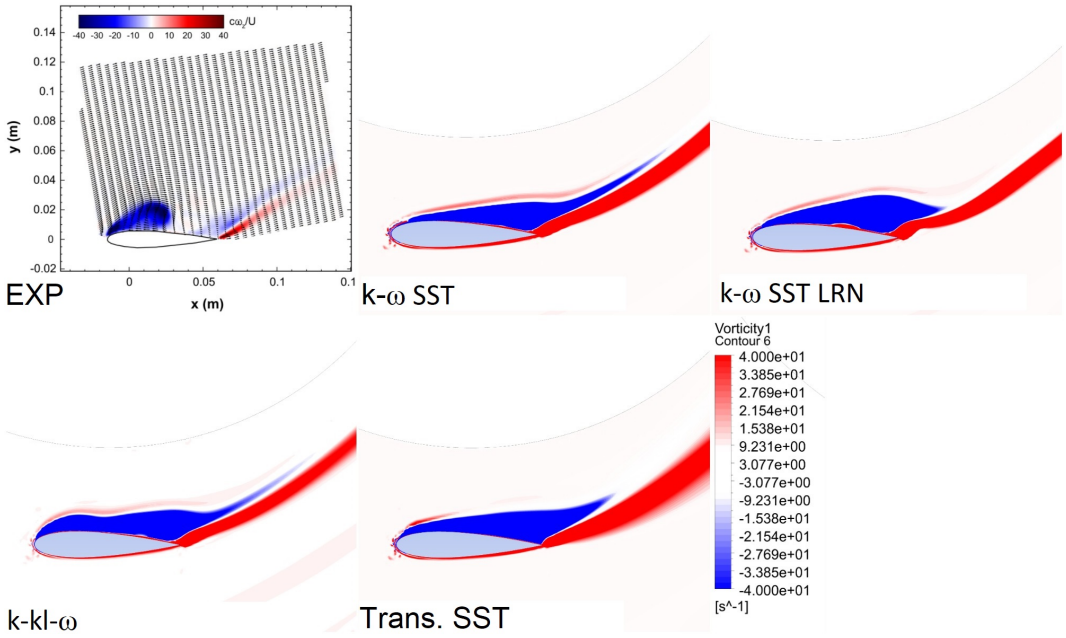

Figure 4.10: Upper left: Buchner's experimental result for Vorticity at TSR=2.0 [8], Upper centre: k-ω SST, Upper right: k-ω SST LRN, Lower left: Transition SST, Lower middle: k-k_l-ω

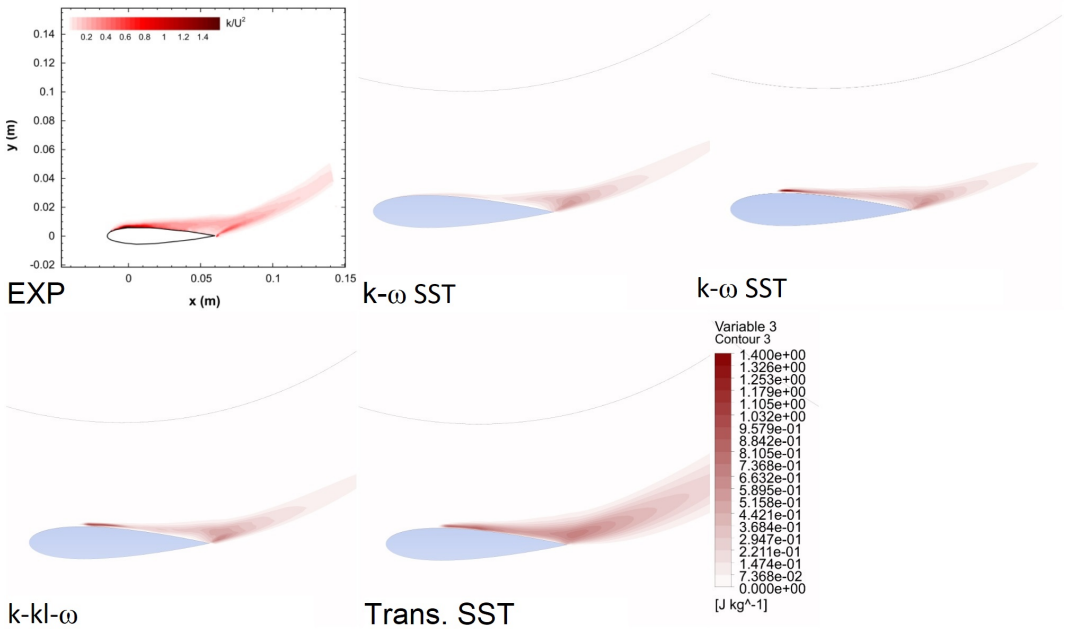

Figure 4.11: Upper left: Buchner's experimental result for Turbulent Kinetic Energy at TSR=3.0 [8], Upper centre: k-ω SST, Upper right: k-ω SST LRN, Lower left: Transition SST, Lower middle: k-k_l-ω

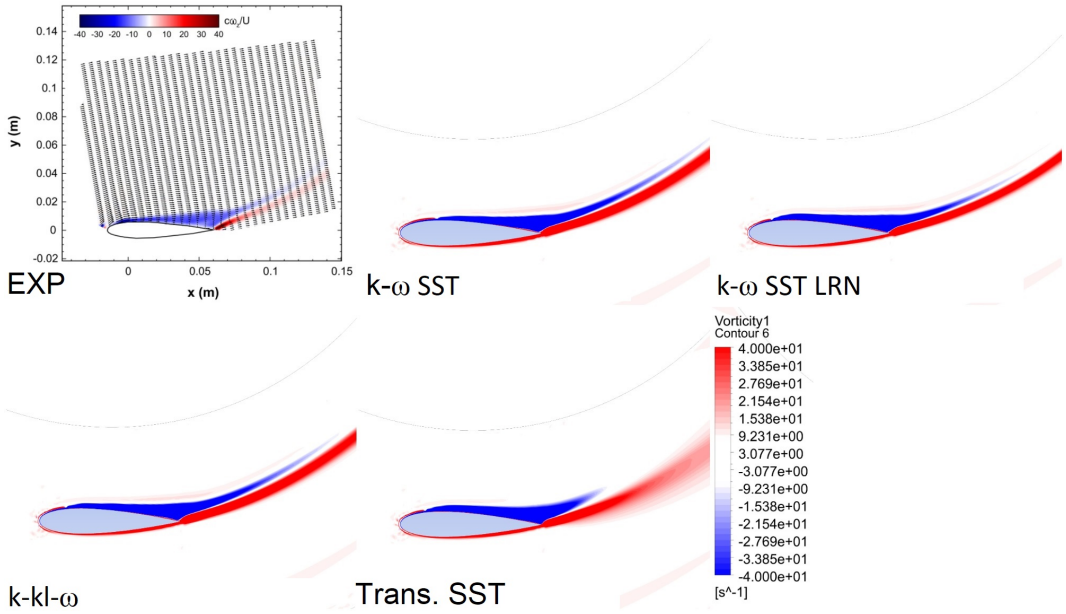

Figure 4.12: Upper left: Buchner's experimental result for Vorticity at TSR=3.0 [8], Upper centre: k-ω SST, Upper right: k-ω SST LRN, Lower left: Transition SST, Lower middle: k-k_l-ω

The experimental result for Turbulent Kinetic Energy at TSR=3.0 shown in the top left of figure 4.11 had a nearly flat wake from a separation close to the leading edge, with another trailing edge separation that produced a tail. In the vorticity map in figure 4.12 there was a positive vorticity lower tail and negative vorticity upper tail from the trailing edge.

All of the models in figures 4.11 and 4.12 failed to predict the position of the initial separation, with all but k-ω SST estimating occurrence of separation at one-third chord. From the vorticity maps it is seen that this was due to a positive vorticity region covering the leading edge, which pushed separation backwards. These differences may be due to surface roughness on the experimental blades which can affect separation[177].

Overall, Transition SST offered the most robust performance for this scenario out of the tested turbulence models, however accuracy was still poor for the blade-wake so other modelling techniques may be required for accurate near blade wake analysis.

4.2.2 Turbulence Model Validation - Far Blade

Castelein examined the near and far blade wake at different azimuthal positions at two TSRs, however here only one TSR (4.5) will be investigated.

Table 4.4: Comparing the normalised area of the blade wake regions of different turbulence models against the Castelein et al. experiment

Condition	Region	Blade area normalised wake area						
Position		0°	45°	135°	180°	225°	270°	315°
Experiment	High	28.8	7.49	N/A	1.53	0.88	0.82	3.40
	Low	15.0	4.02	N/A	1.15	0.69	1.87	12.6
	Ratio	1.93	1.87	N/A	1.33	1.27	0.44	0.27
k-ω SST	High	25.4	7.37	9.98	3.02	0.56	0.61	1.94
	Low	10.1	3.59	4.83	5.35	2.93	4.90	10.8
	Ratio	2.52	2.05	2.07	0.56	0.19	0.13	0.18
	% Dev.	30.9	10.1	N/A	-57.7	-85.1	-71.5	-33.34
k-ω SST LRN	High	26.8	6.56	11.3	5.24	0.72	0.69	2.05
	Low	9.44	3.24	4.58	5.38	3.14	5.34	10.65
	Ratio	2.84	2.02	2.48	0.97	0.23	0.13	0.19
	% Dev.	47.4	8.40	N/A	-27.1	-82.0	-70.8	-28.8
Transition SST	High	26.3	7.82	11.8	3.1	0.93	0.63	2.43
	Low	10.5	3.80	4.44	5.39	3.05	5.52	9.71
	Ratio	2.51	2.06	2.64	0.57	0.30	0.11	0.25
	% Dev.	30.3	10.4	N/A	56.9	76.0	74.1	7.34
k-k_l-ω	High	35.1	7.59	23.3	4.91	0.95	0.85	1.28
	Low	9.07	3.65	2.58	5.13	2.61	6.46	9.36
	Ratio	3.86	2.08	9.02	0.96	0.36	0.13	0.14
	% Dev.	101	11.5	N/A	-28.3	-71.4	-69.9	-49.4

Table 4.4 considers the size of comparable regions of the blade wakes, divided into high velocity regions above 6.5m/s and low velocity regions below 6.5m/s. The size of the wakes are normalised against the area of the blade and a ratio between the size of the two regions is also provided in order to improve comparability and reduce the impact of any measurement inaccuracies. Results for the experiment at 90° and 135° are not provided due to insufficient data available from the original experiment.

It can be seen that at 45 and 270° there was good agreement between the turbulence models, whilst at 180° k-ω SST and Transition SST agreed with each other but disagreed with the similar results of k-ω SST LRN and k-k_l-ω that produced a

ratio closer to the experimental result. The deviation from the experiment at most positions is poor although k-k_l-ω and k-ω SST LRN demonstrated significantly improved accuracy at 180°, and Transition SST at 315°. k-k_l-ω produced very poor estimates at 0° compared to the other models due to significantly overestimating the size of the high velocity region.

Table 4.5: Comparing the normalised area of the blade wake regions of different turbulence models against the Castelein et al. experiment

Turbulence Model	Average Absolute Deviation (%)
k-ω SST	48.11
k-ω SST LRN	44.07
Transition SST	42.51
k-k_l-ω	55.19

The average deviations are shown in Table 4.5, with Transition SST offering the lowest deviation. k-k_l-ω had a very high deviation due to the poor estimate at 0°, and when excluding this position the average deviation for k-k_l-ω (46.1%) is in line with k-ω SST LRN (43.4%) and Transition SST (44.9%), with k-ω SST having a much greater error (51.5%).

The cause of the quantitative results was then evaluated qualitatively. In figures 4.13-4.19 the experimental velocity values as a ratio of freestream velocity are shown. The original colour scheme used helps to highlight certain flow characteristics but it can also make simulation results appear very different if the values are slightly different.

Good agreement was shown between the turbulence models and the experiment at 0° as shown in figure 4.13. At 45° the overall structure of the simulated wakes were similar to the experiment, however the low velocity separation was elongated compared to the original teardrop shape in the experiment, as shown in figure 4.14. Results at 90° were not provided for the experiment but good agreement was shown between the turbulence models. Overall, the results for the SST models had insignificant differences between each other, and with all differing significantly from the experiment.

At 135° a small delay in the separation bubble on the inside of the blade was

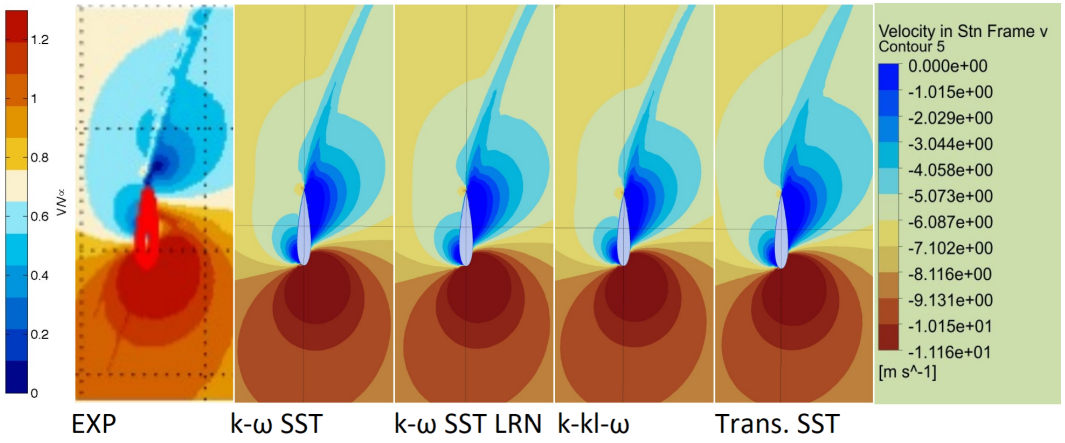

Figure 4.13: Velocity at 0° 1: Experimental[9], 2: k-ω SST, 3: k-ω SST LRN, 4: Transition SST, 5: k-kl-ω

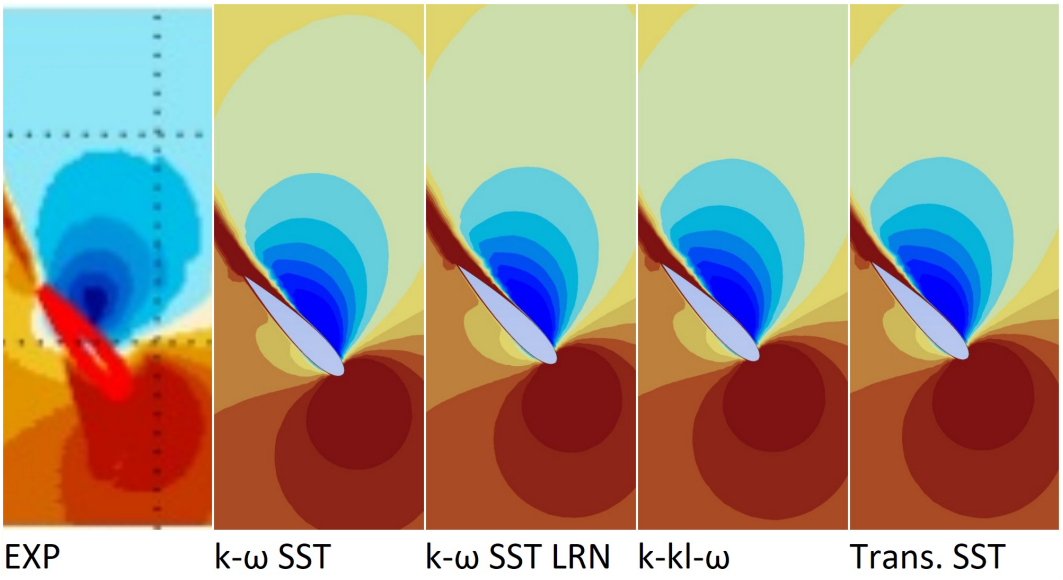

Figure 4.14: Velocity at 45° 1: Experimental[9], 2: k-ω SST, 3: k-ω SST LRN, 4: Transition SST, 5: k-kl-ω

seen in figure 4.15. At 180° a small high velocity region was found at the trailing edge which isn't present in the experimental results. Using k-k_l-ω an improvement was seen with a reduction in the size of the high velocity separation bubble, and increase in the low velocity separation, at both 135 and 180°, however they were still different in size to the experimental results as seen in figures 4.15 and 4.16.

At 225° a much larger high velocity region was found at the inner side of the trailing edge of the blade compared to the experiment, seen in figure 4.17. At 270° the SST turbulence models failed to predict the small separation bubble on the inside

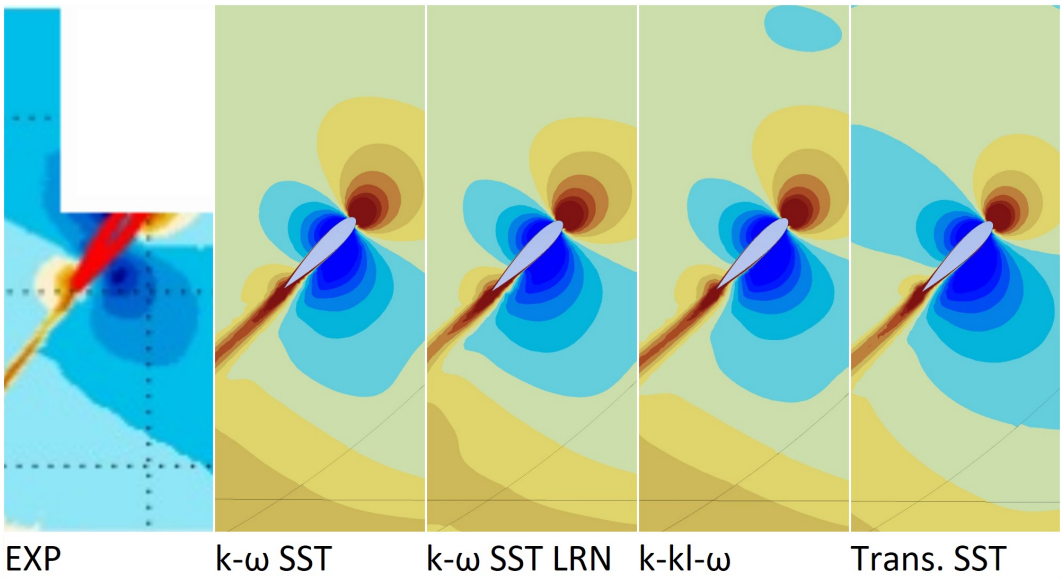

Figure 4.15: Velocity at 135° 1: Experimental[9], 2: k-ω SST, 3: k-ω SST LRN, 4: Transition SST, 5: k-kl-ω

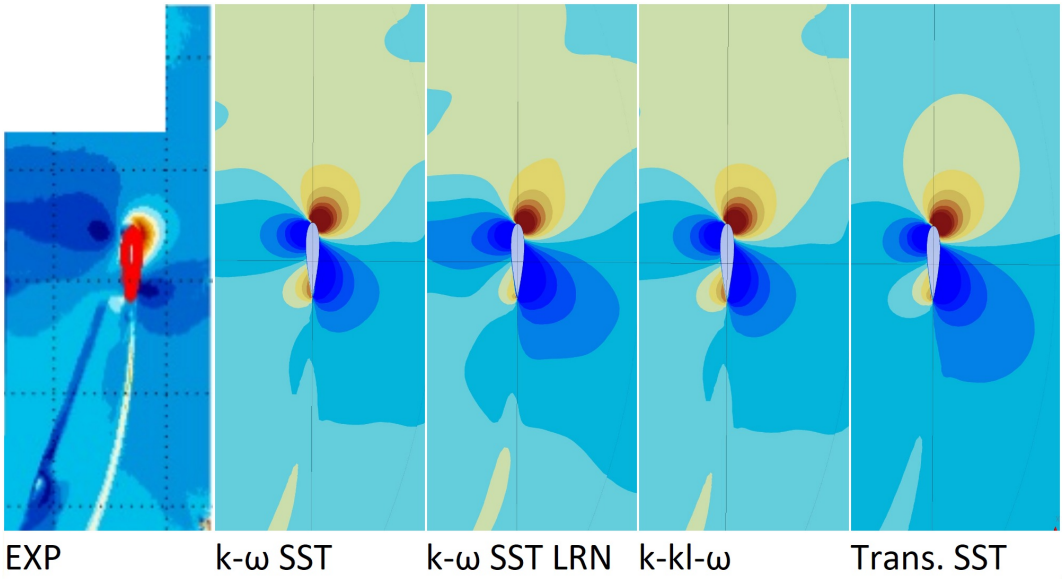

Figure 4.16: Velocity at 180° 1: Experimental[9], 2: k-ω SST, 3: k-ω SST LRN, 4: Transition SST, 5: k-kl-ω

of the blade which resulted in a higher velocity region on the CFD results, as shown in figure 4.18. This issue continued at 315°, shown in figure 4.19.

Overall, a better prediction of the far blade wake was seen with Transition SST which was expected given that this is similar to the instantaneous results from the Tescione validation, however there was still significant inaccuracy. It is unclear

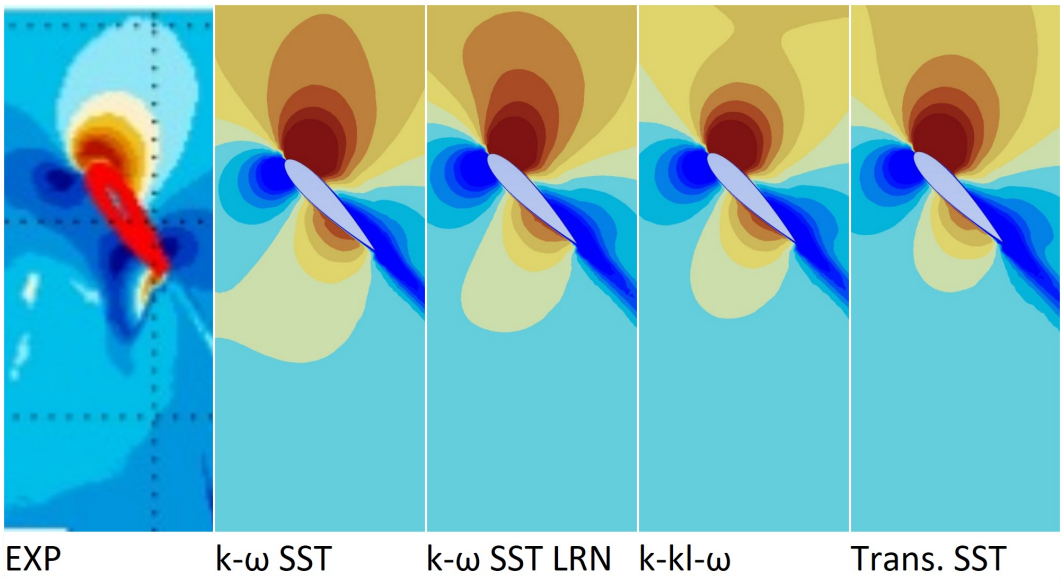

Figure 4.17: Velocity at 225° 1: Experimental[9], 2: k-ω SST, 3: k-ω SST LRN, 4: Transition SST, 5: k-kl-ω

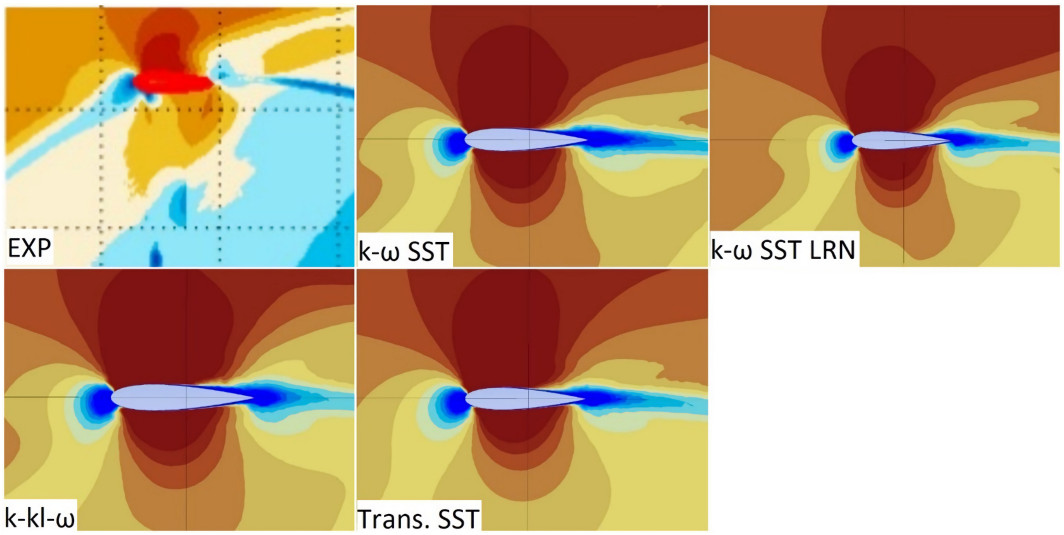

Figure 4.18: Velocity at 270° 1: Experimental[9], 2: k-ω SST, 3: k-ω SST LRN, 4: Transition SST, 5: k-kl-ω

whether this is due to limitations of the turbulence models, 3D effects, or variables which haven't been accounted for.

The difference in results between the turbulence models and the experiment may partially be due to differences in effective angle of attack of the blade, either as a result of the difference in inlet velocity, the simulation setup, or the wind tunnel setup. Another possible cause is the lack of accounting for surface roughness in

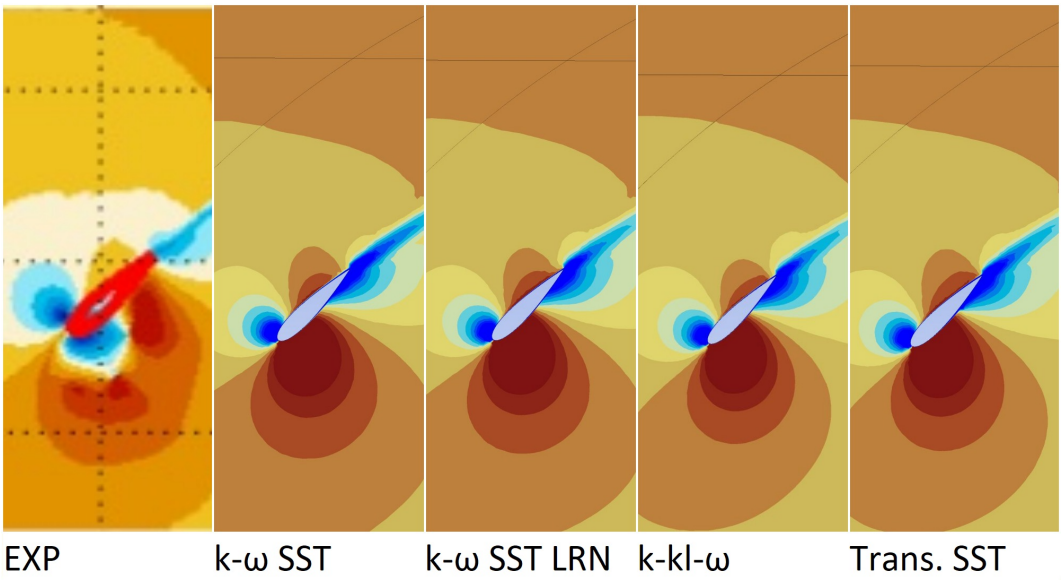

Figure 4.19: Velocity at 315° 1: Experimental[9], 2: k-ω SST, 3: k-ω SST LRN, 4: Transition SST, 5: k-kl-ω

the simulations, as Zhang et al. finds that blade wakes are affected significantly by surface roughness[178].

4.2.3 Turbulence Model Validation - Near Turbine

Tescione et al.[12] considered the wake downstream of the turbine which is important for how turbines interact within arrays, and the near wake within 2D downstream is of high value due to the small distances proposed between turbines in VAWT arrays. This subsection used the Tescione et al. experimental results to compare the accuracy of the different turbulence models in CFD alongside QBlade for predicting the downstream wake. It investigates time-averaged streamwise and cross-stream velocity in both the horizontal and vertical midplanes, however this study focused on the horizontal midplane due to this being most suitable for the more commonly used 2D CFD.

Firstly, the deviation between the simulation and experimental results was considered in Table 4.6 for streamwise velocity, where Transition SST demonstrates the smallest deviation from the experimental baseline at all distances downstream. However, the difference in accuracy between the turbulence models was limited with predictions from both k-ω SST and k-k_l-ω remaining within 1% of Inlet Ve-

locity of each other. QBlade showed poor results with significantly larger deviations from the experiment. All models demonstrated increasing error from the experiment further downstream.

Table 4.6: Deviation between simulation predictions of streamwise velocity downstream of the VAWT compared to the Tescione et al. experiment[12]

Distance Downstream (R)		Transition SST	k-k_l-ω	k-ω SST	k-ω SST LRN	QBlade
1.5	Average Absolute Deviation (m/s)	0.564	0.635	0.638	0.619	3.80
	As % of V_∞	6.07	6.83	6.86	6.16	40.9
2.5	Average Absolute Deviation (m/s)	0.701	0.757	0.785	0.832	4.44
	As % of V_∞	7.53	8.14	8.44	8.95	47.8
4.0	Average Absolute Deviation (m/s)	0.980	1.02	1.07	1.25	5.95
	As % of V_∞	10.5	11.0	11.5	13.5	64.0

In table 4.7 the cross-stream velocity is considered, showing that k-kl-ω offered the lowest error from the experiment up to 2.5R downstream, then Transition SST offered the best accuracy at 4R downstream, with k-ω SST LRN and k-k_l-ω offering slightly reduced accuracy. The errors decreased further downstream due to the trend of decreasing absolute cross-stream velocity.

Table 4.7: Deviation between simulation predictions of cross-stream velocity downstream of the VAWT compared to the Tescione et al. experiment[12]

Distance Downstream (R)		Transition SST	k-k_l-ω	k-ω SST	k-ω SST LRN
1.5	Average Absolute Deviation (m/s)	0.434	0.344	0.455	0.657
	As % of V_∞	4.67	3.70	4.89	7.06
2.5	Average Absolute Deviation (m/s)	0.403	0.244	0.479	0.471
	As % of V_∞	4.34	2.62	5.16	5.07
4.0	Average Absolute Deviation (m/s)	0.192	0.227	0.314	0.217
	As % of V_∞	2.06	2.45	3.38	2.33

Combining the streamwise and cross-stream velocity errors in table 4.8, both Transition SST and k-k_l-ω offered good accuracy with k-k_l-ω offering improved

accuracy up to 2.5R downstream. This may indicate that Transition SST is more appropriate for arrays where the turbines are placed greater than 2.5R apart, whilst k-k_l-ω is appropriate for distances up to 2.5R. k-ω SST may be useful to initialise simulations due to being less computationally intensive, followed by switching to Transition SST or k-k_l-ω.

Table 4.8: Deviation between simulation predictions of total velocity downstream of the VAWT compared to the Tescione et al. experiment[12]

Distance Downstream (R)		Transition SST	k-k_l-ω	k-ω SST	k-ω SST LRN
1.5	Average Absolute Deviation (m/s)	0.999	0.980	1.09	1.28
	As % of V_∞	10.7	10.5	11.8	13.7
2.5	Average Absolute Deviation (m/s)	1.10	1.00	1.26	1.30
	As % of V_∞	11.9	10.8	13.6	14.0
4.0	Average Absolute Deviation (m/s)	1.17	1.25	1.39	1.47
	As % of V_∞	12.6	13.4	14.9	15.8

In order to understand the cause of the deviations, the graphs and contour maps of streamwise velocity were considered, with markers representing sampled points.

From the experimental results in figure 4.20 it was shown that the wake in the experiment has reducing velocity further away from the turbine and there was a greater velocity deficit to the upwind stroke side of the turbine (positive X values), which increased further away from the turbine. The minimum velocity point moved from 2.5m/s at approximately x=+0.05m for 1.5R downstream to 1.8m/s at x=+0.25R for 4.0R downstream.

The turbulence models showed good estimations of the downwind stroke time-averaged streamwise velocity (negative X values) but failed to predict the greater deficit on the upwind stroke as seen in Figure **??**. This inaccuracy became greater further downwind. This has been seen in other research for 2D and 2.5D VAWT simulation by Bachant and Wosnik[42] and Rezaeiha et al.[143], though appears to be solved by using a 3D approach[11]. It should be noted that Rezaeiha's paper uses Tescione's experiment as their experimental reference, and Bachant's turbine is at

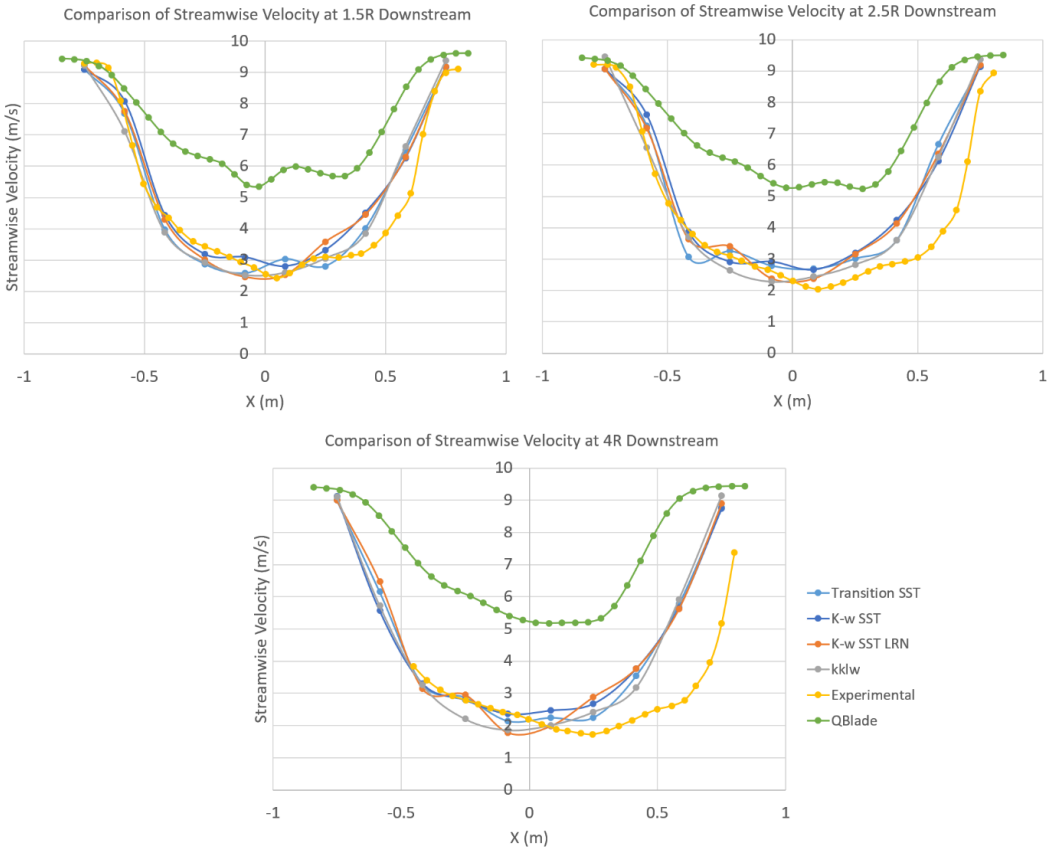

Figure 4.20: Comparing turbulence model results with experimental results for streamwise velocity at 1.5R (upper left), 2.5R (upper right), and 4.0R (lower) downstream

the same scale with similar magnitude of blade Reynolds number. Further research needs to be conducted at commercial scale Reynolds numbers of 10^7 in order to determine whether this is a factor in accuracy of prediction of the turbine wake for utility scale turbines.

k-ω SST and Transition SST produced the most accurate results, with Transition SST better predicting the wider low-velocity region on the upwind side from x=0.2m to 0.5m for 1.5R and 2.5R, and x=0.1m to 0.5m for 4.0R. k-k_l-ω showed a droop on the downwind stroke side compared to the experiment and other turbulence models. It also showed a smoother wake profile throughout the rotations which could affect results for farm design as the intra-rotation fluctuations may alter power output of downwind turbines in some circumstances. Using cubed root of the mean of the cubed velocity fields would help designers account for this as this measures the average power at a given point[179]. This relationship also means

there would be relatively little difference in terms of power prediction for downstream turbines between k-ω SST and Transition SST because the regions where their predictions differ have low velocities.

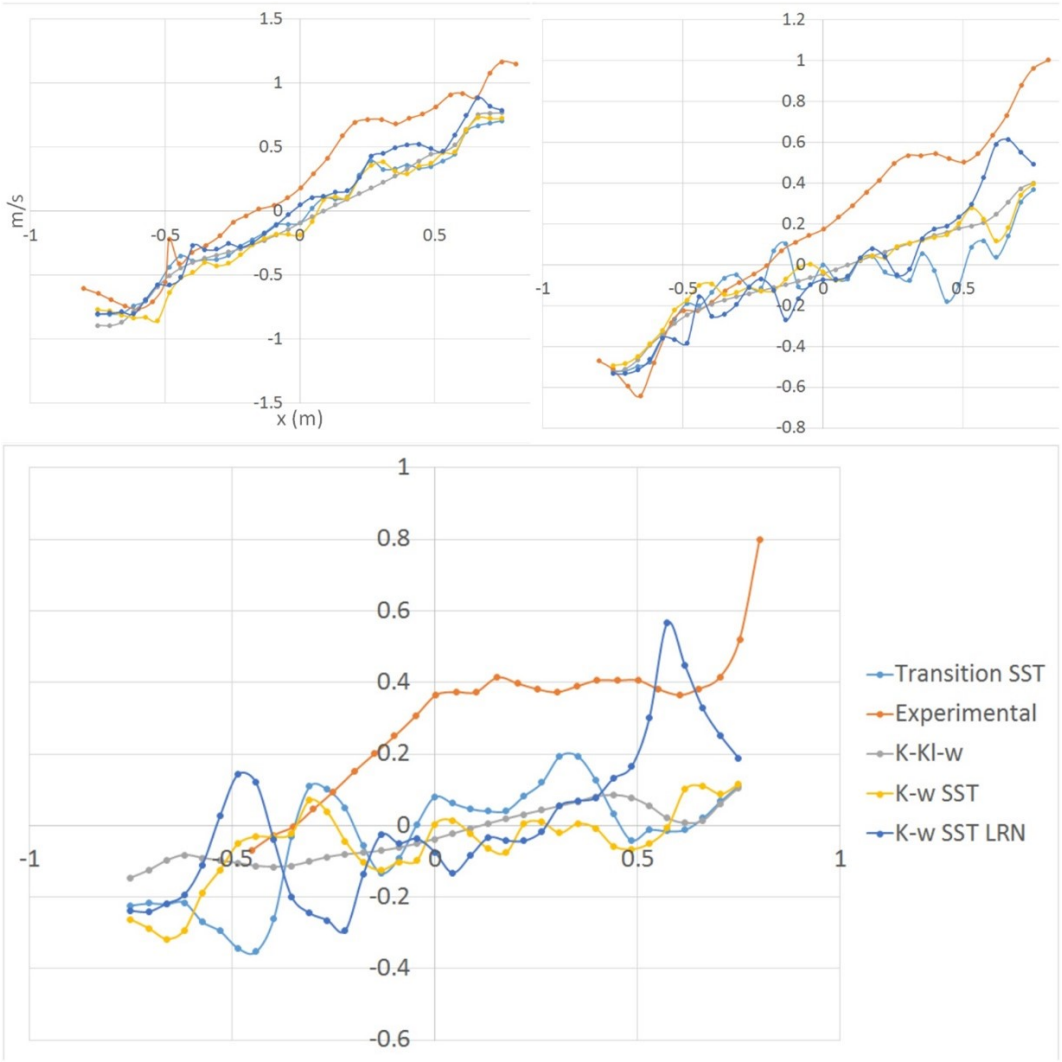

Figure 4.21: Comparing turbulence model results with experimental results for cross-stream velocity at 1.5R (upper left), 2.5R (upper right), and 4.0R (lower) downstream

Considering Cross-stream velocity in figure 4.21, better accuracy was seen at smaller distances downwind, with k-ω SST LRN producing the most similar results to the experiment at 1.5R downwind, although the gradient of the velocity change was lower than expected from the experimental results. At 2.5R downwind all models except for k-kl-ω showed very oscillatory behaviour so there was no clear better turbulence model for predicting Cross-stream velocity at this distance downstream.

At 4.0R the oscillatory behaviour became an even greater issue. For downwind turbines in the mid-wake, especially on the upwind stroke side, the cross-stream velocity constituted a significant component of the total velocity vector, so accounting for this in turbine placement and variable pitch algorithms will be necessary to ensure optimal operation.

The results were also compared against previous CFD in the literature for the Tescione et al. experiment such as Rezaeiha et al.[10] and Lam and Peng[11] shown in figure 4.22. Lam and Peng's results using the k-ω SST model demonstrated an overestimation at all points whilst Rezaeiha et al. shows good agreement or small overestimation in the negative X region whilst k-ω SST and Transition SST in the current study underestimate between -0.4 to -0.1m, with Transition SST showing a greater deviation. In the positive X region the current study demonstrates a significantly reduced deviation from the experiment using k-ω SST and Transition SST compared to Lam and Peng, and Rezaeiha et al.'s use of the same models. The oscillation at the centre in Rezaeiha et al.'s results was also not seen in either the current study or Lam and Peng. This may be due to the choice of Pressure-Velocity coupler or the different meshes used because these studies use similar methodologies otherwise.

By inspecting the full plane of the wake it is possible to visualise characteristics of the flow to help further understand the velocity graphs. Instantaneous values were used here for the CFD results.

It can be determined by inspection of figure 4.23 that the k-k_l-ω model provided the most similar prediction of the instantaneous inner wake streamwise velocity with the other models failing to predict the more cohesive wake formation seen in Tescione's results. All of the models overestimated the velocity at the edges of the wake, and k-k_l-ω predicted a much smoother wake pattern than the experiment and other models. This is an issue for array design if the outer wake is an important variable in the performance of downwind turbines, and in a 3D scenario there will be additional effects from wake contraction in the Z axis alongside tip vortex effects which are not present in the 2D simulation.

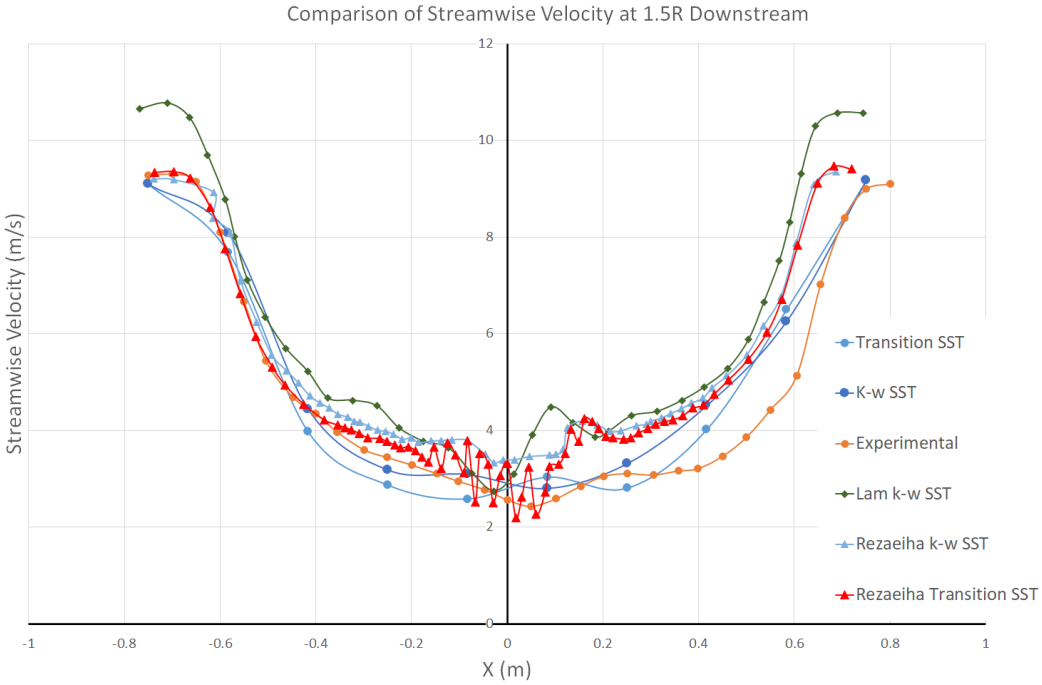

Figure 4.22: Comparison of k-ω SST and Transition SST streamwise velocity results at 1.5R downstream for the current study and previous literature[10][11]

All models underestimated the velocity deficit caused by the shaft, with Transition SST producing slightly higher velocity predictions than the other models. The SST models including k-ω SST, k-ω SST LRN, and Transition SST were better predictors of the blade wake velocity with the impact still being accurately predicted until the third wake artefact downstream. The LRN model produces wavy sprites at the wake edge however while the experimental results show smoother sprites, so the standard k-ω SST and Transition SST are better in this regard.

As shown in the velocity graphs also, the wake tended towards the centre or downwind side in the CFD models whereas it tended further towards the upwind side on the experiment.

Differences occurred in the visualised wakes due to inaccurate replication of the contour boundaries, because whilst the contour colour scheme has been replicated it is not a perfect copy. In the future it would be preferable to use a scheme with smaller velocity bands and a larger colour gradient to improve comparability.

From figure 4.24, a significant departure from the experimental results was seen in all turbulence models. All models showed smaller regions with cross-stream

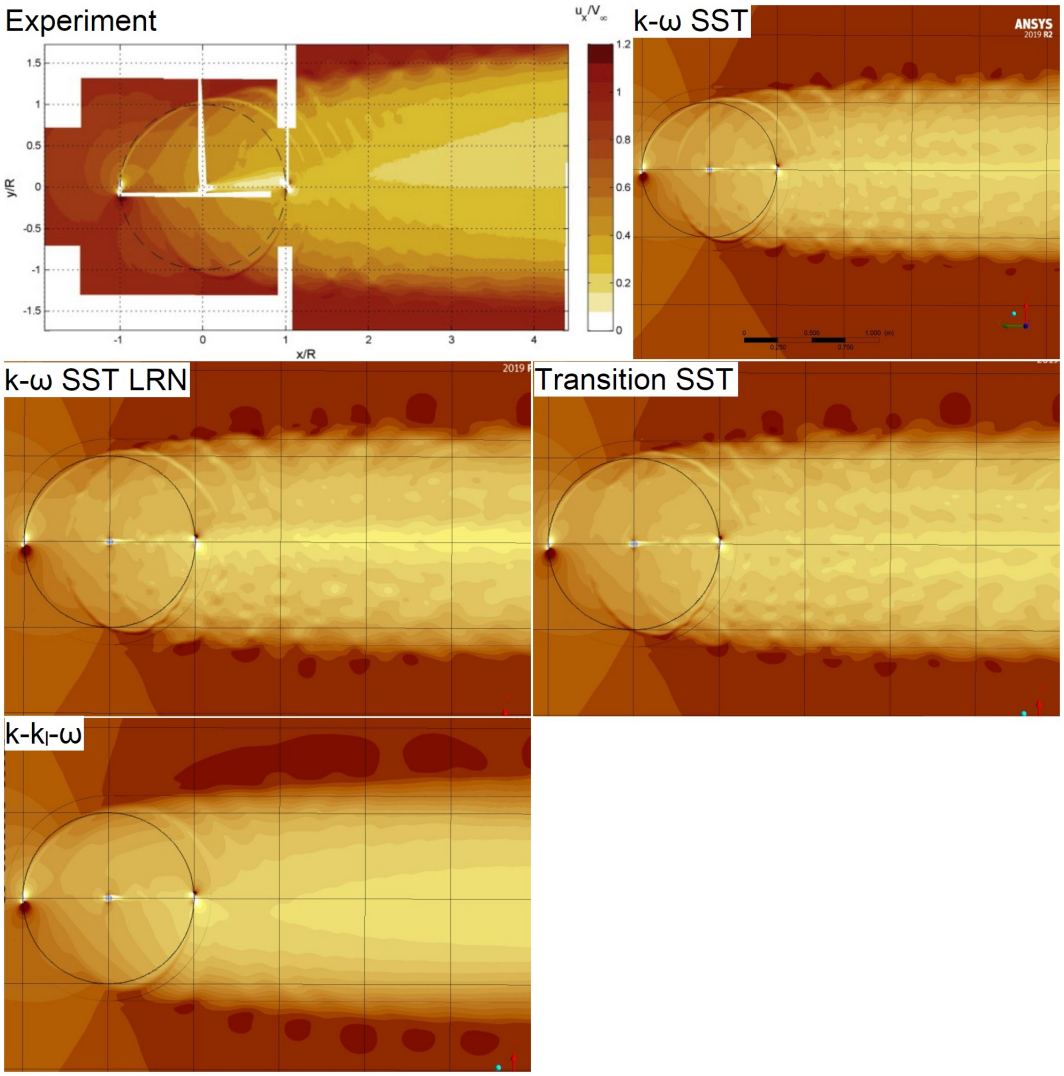

Figure 4.23: Comparison of Experimental SPIV results for streamwise velocity by Tescione and CFD results by Turbulence model. Upper left: Tescione's results[12], Upper right: k-ω SST Centre left: k-ω SST LRN, Centre right: Transition SST, Lower: k-k_l-ω

velocity near zero, alongside larger areas of negative velocity on the upwind side and positive velocity on the downwind side.

All of the CFD models showed good prediction of wake velocity on the upstream side of the turbine region, however Transition SST had a more accurate prediction on the downstream side. Wake artefacts from previous revolutions of the blade with the turbine region were positioned further downstream than their equivalents in the experimental results, and they had a smaller radius of curvature compared to the experiment also. This makes any comparison difficult as any interaction

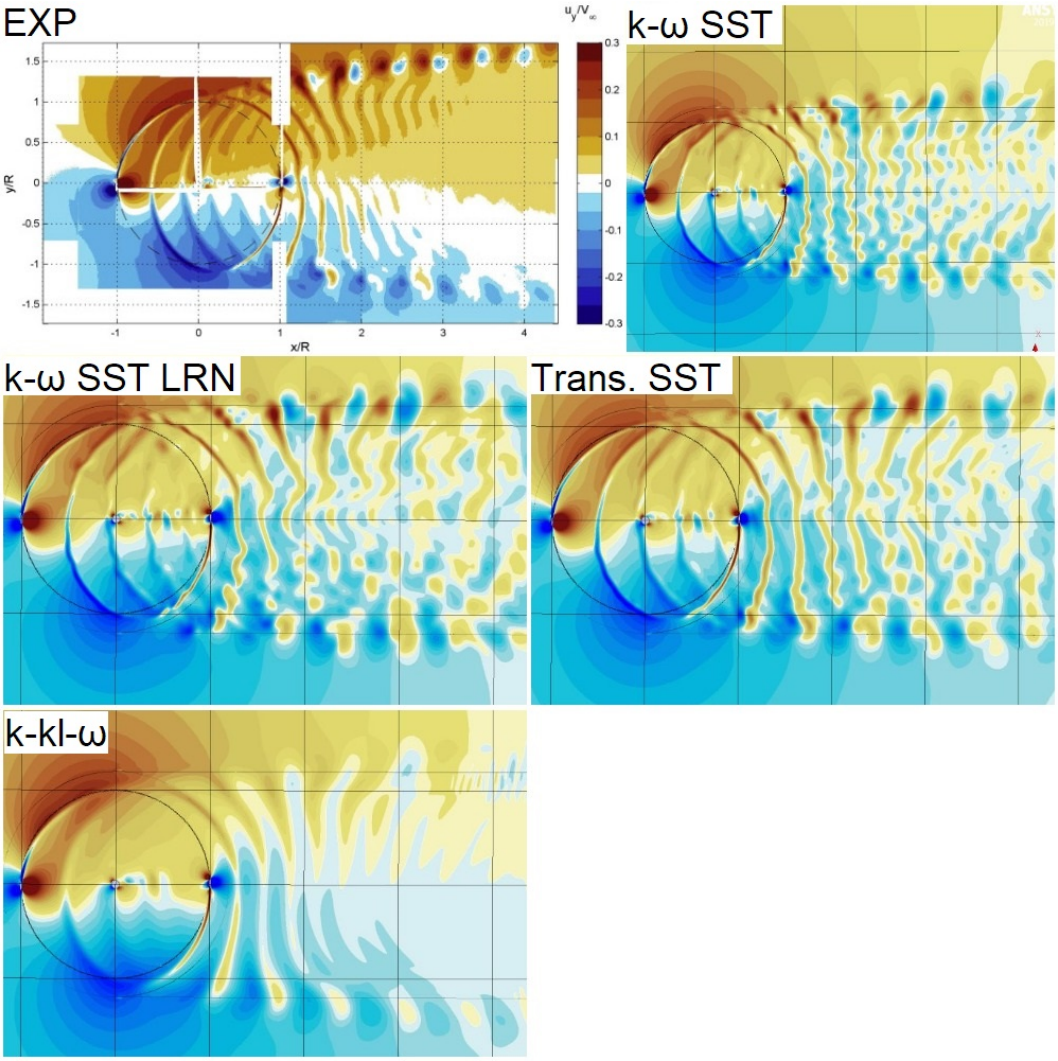

Figure 4.24: Comparison of Experimental SPIV results for cross-stream velocity by Tescione and CFD results by Turbulence model. Upper left: Tescione's results[12], Upper right: k-ω SST Centre left: k-ω SST LRN, Centre right: Transition SST, Lower: k-k_l-ω

between past blade wakes and the rotating blades could alter results significantly.

There was also a repetition of k-k_l-ω producing very different results compared to the other turbulence models, showing a lower cross-stream velocity on the edges of the wake compared to the experiment, in contrast to the high streamwise velocity in these areas.

The difference in the results in this validation compared to Rezaeiha et al.[143] and Lam and Peng[11] could be due to two variables: meshing or pressure-velocity coupler. The mesh used here has a much higher number of cells compared to Reza-

eiha et al.'s and Lam and Peng's (1,351,811 vs. 402,999 and 430,000) and in particular this mesh uses a refined wake zone which wasn't used by either of these studies which both only refined around the blade regions. The other change is that Rezaeiha used the SIMPLE pressure-velocity coupler whilst Lam and Peng used SIMPLEC whereas Coupled was used in this study, however this was shown in the Verification subsection 3.2.13 to have an insignificant impact on results.

Overall, Transition SST offered the most accurate model however users should be aware of velocity being overestimated in the upwind side wake. k-ω SST offered a good alternative for conducting a large number of simulations or as an initial estimate due to its lower computational time and similar accuracy. It is also clear that small deviations in methodology can make a significant difference for VAWT wake prediction as shown by the disparities in results between the current study, Rezaeiha et al., and Lam and Peng.

4.2.4 Turbulence Model Validation - Near Array

A co-rotating turbine pair based upon the experiment conducted by Lam and Peng[100] was considered to evaluate the accuracy of different turbulence models for predicting array performance. This also investigated the wake further downstream compared to Tescione et al.

In figure 4.25 it can be seen that k-ω SST and Transition SST produced similar results, albeit with Transition SST finding a deeper but thinner trough for the right turbine wake. Both of these models also found velocity reversal within the wake, and are clearly the less accurate models.

In contrast, k-ω SSTI demonstrated improved predictions with closer minima values and positions to the experiment, alongside good estimation of the central peak, however the trough positions and velocities were still significantly different to the experimental results and would not allow for accurate farm design validation via CFD. The estimation of velocity for the left trough was significantly improved compared to the other models with this estimated at 2.9m/s compared to 3.9m/s in the experiment, and negative values for k-ω SST and Transition SST. However, this was still a significant underestimation of 26% for velocity and 59% for power at

the minima. The velocity estimations for the right trough were similar for all three tested turbulence models

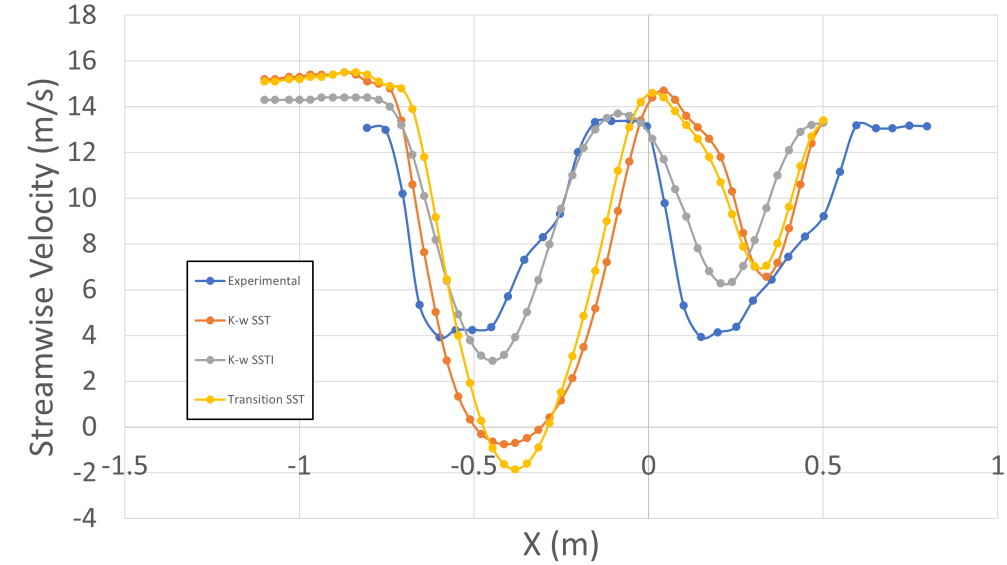

Figure 4.25: Validation of Turbulence Models for Streamwise Velocity at 2D Downstream

This demonstrates that the k-ω SSTI model was better at predicting downstroke-side shift, especially in the right hand turbine, however it was insufficiently accurate to capture the trough position of the left hand turbine. It also predicted faster velocity recovery for the right hand turbine compared to the experiment, which may result in CFD array optimisation predicting smaller spacings between turbines than experiments.

AT 4D downstream, the k-ω SST and k-ω SSTI models produce reasonable estimates of the trough positions, but significantly overestimate the velocity at these positions. Neither accurately predict the central peak, in contrast to the very good prediction by k-ω SSTI at 2D downstream. When considering results beyond 4D downstream, CFD results showed limited or no resemblance to the experimental results as seen in figures 4.26-4.28.

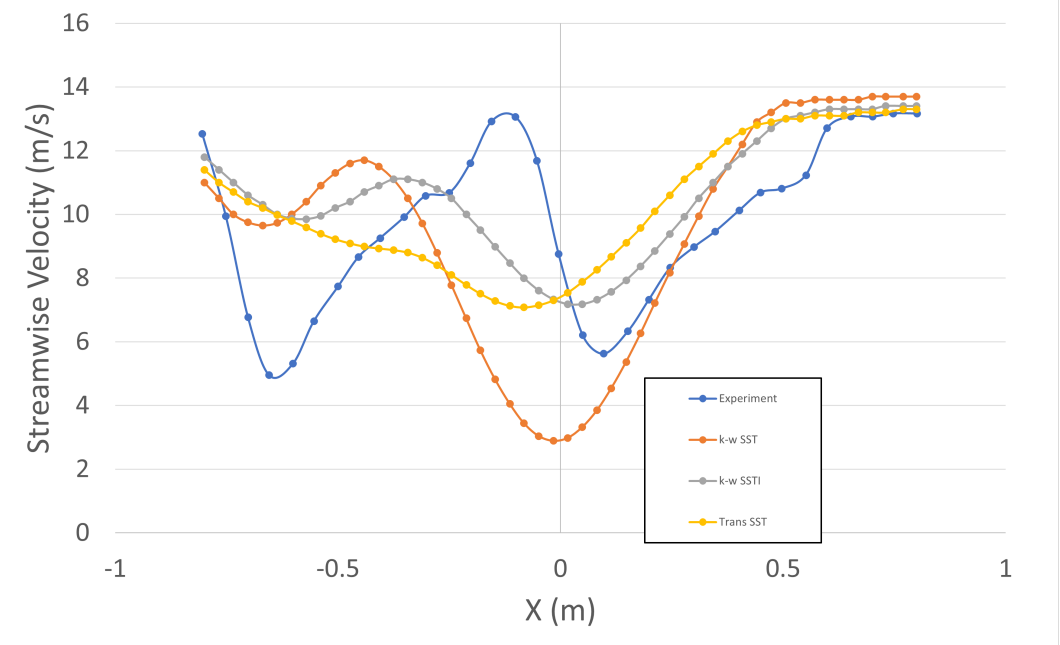

Figure 4.26: Validation of Turbulence Models for Streamwise Velocity at 4D Downstream

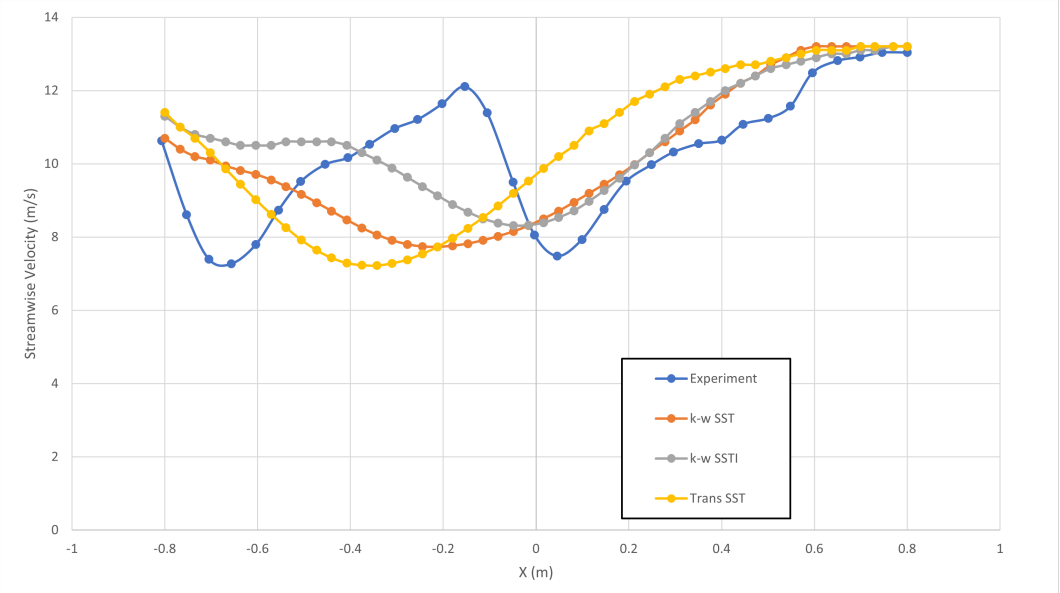

Figure 4.27: Validation of Turbulence Models for Streamwise Velocity at 6D Downstream

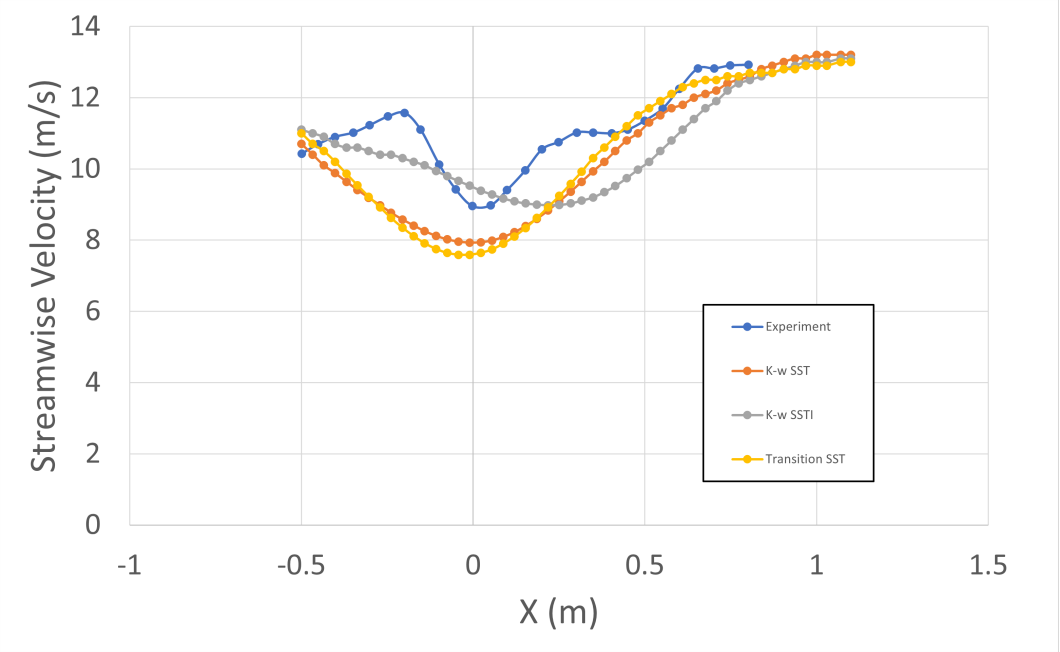

Figure 4.28: Validation of Turbulence Models for Streamwise Velocity at 8D Downstream

The cross-stream results in figures 4.29-4.31 confirmed that there are likely to be additional causes of inaccuracy for simulating arrays using the chosen 2D CFD methods compared to individual turbines, or that the predicted flow within the co-rotating array amplified the impact. All of the turbulence models predict similar patterns, however k-ω SSTI has smaller peaks and troughs compared to the other turbulence models and the experiment. These help to explain the downstroke shift patterns in the turbulence models due to the reduction in the cross-stream velocity component compared to the experiment, alongside much wider peaks.

Through inspection of figure 4.25 it is seen that for both left and right turbines using all turbulence models at 2D downstream, there was an increase in streamwise velocity beyond the inlet velocity, in some cases greater than 1m/s. Through inspecting the left turbine wake in figure 4.32 it can also be seen that the wake of the blade during the downstroke caused this increase, and that the increase continued late into the downstroke at approximately 160° from the upstream direction. This late continuation of the wake causing an increase in velocity appears to have induced the negative cross-stream velocity and resultant shift in the trough positions compared to the experiment. This would indicate that future research on validating

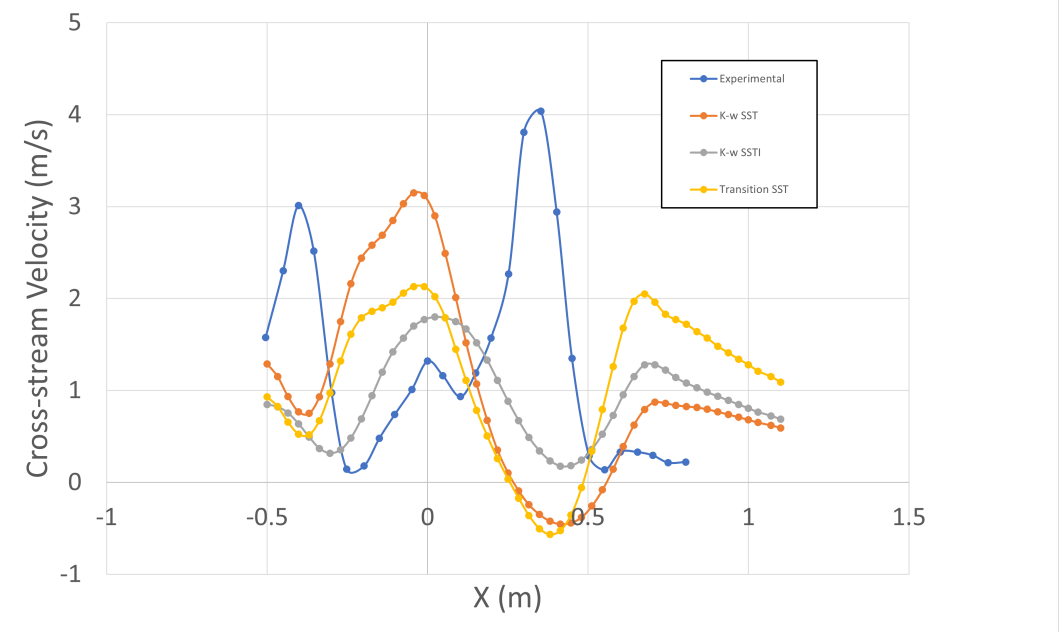

Figure 4.29: Validation of Turbulence Models for Cross-stream Velocity at 2D Downstream

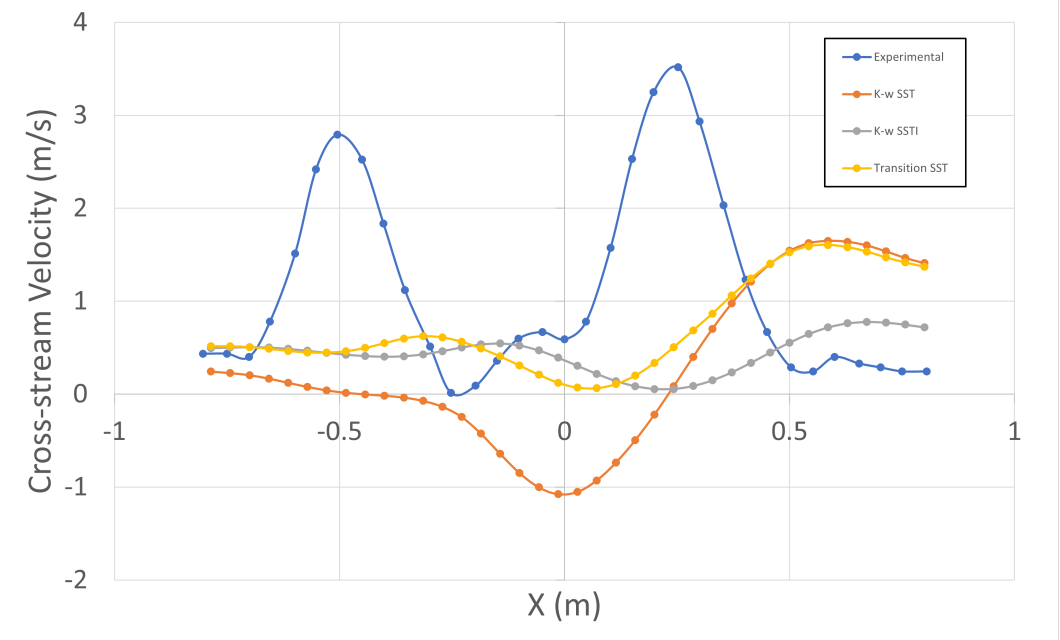

Figure 4.30: Validation of Turbulence Models for Cross-stream Velocity at 4D Downstream

2D CFD for VAWTs should focus on finding or creating a turbulence model which accurately predicts the blade wake in the region of 90° to 180° from the upstream direction.

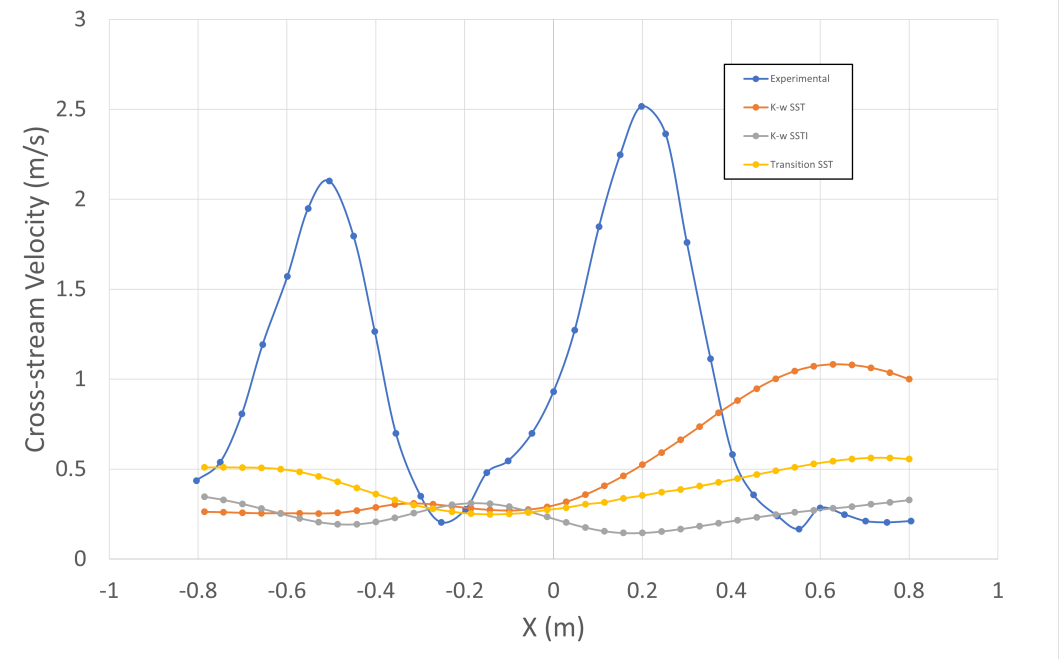

Figure 4.31: Validation of Turbulence Models for Cross-stream Velocity at 6D Downstream

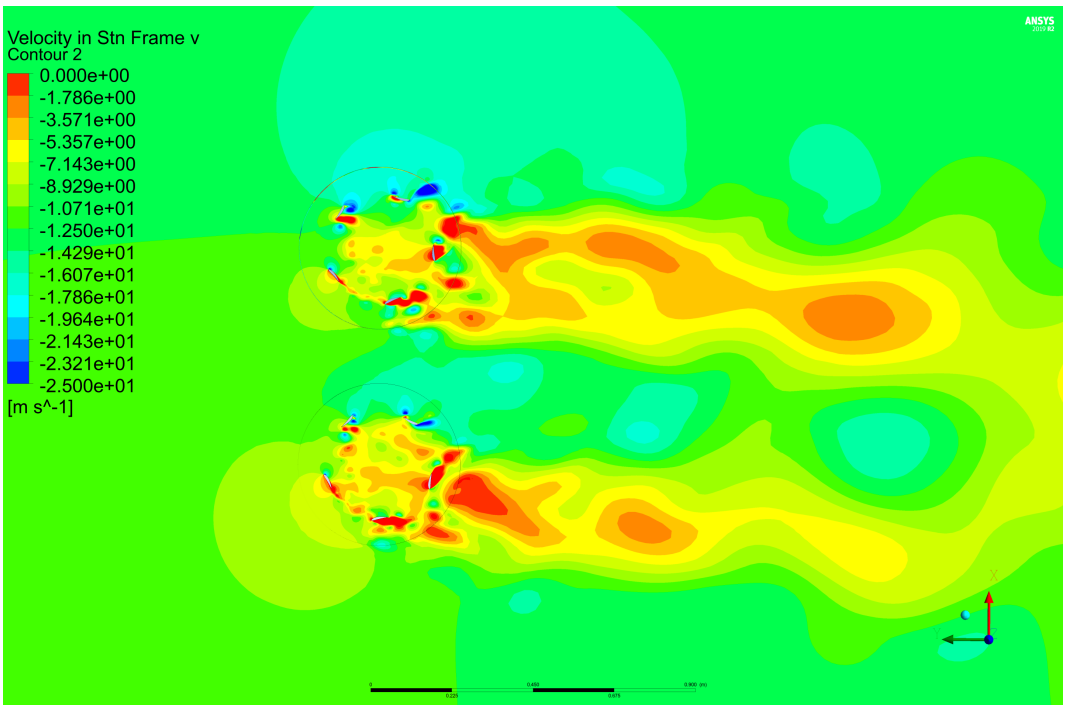

Figure 4.32: Streamwise Velocity Contour for Left Turbine (k-ω SSTI)

It is possible that this may remain an issue which is not solvable using 2D CFD, and there is evidence for and against this idea. Shamsoddin and Porté-Agel[180] used 3D CFD using Large Eddy Simulation and the Actuator Line Model, which

would be expected to give more accurate results due to it being a more direct form of numerical simulation. This study utilised a VAWT design where a ring connects the ends of the blades which would reduce tip effects, emulating blades of infinite length and therefore it should provide similar results to a 2D CFD setup. Their results demonstrated insignificant shift of the streamwise velocity minima position in the turbine wake, matching the findings for the single turbine 2D CFD results as expected.

However similar results were seen by Posa et al.[13] and Lei et al.[130] for turbines with no tip devices, showing that both the experiments and 3D CFD using LES, DDES, and k-ω SST had insignificant shift of the minima position also, so not all VAWTs will demonstrate this behaviour. In the study by Posa et al., the shift, and failure for CFD to predict the shift, was seen in the low TSR condition but not the high TSR condition, although this was not seen between the low and high TSR conditions in Lei et al.

The difference between these two studies and Shamsoddin and Porté-Agel is that Lei et al. and Shamsoddin and Porté-Agel used significantly higher Reynolds numbers, so the shift could be related to Reynolds independence which is a well-documented phenomena for prediction of power coefficient of VAWTs[42][5][24], and may be a phenomena which CFD struggles with[43]. However the chord Reynolds number (Re_c) which is being experienced by the VAWT in both low and high TSR conditions is far below that expected for Reynolds independence for power coefficient, approximately $2x10^5$, whereas Posa et al.'s results would indicate that Reynolds independence for the wake can occur at approximately $3x10^4$. The difference between the results for the low and high TSR conditions implies that the simplified chord Reynolds number which does not take rotational speed into account is not sufficient for predicting whether a shift will occur.

The shift could be due to the blade reaching low effective Reynolds numbers as a result of the rotation, where the crossover point would occur at TSR=1 representing the point at which a blade positioned at the 90°position would have an effective Reynolds number of zero. Although this logic can be applied to any point

in the downstroke where the streamwise velocity of the blade minus the streamwise velocity of the airflow is greater than zero. It would then be expected that CFD estimates would be incorrect for TSRs above 1 if the effective Reynolds number remained sufficiently low and the turbulence model was inaccurate for low Reynolds number scenarios. For Posa et al. the change in Re_c between TSR=1 and TSR=1.35, where the shift still occurred in the experiment, is approximately 10,531 whilst for TSR 2.21, where the shift was no longer seen, this is approximately 66,821. The range for wake Reynolds independence can be further narrowed down using Lei et al.'s results, where the change in Re_c between TSR=1 and TSR=1.38, where no shift is found in their results, is 54,014.

Tescione et al.'s experiment[12] demonstrated a shift towards the upstroke side which is the opposite direction to expected. It also used a TSR of 4.5, a Re_c change of 132,691, and a low turbulence intensity of 0.5%, all of which appear to be indicators of reduced shift based upon results and considerations presented in this thesis so far. So Tescione's study is evidence against these hypotheses although it may have confounding factors which affect the results. For example, the cross-stream velocity profiles found by Tescione et al. indicate that the inlet cross-stream velocity may not have a uniform profile and so this would have affected how the blades interact with the airflow in comparison to other turbines due to the blades experiencing a different effective velocity and direction compared to a uniform inlet profile.

In the experiments used as baselines for the results presented in this study, the TSR is below 1 so the blades will inherently encounter low effective Reynolds number, or even reversed effective wind speed relative to the normal aerofoil direction, during the downstroke. Increasing inaccuracy with negative effective Reynolds number would also explain the array results where the velocity of the airflow was accelerated between the two turbines and so small effective blade Reynolds numbers or reversed flow would be more likely to occur on the downstroke.

Lam and Peng[11] found that 3D CFD using k-ω SST and DES turbulence models still failed to predict the shift in the minima position found in their experimental baseline, reinforcing that the issue may be unrelated to the number of

dimensions used.

Further research is needed to gather evidence specifically on these hypotheses, focusing on how the accuracy of CFD is affected by turbulence intensity and low or negative effective Reynolds number during the downstroke.

4.2.5 2D vs. 3D

Simulations in 3D were run again using the Tescione et al. experiment as a basis which also allowed a comparison to the 2D results. Simulations were run for the k-ε Realizable, k-ω SST, and Transition SST turbulence models and were initially run until the average velocity at a 1.5m line placed 2D downstream and the torque plateaued, this gave the following results in table 4.9. All of the models showed similar results for average velocity, however the results for torque varied significantly, even between the SST models.

Turbulence Model	Average Velocity (m/s)	Torque (Nm)
3D k-ε Realizable	4.7	0.246
3D k-ω SST	4.8	0.794
3D Transition SST	4.7	0.998
2D k-ω SST	4.8	1.498
3D Transition SST	4.7	1.773

Table 4.9: Comparison of Average Velocity and Torque for the Turbulence Models used in 3D Simulations of Tescione et al.[12]

In figures 4.33 and 4.34 the 3D results are compared to previous equivalent 2D results and the experiment. Firstly in figure 4.33 for streamwise velocity, it can be seen that the 3D CFD did not predict the asymmetry of the wake seen in the experiment, and whilst the domain dimensions and blockage ratio were matched to the experiment, the trough caused by the wake did not recover as quickly at the edges as in the experiment or 2D results. The minimum velocity was also higher and there were no oscillations in the line like in the 2D results and experiment. In figure 4.34 for Cross-stream velocity, it can be seen that there was very little cross-stream velocity induced in the wake by the 3D turbine simulations compared to the experiment, which would account for the symmetry seen in the streamwise velocity results.

Comparing the turbulence models, the minimum velocity was higher when using k-ε Realizable and therefore less accurate than Transition SST, however the difference was small and so could be an acceptable trade-off in some circumstances given that both models otherwise demonstrate the same trend.

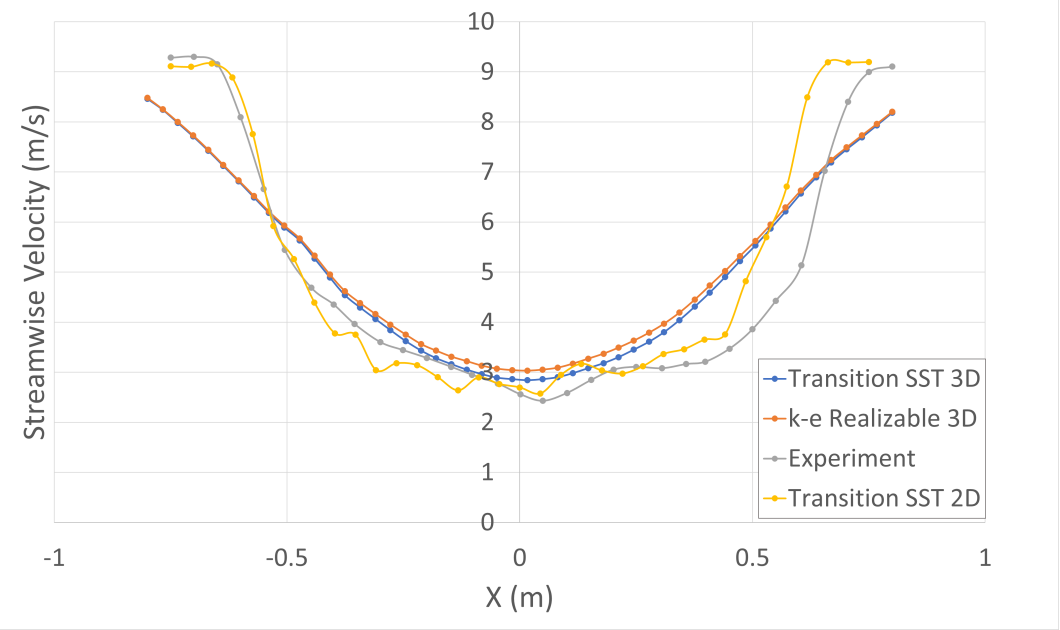

Figure 4.33: Comparison of Streamwise Velocity at 1.5R downstream of the turbine for 2D and 3D CFD against the Tescione et al. experiment[12]

There are several possible reasons for the comparatively worse results using 3D compared to 2D based upon the differences in methodology. Firstly, as covered in subsection 4.2.4, it is possible that a 3D approach alone was not sufficient to replicate the downstream wake asymmetry seen in some VAWT experiments. This would account for why the 3D results are not more accurate than 2D but would not explain why they are less accurate.

The replication of the domain may have affected the results because the 3D simulation does not include the shaft whereas the 2D simulation does, this will be covered in the next subsection 4.2.6. Whilst the blockage ratio was lower for the 3D domain, the width of the domain was much smaller and symmetry is not applied to the sides of the domain so this could have caused blockage effects, although the domain has been replicated like-for-like to the experiment so these should have had an equivalent effect. The high density mesh in the wake region was also not fully repli-

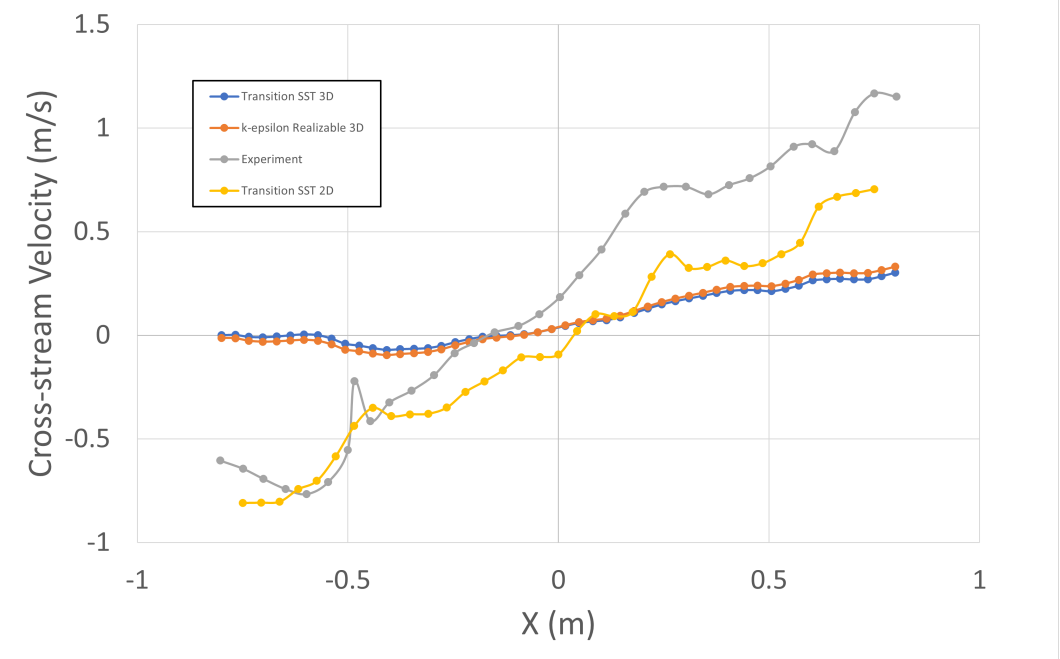

Figure 4.34: Comparison of Cross-stream Velocity at 1.5R downstream of the turbine for 2D and 3D CFD against the Tescione et al. experiment[12]

cated in the 3D simulation compared to the 2D simulations and this may also have affected the wake results as evidenced by the differences between this study and Rezaeiha et al.[10] and Lam and Peng[11]. The use of horizontal midplane symmetry to halve the cell count may also have impacted results given that measurements were taken on this plane, so further verification is needed against completing a full turbine simulation.

Using first order spatial discretisations may have impacted accuracy compared to the second order discretisations used for the 2D simulations. Some settings which were verified to have an insignificant effect for 2D simulations may have a significant impact in 3D, for example the use of SIMPLE in the 3D simulation due to the inability to use Coupled as used in the 2D simulation.

Finally, the verification procedure of averaging velocity across a line may not have been sufficient to capture the differences that are being analysed, which especially applies to time step as seen in figure 3.14 where the average velocity across the evaluated line would be similar across the 0.1, 0.02, and 0.004° conditions. This could imply that time steps must be much smaller than those used in the literature

(subsection 2.5.6) in order to achieve accurate wake prediction, even for the high TSR used by Tescione et al.

4.2.6 Impact of Shaft and Struts

The shaft and struts were added to the 3D simulation used in subsection 4.2.5 in order to consider the impact of these on the downstream wake. As shown in figures 4.35 and 4.36, there was a small difference however this occurred on the downstroke side of the turbine which improves accuracy albeit not in the area of greatest interest which is the upstroke side asymmetry. Given the high additional computational cost of including the shaft and struts in the mesh, with the mesh growing from 19.5M cells to 23.7M cells, a 21.5% increase, it is unlikely that the greater accuracy from this alone would provide sufficient benefit to warrant their inclusion in 3D array simulations.

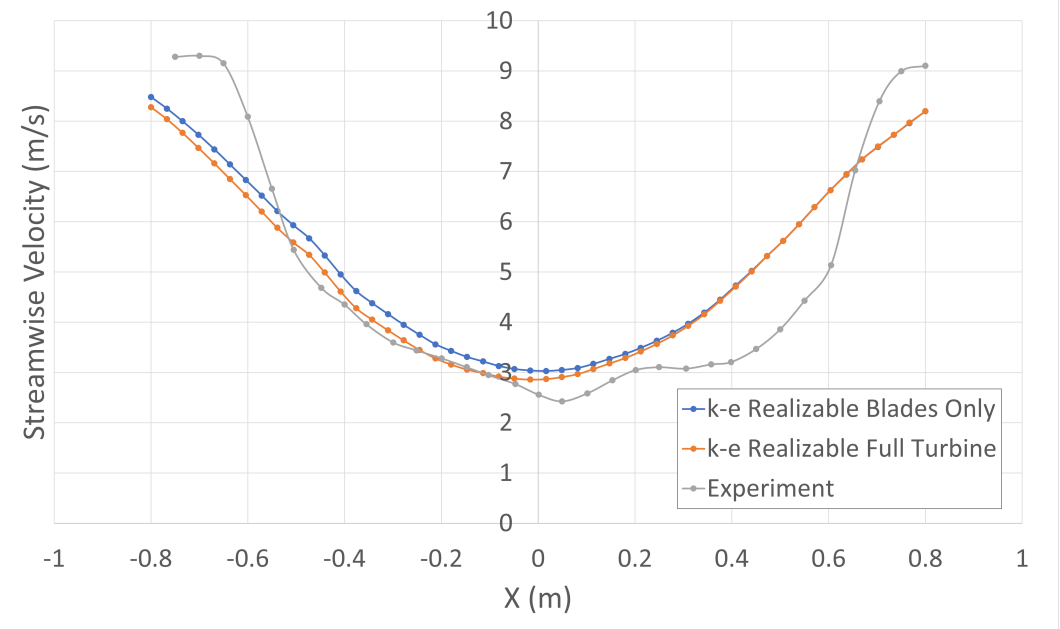

Figure 4.35: Comparison of Streamwise Velocity at 1.5R downstream of the turbine for 3D CFD models with and without shaft and struts against the Tescione et al. experiment[12]

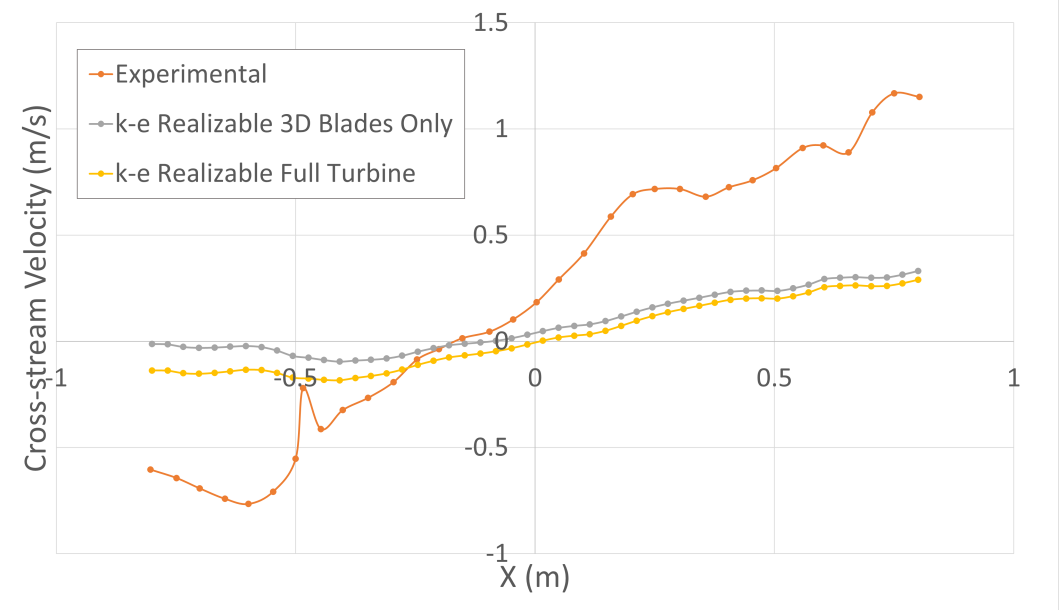

Figure 4.36: Comparison of Cross-stream Velocity at 1.5R downstream of the turbine for 3D CFD models with and without shaft and struts against the Tescione et al. experiment[12]

4.3 Impact of Field Representative Values on VAWT Simulation

This section considers the impact of small changes in turbulence intensity on the accuracy of CFD in order to advise upon the level of detail needed to appropriately recreate experiments in CFD simulations for validations. It also considers how changes in Turbulence Intensity can affect VAWT wakes.

Firstly, the arrangement studied by Peng et al. is analysed, considering the impact on streamwise velocity at 2D downstream of changing inlet Turbulence Intensity from the original 2.5% to 0% in figure 4.37. It can be seen that the introduction of a small amount of turbulence intensity resulted in a significant change in the wake, with much greater asymmetry. The 0% intensity condition showed a slight asymmetry with this resulting in the minima at 1.61m/s shifting from the centre to 0.04m, however when accounting for this shift the wake was otherwise symmetrical with the wake recovering to 12m/s at -0.2m on one side compared to 0.28m on the other side. In contrast, for the 2.5% intensity condition the primary minima

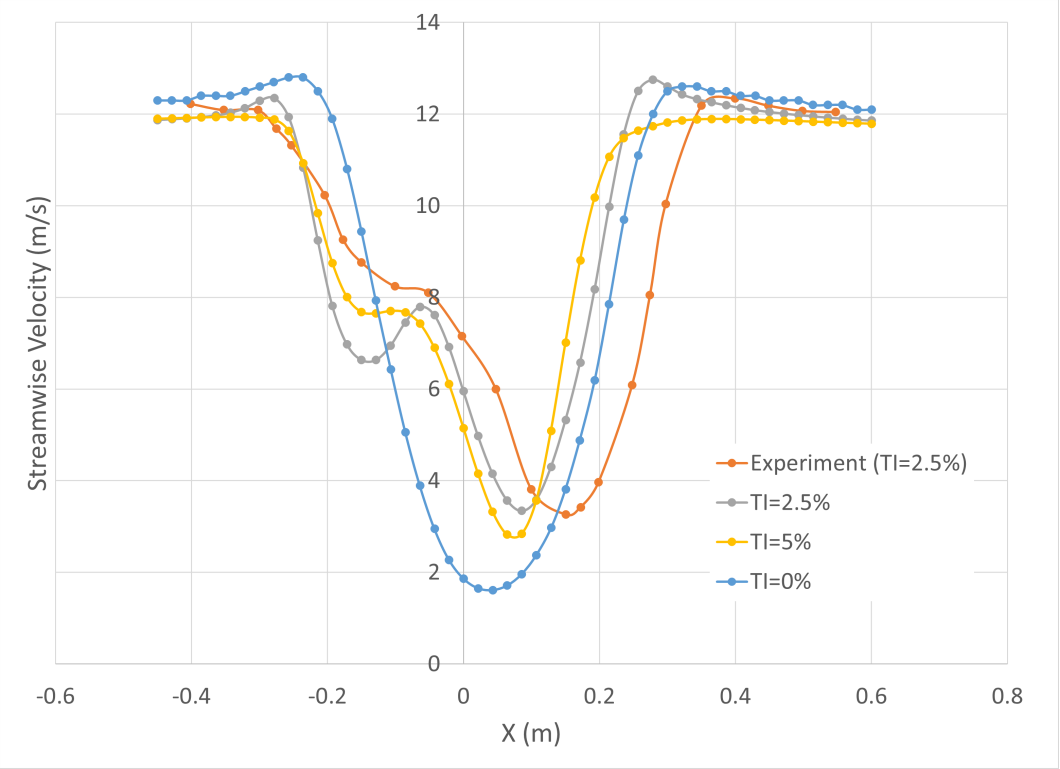

Figure 4.37: Impact of Turbulence Intensity on Streamwise Velocity at 2D downstream for Peng et al.

of 2.8m/s occurred at 0.07m, with a secondary minima of 8.1m/s at -0.15m. The recovery to 12m/s on the other hand was symmetrical with both sides recovering to this velocity at $\pm$0.28m.

Compared to the experiment, the 2.5% simulation underestimated the velocity at the minima and the shift to the positive X direction. This could be the result of CFD underestimating the impact of turbulence intensity on the results, Peng et al. underestimating the turbulence intensity in their wind tunnel, or the differences in the domains affecting the turbulence intensity at the position of the turbine and downstream in its wake.

This demonstrates that high accuracy of measurement of the turbulence intensity in the wind tunnel and resultantly the correct implementation of the turbulence intensity in CFD simulation is necessary to ensure that a validation is a valid representation of the accuracy of a CFD procedure.

A further increase in Turbulence Intensity to 5% was also considered, with

this resulting in a plateau which is more similar to the experimental result, unlike the minor trough seen in the 2.5% CFD results. The major trough is also thinner and shifted slightly back towards the centre. This could demonstrate the need for future study of Turbulence Intensity in small increments down to the order of 0.1% in order to better understand the effect of Turbulence Intensity on VAWT wakes for certain turbines. This could be important for understanding potential sources of error between CFD and experimental results.

Secondly, Posa et al. is analysed, considering the impact on streamwise velocity at 1D downstream of changing Turbulence Intensity from the estimated 2.5% to the IEC64100 field representative 12% in figure 4.38, it also compared the impact of including the shaft on 2D simulations. The shaft showed a significant impact on the wake, with the wake showing much greater resemblance to the experiment when the shaft is included. Notably, the results here showed reduced error compared to the 3D LES results conducted by Posa et al. as a result of the more accurate estimation of the minima, however the LES results more accurately replicate the shape of the wake, with the small trough on the upstroke side being correctly replicated whilst in the 2D URANS simulation there was a small peak in this position instead. The 2D URANS also predicted a wider trough on the downstroke side of approximately 0.033m, whilst the differences in the trough between the 3D LES and experiment are accounted for by the offset in the velocity minima.

In comparing the two turbulence intensity conditions, it can be seen that the differences between 2.5% and 12% were much smaller here than between 0% and 2.5% for the Peng et al. simulations. There are several possible causes for this: the line of measurement in Posa et al. was closer to the turbine than in Peng et al. and so errors have had less opportunity to accrue, the combination of the setup used being more conducive to accurate CFD simulations, potentially including estimation of the impact of turbulence intensity, and the existence of a point of turbulence intensity independence for VAWT wakes in some scenarios. The existence of a point of turbulence intensity independence could be advantageous regarding the use of wind tunnels for VAWT testing because most wind tunnels which have been used

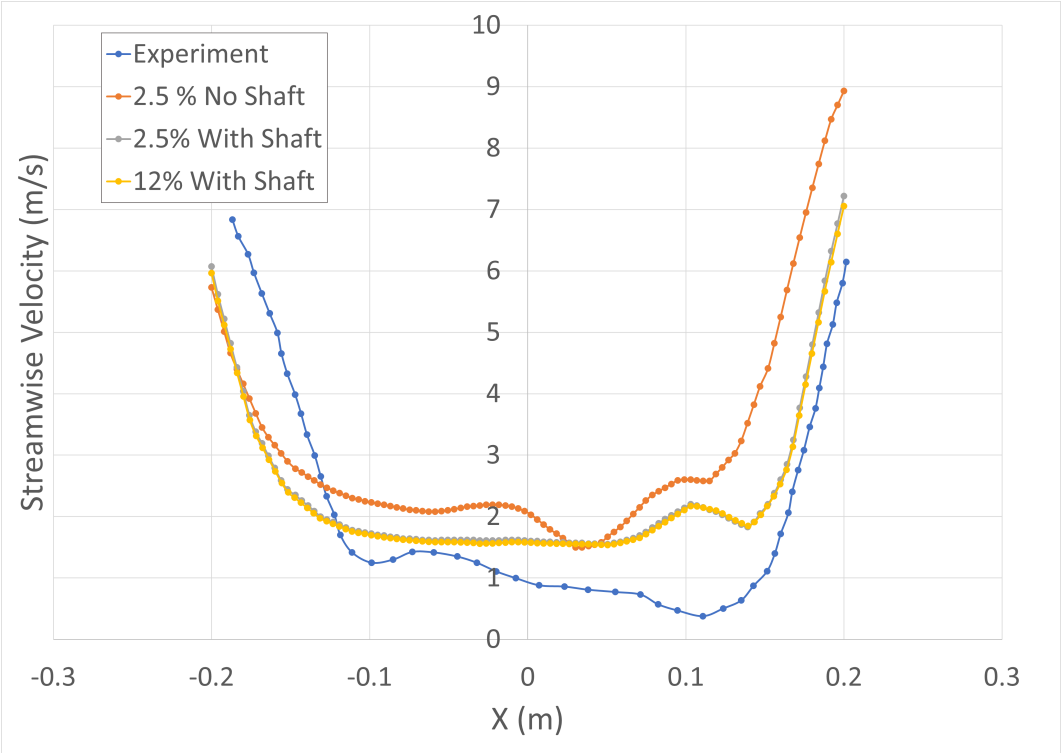

Figure 4.38: Impact of Turbulence Intensity on Streamwise Velocity at 2D downstream for Posa et al.

for VAWT experiments are limited to low turbulence intensities which cannot reach the IEC64100 range.

Chapter 5

Conclusions

This chapter concludes the studies conducted in this thesis. The aim of this thesis was stated in section 2.10 as ”To improve the design procedure for Vertical Axis Wind Turbine arrays through analysis of array layout to determine potential improvement in power output and to evaluate the procedure for numerical analysis”. Achievement of this aim would provide a more standardised procedure for VAWT simulation and array design. Such a methodology would allow for more rapid development of commercially viable VAWTs and VAWT arrays by enabling rapid accurate simulation of VAWT arrays to determine the optimal configurations for power output.

5.1 Main Findings

The main findings below are listed in correlation with the objectives set out in 2.11:

1. A review of the literature was conducted in order to determine gaps in the research to drive this thesis. It was found that there was a need for further direct comparisons of array designs, including the use of optimisation procedures and how turbine design can affect array design. There was need for improvement in VAWT experimental and simulation guidelines in order to improve applicability alongside standardisation and therefore comparability. Part of this necessary improvement is related to the understanding of how different variables such as Reynolds number and Turbulence Intensity affect operation of VAWTs.

2. ANSYS FLUENT was used to conduct CFD simulations on a series of array layouts based upon the literature including Grid, Truss, Biomimetic, Pair, and Hybrid layouts in order to determine the C_{AP} of each design and to inspect the mechanisms of action for any change in C_{AP} compared to an isolated turbine baseline. It was found that the Truss layout offered the highest C_{AP} at 0.425, compared to the Biomimetic layout at 0.356, Pairs at 0.383, Isolated turbine at 0.252, and Grid at 0.131. This represented a 69% increase over the isolated turbine. The mechanism of action was determined to be the Venturi effect with increases in velocity and cross-stream velocity suppression as a result of upstream turbines.

3. A gradient-based optimisation procedure was completed in order to further optimise the spacings used by the Truss configuration. The optimisation procedure resulted in an increase in C_{AP} to 0.453 from 0.425 in the baseline Truss configuration. This is an 80% increase over the baseline isolated turbine.

4. Using the optimised Truss configuration, the original high solidity σ=0.883 turbine was replaced with a low solidity σ=0.12 turbine by reducing the chord length accordingly. It was found that this array had a reduced C_{AP} of 0.355 compared to the high solidity baseline.

5. During the review of the literature, significant evidence was found for differences in VAWT C_p curves between turbines conducted in typical wind tunnel conditions and those conducted in the field. The main causes of these were dependence on Reynolds Number and Turbulence Intensity. The use of field experiments with use of LiDAR for recording wakes may offer a solution for VAWT experiments which is cheaper compared to sufficiently large wind tunnels, and more utility-applicable compared to small wind tunnels.

6. Through the CFD validations of various turbulence models across different regions and conditions of the VAWT flow problem, it was found that k-ω SSTI, Transition SST, and k-k_l-ω offered the most promising options for CFD analysis.

7. Simulations were conducted to analyse the change in downstream wake for two VAWTs depending on their Turbulence Intensity. For the first VAWT it was found that changing from the baseline 2.5% intensity to 0% had a drastic impact on the wake, resulting in much greater symmetry. In contrast, for the second VAWT, a change from 2.5% to a field-representative 12% had limited effect. Given that wind tunnels typically operate at low intensities, small inaccuracies in measurements or changes throughout the domain may have a significant impact on the accuracy of CFD simulations if the conditions are not sufficient for Turbulence Intensity independence.

5.2 Contribution to Knowledge

Per section 2.9, a series of gaps were found in the research on VAWTs through the literature review. Through the research conducted in this thesis, the following contributions to knowledge were made:

1. Using CFD simulation, a direct comparison between the array power coefficients of several VAWT array layouts was conducted. Out of the compared designs, the Truss formation resulted in the highest power coefficient of 0.425 which was higher than the other tested formations and the isolated turbine baseline.

2. Mechanisms for increased power coefficients in VAWT arrays have been identified. Namely, there is evidence of VAWTs creating a constriction which causes the Venturi effect, resulting in accelerated flow in a more preferable direction for downstream turbines. This causes a significant increase in power coefficient of downstream turbines without breaking the Betz limit, and works best when there are two turbines upstream of a downstream turbine.

3. Gradient-based optimisation has demonstrated the ability to deliver good results for optimising wake arrays, with low resource requirements.

4. Solidity of a turbine has been demonstrated to affect performance of a given array design, with an array using a low solidity turbine σ=0.12 having an

array power coefficient which was 21.6% lower than the high solidity turbine σ=0.883.

5. The potential for VAWTs to offer significantly higher power density than HAWTs has been confirmed, however the potential power density is approximately half of what has been previously reported, likely due to optimising for efficiency in this thesis instead of power density and the use of different approaches to the methodology including turbine design.

6. CFD simulation and verification procedure have proven to require high stringency compared to the literature, with very small time steps required for convergence compared to the literature in some scenarios. For a low TSR turbine, time steps as low as 0.02° or lower may be required for convergence. Some experiments may require a high density mesh region downstream of the turbine in order to enable accurate simulation.

7. Transition SST offered the lowest error of the turbulence models tested for predicting VAWT wakes, however given the high computational cost of this model it is suitable to initiate the CFD simulation using lower cost models such as k-ω SST given the small additional error such models cause. For 3D, the differences between k-ε Realizable and Transition SST are insignificant, and so the additional computational cost of using a mesh which achieves y^+=1 combined with the additional cost of using Transition SST is unlikely to be a reasonable trade-off.

8. The tested CFD methods are insufficient for universally accurate array simulation in the tested scenarios due to poor predictions of cross-stream velocity which result in compounding errors further downstream. However, they can predict the minimum streamwise velocity with sufficient accuracy to predict the optimal power output and there are some scenarios where high accuracy is demonstrated.

9. The choice of 2D or 3D CFD is not the primary cause of failure to predict

wake asymmetry in 2D models because this also occurs in 3D models.

10. Using shafts and struts in VAWT simulation will significantly affect the prediction of the depth, width, and position of the downstream wake, however in some scenarios this loss of accuracy alone may not be sufficient to warrant the additional computational resource requirements of the dense mesh around these structure.

11. There is strong evidence for the existence of Reynolds number and Turbulence Intensity dependence with VAWTs, with both occurring up to a point where independence occurs with this point varying dependent on the turbine design. These dependencies impact the accuracy of simulations and so accurate measurements and recreation of these variables are necessary to ensure that CFD validations are representative. They also question whether the methods typically used in VAWT experiments are applicable to the commercialisation of VAWTs.

12. 3 peer-reviewed journal articles have been published as a result of this thesis[108][181][182].

5.3 Further Work

The research conducted in this thesis provides a basis for future work, which is listed below:

1. Comparison of a gradient optimised Truss array with a Monte Carlo optimised array layout using CFD simulation in order to determine the potential benefit of randomised optimisation compared to a stock design. This can include a more comprehensive accounting for wind direction.

2. 3D CFD simulation of arrays in order to determine the impact of varying turbine aspect ratio on array design.

3. Run simulations to determine whether two turbines solely differentiated by

solidity value produce different array designs when array designs are optimised.

4. Further refinement of the CFD procedure should be completed in order to further improve accuracy to allow more confident array design. This should include measuring the surface roughness of the VAWT blades used for a physical experiment and replicating this in CFD, and analysing the impact of the choice of spatial discretisation settings. Refinement is particularly necessary for 3D URANS CFD given the additional costs compared to 2D.

5. Evaluate the causes of the failure of CFD to accurately predict VAWT wake asymmetry in some turbines, considering Reynolds number and Turbulence Intensity as the main potential causes. A better understanding of the causes of inaccuracy will allow these issues to be addressed.

6. Develop a turbulence model aimed at solving the causes of the failure of CFD to accurately predict VAWT wake asymmetry. A new URANS turbulence model would significantly reduce the resources required compared to LES and Hybrid options and therefore speed up VAWT development.

7. Investigate the potential variables which affect Reynolds number and Turbulence Intensity dependence so that experiments can be designed to meet the bare-minimum requirements for applicability in utility-scale conditions and therefore be more available to researchers.

References

[1] Herbert J Sutherland, Dale E Berg, and Thomas D Ashwill. SANDIA REPORT A Retrospective of VAWT Technology. Technical report, 2012.

[2] Andrea Alaimo, Antonio Esposito, Antonio Messineo, Calogero Orlando, and Davide Tumino. 3D CFD analysis of a vertical axis wind turbine. *Energies*, 8(4):3013–3033, 2015.

[3] Changping Liang, Deke Xi, Sen Zhang, and Qiuping Yang. IOP Conference Series: Earth and Environmental Science Effects of Solidity on Aerodynamic Performance of H-Type Vertical Axis Wind Turbine Effects of Solidity on Aerodynamic Performance of H-Type Vertical Axis Wind Turbine. *IOP Conf. Ser.: Earth Environ. Sci*, 170:42061, 2018.

[4] Shawn Armstrong, Andrzej Fiedler, and Stephen Tullis. Flow separation on a high Reynolds number, high solidity vertical axis wind turbine with straight and canted blades and canted blades with fences. *Renewable Energy*, 41:13–22, may 2012.

[5] Andrzej J Fiedler and Stephen Tullis. Blade Offset and Pitch Effects on a High Solidity Vertical Axis Wind Turbine. Technical report, 2009.

[6] Qing'an Li, Takao Maeda, Yasunari Kamada, Junsuke Murata, Masayuki Yamamoto, Tatsuhiko Ogasawara, Kento Shimizu, and Tetsuya Kogaki. Study on power performance for straight-bladed vertical axis wind turbine by field and wind tunnel test. *Renewable Energy*, 90:291–300, may 2016.

[7] Francesco Balduzzi, Alessandro Bianchini, Riccardo Maleci, Giovanni Ferrara, and Lorenzo Ferrari. Critical issues in the CFD simulation of Darrieus wind turbines. *Renewable Energy*, 85:419–435, jan 2016.

[8] A-J. Buchner, M.W. Lohry, L. Martinelli, J. Soria, and A.J. Smits. Dynamic stall in vertical axis wind turbines: Comparing experiments and computations. *Journal of Wind Engineering and Industrial Aerodynamics*, 146:163–171, nov 2015.

[9] Dieter Castelein, Daniele Ragni, Giuseppe Tescione, Carlos Simão Ferreira, D Castelein, D Ragni, G Tescione, CJ Simão Ferreira, and M Gaunaa. Creating a benchmark of Vertical Axis Wind Turbines in Dynamic Stall for validating numerical models. 2015.

[10] Abdolrahim Rezaeiha, Hamid Montazeri, and Bert Blocken. On the accuracy of turbulence models for CFD simulations of vertical axis wind turbines. *Energy*, 180:838–857, aug 2019.

[11] H.F. Lam and H.Y. Peng. Study of wake characteristics of a vertical axis wind turbine by two- and three-dimensional computational fluid dynamics simulations. *Renewable Energy*, 90:386–398, may 2016.

[12] G. Tescione, D. Ragni, C. He, C.J. Simão Ferreira, and G.J.W. van Bussel. Near wake flow analysis of a vertical axis wind turbine by stereoscopic particle image velocimetry. *Renewable Energy*, 70:47–61, oct 2014.

[13] Antonio Posa, Colin M. Parker, Megan C. Leftwich, and Elias Balaras. Wake structure of a single vertical axis wind turbine. *International Journal of Heat and Fluid Flow*, 61:75–84, oct 2016.

[14] Energy Department for Business and Industrial Strategy. UK Energy Statistics 2019. Technical report, BEIS, London, mar 2020.

[15] Energy Department for Business and Industrial Strategy. Electricity Generation Costs 2020. Technical report, BEIS, London, aug 2020.

[16] BEIS. Energy Trends and Prices Statistical Release March 2022. Technical report, BEIS, mar 2021.

[17] Albert Betz and D. G. Randall. *Introduction to the theory of flow machines*. 1966.

[18] John O Dabiri. Potential order-of-magnitude enhancement of wind farm power density via counter-rotating vertical-axis wind turbine arrays. 2011.

[19] M C Claessens. *The Design and Testing of Airfoils for Application in Small Vertical Axis Wind Turbines*. PhD thesis, TU Delft, 2006.

[20] Carlos Simão Ferreira and Ben Geurts. Aerofoil optimization for vertical-axis wind turbines. *Wind Energy*, 18(8):1371–1385, aug 2015.

[21] Jian Chen, Liu Chen, Hongtao Xu, Hongxing Yang, Changwen Ye, and Di Liu. Performance improvement of a vertical axis wind turbine by comprehensive assessment of an airfoil family. *Energy*, 114:318–331, nov 2016.

[22] Delphine De Tavernier, Carlos Ferreira, and Gerard Bussel. Airfoil optimisation for vertical-axis wind turbines with variable pitch. *Wind Energy*, 22(4):547–562, apr 2019.

[23] Ion Paraschivoiu, Octavian Trifu, and F. Saeed. H-Darrieus wind turbine with blade pitch control. *International Journal of Rotating Machinery*, 2009, 2009.

[24] B F Blackwell, R E Sheldahl, and L V Feltz. Wind tunnel performance data for the Darrieus wind turbine with NACA 0012 blades. (May), 1976.

[25] Robert E Akins, Dale E Berg, and W Tait Cyrus. SANDIA REPORT Measurements and Calculations of Aerodynamic Torques for a Vertical-Axis Wind Turbine. Technical report, 1987.

[26] PL Delafin, T Nishino, L Wang, and A Kolios. Effect of the number of blades and solidity on the performance of a vertical axis wind turbine Related

content Effects of Solidity on Aerodynamic Performance of H-Type Vertical Axis Wind Turbine. *Journal of physics: Conference Series*, 753, 2016.

[27] Wendi Liu and Qing Xiao. Investigation on Darrieus type straight blade vertical axis wind turbine with flexible blade. *Ocean Engineering*, 110:339–356, 2015.

[28] L. Battisti, A. Brighenti, E. Benini, and M. Raciti Castelli. Analysis of Different Blade Architectures on small VAWT Performance. *Journal of Physics: Conference Series*, 753:062009, sep 2016.

[29] Young-Tae Lee and Hee-Chang Lim. Numerical study of the aerodynamic performance of a 500 W Darrieus-type vertical-axis wind turbine. *Renewable Energy*, 83:407–415, nov 2015.

[30] Remi Gosselin. *Analysis and optimization of vertical axis turbines*. PhD thesis, Université Laval, 2015.

[31] Frank Scheurich and Richard E. Brown. Modelling the aerodynamics of vertical-axis wind turbines in unsteady wind conditions. *Wind Energy*, 16(1):91–107, jan 2013.

[32] Brian Hand and Andrew Cashman. Conceptual design of a large-scale floating offshore vertical axis wind turbine. *Energy Procedia*, 142:83–88, dec 2017.

[33] Mathijs Peeters, Gilberto Santo, Joris Degroote, and Wim Van Paepegem. The concept of segmented wind turbine blades: A review. *Energies*, 10(8):1–20, 2017.

[34] J Cotrell, T Stehly, J Johnson, J O Roberts, Z Parker, G Scott, and D Heimiller. Analysis of Transportation and Logistics Challenges Affecting the Deployment of Larger Wind Turbines: Summary of Results. Technical report, NREL, Golden, CO, 2014.

[35] Mahamed Hussain, Mostafa Sahed, Agnimitra Mazarbhuiya, Kaushal Biswas, and Sharma Kumar. Performance investigations of modified asymmetric blade H-Darrieus VAWT rotors. *J. Renewable Sustainable Energy*, 10:33302, 2018.

[36] British Standards. Wind Turbine—Part 1: Design Requirements, IEC 61400-1. Technical report, 2005.

[37] R. E. Sheldahl, P. Klimas, and L. Feltz. Aerodynamic Performance of a 5-Metre- Diameter Darrieus Turbine With Extruded Aluminum NACA-0015 Blades. *Sandia Laboratories*, 1980.

[38] S. Brusca, R. Lanzafame, and M. Messina. Design of a vertical-axis wind turbine: how the aspect ratio affects the turbine's performance. *International Journal of Energy and Environmental Engineering*, 5(4):333–340, dec 2014.

[39] Stefania Zanforlin and Stefano Deluca. Effects of the Reynolds number and the tip losses on the optimal aspect ratio of straight-bladed Vertical Axis Wind Turbines. *Energy*, 148:179–195, apr 2018.

[40] Sung-Cheoul Roh and Kang Seung-Hee. Effects of a blade profile, the Reynolds number, and the solidity on the performance of a straight bladed vertical axis wind turbine. *Journal of Mechanical Science and Technology*, 27(11):3299–3307, 2013.

[41] K. McLaren, S. Tullis, and S. Ziada. Computational fluid dynamics simulation of the aerodynamics of a high solidity, small-scale vertical axis wind turbine. *Wind Energy*, 15(3):349–361, apr 2012.

[42] Peter Bachant, Martin Wosnik, Peter Bachant, and Martin Wosnik. Effects of Reynolds Number on the Energy Conversion and Near-Wake Dynamics of a High Solidity Vertical-Axis Cross-Flow Turbine. *Energies*, 9(2):73, jan 2016.

[43] Abdolrahim Rezaeiha, Hamid Montazeri, and Bert Blocken. Characterization of aerodynamic performance of vertical axis wind turbines: Impact of operational parameters. *Energy Conversion and Management*, 169:45–77, aug 2018.

[44] Mahdi Torabi Asr, Erfan Zal Nezhad, Faizal Mustapha, and Surjatin Wiriadidjaja. Study on start-up characteristics of H-Darrieus vertical axis wind turbines comprising NACA 4-digit series blade airfoils. *Energy*, 112:528–537, oct 2016.

[45] Louis Angelo Danao, Ning Qin, and Robert Howell. A numerical study of blade thickness and camber effects on vertical axis wind turbines. *Proceedings of the Institution of Mechanical Engineers, Part A: Journal of Power and Energy*, 226(7):867–881, nov 2012.

[46] Mazharul Islam, David S-K. Ting, and Amir Fartaj. Design of a Special-Purpose Airfoil for Smaller-Capacity Straight-Bladed VAWT. *Wind Engineering*, 31(6):401–424, dec 2007.

[47] Carlos Simão Ferreira. *The near wake of the VAWT 2D and 3D views of the VAWT aerodynamics The near wake of the VAWT*. PhD thesis, TU Delft, 2009.

[48] M. Elkhoury, T. Kiwata, and E. Aoun. Experimental and numerical investigation of a three-dimensional vertical-axis wind turbine with variable-pitch. *Journal of Wind Engineering and Industrial Aerodynamics*, 139:111–123, apr 2015.

[49] Gabriele Bedon, Stefano De Betta, and Ernesto Benini. Performance-optimized airfoil for Darrieus wind turbines. *Renewable Energy*, 94:328–340, aug 2016.

[50] Jabir Ubaid Parakkal, Khadije El Kadi, Ameen El-Sinawi, Sherine Elagroudy, and Isam Janajreh. Numerical analysis of VAWT wind turbines:

Joukowski vs classical NACA rotor's blades. *Energy Procedia*, 158:1194–1201, feb 2019.

[51] M.H. Mohamed, A.M. Ali, and A.A. Hafiz. CFD analysis for H-rotor Darrieus turbine as a low speed wind energy converter. *Engineering Science and Technology, an International Journal*, 18(1):1–13, mar 2015.

[52] M.H. Mohamed. Performance investigation of H-rotor Darrieus turbine with new airfoil shapes. *Energy*, 47(1):522–530, nov 2012.

[53] Francesco Balduzzi, Alessandro Bianchini, Riccardo Maleci, Giovanni Ferrara, and Lorenzo Ferrari. Blade Design Criteria to Compensate the Flow Curvature Effects in H-Darrieus Wind Turbines. *Journal of Turbomachinery*, 137(1):011006, sep 2014.

[54] Alessandro Bianchini, Francesco Balduzzi, Giovanni Ferrara, and Lorenzo Ferrari. Virtual incidence effect on rotating airfoils in Darrieus wind turbines. *Energy Conversion and Management*, 111:329–338, mar 2016.

[55] Ning Ma, Hang Lei, Zhaolong Han, Dai Zhou, Yan Bao, Kai Zhang, Lei Zhou, and Caiyong Chen. Airfoil optimization to improve power performance of a high-solidity vertical axis wind turbine at a moderate tip speed ratio. *Energy*, 150:236–252, may 2018.

[56] Travis J. Carrigan, Brian H. Dennis, Zhen X. Han, and Bo P. Wang. Aerodynamic Shape Optimization of a Vertical-Axis Wind Turbine Using Differential Evolution. *ISRN Renewable Energy*, 2012:1–16, 2012.

[57] M. Jafaryar, R. Kamrani, M. Gorji-Bandpy, M. Hatami, and D.D. Ganji. Numerical optimization of the asymmetric blades mounted on a vertical axis cross-flow wind turbine. *International Communications in Heat and Mass Transfer*, 70:93–104, jan 2016.

[58] A. Sagharichi, M. Zamani, and A. Ghasemi. Effect of solidity on the performance of variable-pitch vertical axis wind turbine. *Energy*, 161:753–775, oct 2018.

[59] Abdolrahim Rezaeiha, Hamid Montazeri, and Bert Blocken. Towards optimal aerodynamic design of vertical axis wind turbines: Impact of solidity and number of blades. *Energy*, 165:1129–1148, dec 2018.

[60] Robert Howell, Ning Qin, Jonathan Edwards, and Naveed Durrani. Wind tunnel and numerical study of a small vertical axis wind turbine. *Renewable Energy*, 35(2):412–422, feb 2010.

[61] Palash Jain and A. Abhishek. Performance prediction and fundamental understanding of small scale vertical axis wind turbine with variable amplitude blade pitching. *Renewable Energy*, 97:97–113, nov 2016.

[62] M.H. Mohamed. Impacts of solidity and hybrid system in small wind turbines performance. *Energy*, 57:495–504, aug 2013.

[63] H.Y. Peng, H.F. Lam, and H.J. Liu. Power performance assessment of H-rotor vertical axis wind turbines with different aspect ratios in turbulent flows via experiments. *Energy*, 173:121–132, apr 2019.

[64] Seyed Hossein Hezaveh, Elie Bou-Zeid, Mark W. Lohry, and Luigi Martinelli. Simulation and wake analysis of a single vertical axis wind turbine. *Wind Energy*, 20(4):713–730, apr 2017.

[65] Abdolrahim Rezaeiha, Ivo Kalkman, and Bert Blocken. Effect of pitch angle on power performance and aerodynamics of a vertical axis wind turbine. *Applied Energy*, 197:132–150, jul 2017.

[66] Gebreel Abdalrahman, William Melek, and Fue-Sang Lien. Pitch angle control for a small-scale Darrieus vertical axis wind turbine with straight blades (H-Type VAWT). *Renewable Energy*, 114:1353–1362, dec 2017.

[67] V. Samsonov and P. Baklushin. Comparison of different ways for VAWT aerodynamic control. *Journal of Wind Engineering and Industrial Aerodynamics*, 39(1-3):427–433, jan 1992.

[68] Yan Yan, Eldad Avital, and John Williams. CFD Analysis for the Performance of Gurney Flap on Aerofoil and Vertical Axis Turbine. 2019.

[69] Ion Malael, Radu Bogateanu, Horia Dumitrescu, and Corresponding Author. Theoretical performances of double Gurney Flap equipped the VAWTs. *INCAS BULLETIN*, 4:93–99, 2012.

[70] Haitian Zhu, Wenxing Hao, Chun Li, and Qinwei Ding. Numerical study of effect of solidity on vertical axis wind turbine with Gurney flap. *Journal of Wind Engineering and Industrial Aerodynamics*, 186:17–31, mar 2019.

[71] Junwei Zhong, Jingyin Li, and Penghua Guo. Effects of leading-edge rod on dynamic stall performance of a wind turbine airfoil. *Journal of Power and Energy*, 231(8):753–769, 2017.

[72] Yichen Jiang, Chenlu He, Peidong Zhao, and Tiezhi Sun. Investigation of Blade Tip Shape for Improving VAWT Performance. *Journal of Marine Science and Engineering*, 8(225), 2020.

[73] Thierry Villeneuve, Matthieu Boudreau, and Guy Dumas. Improving the efficiency and the wake recovery rate of vertical-axis turbines using detached end-plates. *Renewable Energy*, 150:31–45, may 2020.

[74] Santiago Laín, Manuel Taborda, and Omar López. Numerical Study of the Effect of Winglets on the Performance of a Straight Blade Darrieus Water Turbine. *Energies*, 11(2):297, jan 2018.

[75] Tian-tian Zhang, Mohamed Elsakka, Wei Huang, Zhen-guo Wang, Derek B. Ingham, Lin Ma, and Mohamed Pourkashanian. Winglet design for vertical axis wind turbines based on a design of experiment and CFD approach. *Energy Conversion and Management*, 195:712–726, sep 2019.

[76] Binyamin Sasson and David Greenblatt. Effect of Leading-Edge Slot Blowing on a Vertical Axis Wind Turbine. *AIAA Journal*, 49(9):1932–1942, sep 2011.

[77] Abdolrahim Rezaeiha, Hamid Montazeri, and Bert Blocken. Active flow control for power enhancement of vertical axis wind turbines: Leading-edge slot suction. *Energy*, 189:116131, dec 2019.

[78] Haitian Zhu, Wenxing Hao, Chun Li, and Qinwei Ding. Simulation on flow control strategy of synthetic jet in an vertical axis wind turbine. *Aerospace Science and Technology*, 77:439–448, jun 2018.

[79] Omar S. Mohamed, Ahmed A. Ibrahim, Ahmed K. Etman, Amr A. Abdelfatah, and Ahmed M.R. Elbaz. Numerical investigation of Darrieus wind turbine with slotted airfoil blades. *Energy Conversion and Management: X*, 5:100026, jan 2020.

[80] Ning Qin, Robert Howell, Naveed Durrani, Kenichi Hamada, and Tomos Smith. Unsteady Flow Simulation and Dynamic Stall Behaviour of Vertical Axis Wind Turbine Blades. *Wind Engineering*, 35(4):511–527, aug 2011.

[81] Anders Goude, Staffan Lundin, and Mats Leijon. A parameter study of the influence of struts on the performance of a vertical-axis marine current turbine. In *8th European Wave and Tidal Energy Conference*, pages 477–482, Uppsala, Sweden, 2009.

[82] Victor Mendoza. Aerodynamic Studies of Vertical Axis Wind Turbines using the Actuator Line Model. Digital Comprehensive Summaries of Uppsala Dissertations from the Faculty of Science and Technology 1671. volume 85, 2018.

[83] Zhenyu Wang and Mei Zhuang. Leading-edge serrations for performance improvement on a vertical-axis wind turbine at low tip-speed-ratios. *Applied Energy*, 208:1184–1197, dec 2017.

[84] Mahdi Zamani, Saeed Nazari, Sajad A. Moshizi, and Mohammad Javad Maghrebi. Three dimensional simulation of J-shaped Darrieus vertical axis wind turbine. *Energy*, 116(December):1243–1255, 2016.

[85] Mahdi Zamani, Mohammad Javad Maghrebi, and Seyed Rasoul Varedi. Starting torque improvement using J-shaped straight-bladed Darrieus vertical axis wind turbine by means of numerical simulation. *Renewable Energy*, 95:109–126, sep 2016.

[86] Lin Pan, Haodong Xiao, Yanwei Zhang, and Zhaoyang Shi. Research on Aerodynamic Performance of J-type Blade Vertical Axis Wind Turbine. In *2020 Chinese Control And Decision Conference (CCDC)*, pages 5454–5459, Hefei, China, aug 2020. IEEE.

[87] Wen-Tong Chong, Wan Khairul Muzammil, Kok-Hoe Wong, Chin-Tsan Wang, Mohammed Gwani, Yung-Jeh Chu, and Sin-Chew Poh. Cross axis wind turbine: Pushing the limit of wind turbine technology with complementary design. *Applied Energy*, 207:78–95, dec 2017.

[88] Wen-Tong Chong, Wan Khairul Muzammil, Hwai-Chyuan Ong, Kamaruzzaman Sopian, Mohammed Gwani, Ahmad Fazlizan, and Sin-Chew Poh. Performance analysis of the deflector integrated cross axis wind turbine. *Renewable Energy*, 138:675–690, aug 2019.

[89] Wei-Cheng Wang, Wen Tong Chong, and Tien-Hsin Chao. Performance analysis of a cross-axis wind turbine from wind tunnel experiments. *Journal of Wind Engineering and Industrial Aerodynamics*, 174:312–329, mar 2018.

[90] Manabu Takao, Hideki Kuma, Takao Maeda, Yasunari Kamada, Michiaki Oki, and Atsushi Minoda. A straight-bladed vertical axis wind turbine with a directed guide vane row — Effect of guide vane geometry on the performance —. *Journal of Thermal Science*, 18(1):54–57, mar 2009.

[91] Rosario Nobile, Maria Vahdati, Janet F. Barlow, and Anthony Mewburn-Crook. Unsteady flow simulation of a vertical axis augmented wind turbine:

A two-dimensional study. *Journal of Wind Engineering and Industrial Aerodynamics*, 125:168–179, feb 2014.

[92] S. Zanforlin and S. Letizia. Improving the Performance of Wind Turbines in Urban Environment by Integrating the Action of a Diffuser with the Aerodynamics of the Rooftops. *Energy Procedia*, 82:774–781, dec 2015.

[93] Benjamin Strom, Steven L. Brunton, and Brian Polagye. Intracycle angular velocity control of cross-flow turbines. *Nature Energy*, 2(8):17103, aug 2017.

[94] G Mosetti, C Poloni, and B Diviacco. Optimization of wind turbine positioning in large windfarms by means of a genetic algorithm. Technical report, 1994.

[95] Johan Meyers and Charles Meneveau. Optimal turbine spacing in fully developed wind farm boundary layers. *Wind Energy*, 15(2):305–317, mar 2012.

[96] Abdullah Mobin Chowdhury, Hiromichi Akimoto, and Yutaka Hara. Comparative CFD analysis of Vertical Axis Wind Turbine in upright and tilted configuration. *Renewable Energy*, 85:327–337, jan 2016.

[97] Mojtaba Ahmadi-Baloutaki, Rupp Carriveau, and David S-K. Ting. A wind tunnel study on the aerodynamic interaction of vertical axis wind turbines in array configurations. *Renewable Energy*, 96:904–913, oct 2016.

[98] Stefania Zanforlin and Takafumi Nishino. Fluid dynamic mechanisms of enhanced power generation by closely spaced vertical axis wind turbines. *Renewable Energy*, 99:1213–1226, dec 2016.

[99] Stefania Zanforlin. Advantages of vertical axis tidal turbines set in close proximity: A comparative CFD investigation in the English Channel. *Ocean Engineering*, 156:358–372, may 2018.

[100] H.F. Lam and H.Y. Peng. Measurements of the wake characteristics of co- and counter-rotating twin H-rotor vertical axis wind turbines. *Energy*, 131:13–26, jul 2017.

[101] D De Tavernier, C Ferreira, A Li, U S Paulsen, and H A Madsen. Towards the understanding of vertical-axis wind turbines in double-rotor configuration. Towards the understanding of vertical-axis wind turbines in double-rotor configuration. page 22015, 2018.

[102] Simone Giorgetti, Giulio Pellegrini, and Stefania Zanforlin. CFD Investigation on the Aerodynamic Interferences between Medium-solidity Darrieus Vertical Axis Wind Turbines. *Energy Procedia*, 81:227–239, dec 2015.

[103] Ian D. Brownstein, Nathaniel J. Wei, and John O. Dabiri. Aerodynamically Interacting Vertical-Axis Wind Turbines: Performance Enhancement and Three-Dimensional Flow. *Energies*, 12(14):2724, 2019.

[104] Sadra Sahebzadeh, Abdolrahim Rezaeiha, and Hamid Montazeri. Towards optimal layout design of vertical-axis wind-turbine farms: Double rotor arrangements. *Energy Conversion and Management*, 226:113527, dec 2020.

[105] Robert W Whittlesey, Sebastian Liska, and John O Dabiri. Fish schooling as a basis for vertical axis wind turbine farm design. *Bioinspiration & Biomimetics*, 5(3):035005, sep 2010.

[106] Seyed Hossein Hezaveh, Elie Bou-Zeid, John Dabiri, Matthias Kinzel, Gerard Cortina, and Luigi Martinelli. Increasing the Power Production of Vertical-Axis Wind-Turbine Farms Using Synergistic Clustering. *Boundary-Layer Meteorology*, 169(2):275–296, nov 2018.

[107] Ammar Naseem, Zaib Ali, and Emad Uddin. On Power Augmentation of VAWT in the wake of a bluff body. In *Proceedings of the 6th International Conference of Fluid Flow, Heat and Mass Transfer (FFHMT'19)*, page 108, Ottawa, Canada, 2019.

[108] Andrew Barnes and Ben Hughes. Determining the impact of VAWT farm configurations on power output. *Renewable Energy*, 143:1111–1120, may 2019.

[109] H.Y. Peng, Z.D. Han, H.J. Liu, K. Lin, and H.F. Lam. Assessment and optimization of the power performance of twin vertical axis wind turbines via numerical simulations. *Renewable Energy*, 147:43–54, mar 2020.

[110] Aaron S. Alexander and Arvind Santhanakrishnan. Mechanisms of power augmentation in two side-by-side vertical axis wind turbines. *Renewable Energy*, 148:600–610, apr 2020.

[111] Ian D. Brownstein, Matthias Kinzel, and John O. Dabiri. Performance enhancement of downstream vertical-axis wind turbines. *Journal of Renewable and Sustainable Energy*, 8(5):053306, sep 2016.

[112] Steven Beresh. Can PIV Measure a Full-Scale Wind Turbine ? Why do we want PIV ?, 2020.

[113] H.Y. Peng, H.F. Lam, and C.F. Lee. Investigation into the wake aerodynamics of a five-straight-bladed vertical axis wind turbine by wind tunnel tests. *Journal of Wind Engineering and Industrial Aerodynamics*, 155:23–35, aug 2016.

[114] Haiying Sun, Xiaoxia Gao, and Hongxing Yang. A review of full-scale wind-field measurements of the wind-turbine wake effect and a measurement of the wake-interaction effect. *Renewable and Sustainable Energy Reviews*, 132:110042, oct 2020.

[115] P. Schito, I. Bayati, M. Belloli, L. Bernini, V. Dossena, and A. Zasso. Numerical Wind Tunnel Tests of an Open Data IPC-VAWT. Technical report, 2018.

[116] Belabes Belkacem and Marius Paraschivoiu. Numerical study of the effect of turbulence intensity on VAWT performance. *Energy*, page 121139, jun 2021.

[117] Vincent F-C. Rolin and Fernando Porté-Agel. Experimental investigation of vertical-axis wind-turbine wakes in boundary layer flow. *Renewable Energy*, 118:1–13, apr 2018.

[118] C. H.J. Stork, C. P. Butterfield, W. Holley, P. H. Madsen, and P. H. Jensen. Wind conditions for wind turbine design proposals for revision of the IEC 1400-1 standard. *Journal of Wind Engineering and Industrial Aerodynamics*, 74-76:443–454, apr 1998.

[119] Alessandro Bianchini, Lorenzo Ferrari, and Sandro Magnani. START-UP BEHAVIOR OF A THREE-BLADED H-DARRIEUS VAWT: EXPERIMENTAL AND NUMERICAL ANALYSIS. In *ASME Turbo Expo 2011*, 2011.

[120] Alexandrina Untaroiu, Houston G. Wood, Paul E. Allaire, and Robert J. Ribando. Investigation of Self-Starting Capability of Vertical Axis Wind Turbines Using a Computational Fluid Dynamics Approach. *Journal of Solar Energy Engineering*, 133(4):041010, nov 2011.

[121] Andreu Carbó Molina, Tim De Troyer, Tommaso Massai, Antoine Vergaerde, Mark C. Runacres, and Gianni Bartoli. Effect of turbulence on the performance of VAWTs: An experimental study in two different wind tunnels. *Journal of Wind Engineering and Industrial Aerodynamics*, 193, oct 2019.

[122] Limin Kuang, Hang Lei, Dai Zhou, Zhaolong Han, Yan Bao, and Yongsheng Zhao. Numerical Investigation of Effects of Turbulence Intensity on Aerodynamic Performance for Straight-Bladed Vertical-Axis Wind Turbines. *Journal of Energy Engineering*, 147(1):04020087, 2021.

[123] C. A. Lopez-Villalobos, O. Rodriguez-Hernandez, R. Campos-Amezcua, Guillermo Hernandez-Cruz, O. A. Jaramillo, and J. L. Mendoza. Wind turbulence intensity at la Ventosa, Mexico: A comparative study with the IEC61400 standards. *Energies*, 11(11):1–19, 2018.

[124] Louis Angelo Danao, Jonathan Edwards, Okeoghene Eboibi, and Robert Howell. A numerical investigation into the influence of unsteady wind on

the performance and aerodynamics of a vertical axis wind turbine. *Applied Energy*, 116:111–124, mar 2014.

[125] Zhenlong Wu, Galih Bangga, and Yihua Cao. Effects of lateral wind gusts on vertical axis wind turbines. *Energy*, 167:1212–1223, jan 2019.

[126] Marco Raciti Castelli, Guido Ardizzon, Lorenzo Battisti, Ernesto Benini, and Giorgio Pavesi. Modeling Strategy and Numerical Validation for a Darrieus Vertical Axis Micro-Wind Turbine. In *Volume 7: Fluid Flow, Heat Transfer and Thermal Systems, Parts A and B*, pages 409–418. ASME, jan 2010.

[127] A Orlandi, M Collu, S Zanforlin, and A Shires. 3D URANS Analysis of a Vertical Axis Wind Turbine in Skewed Flows. 2015.

[128] Chao Li, Songye Zhu, You-lin Xu, and Yiqing Xiao. 2.5D large eddy simulation of vertical axis wind turbine in consideration of high angle of attack flow. *Renewable Energy*, 51:317–330, mar 2013.

[129] Jiao He, Xin Jin, Shuangyi Xie, Le Cao, Yaming Wang, Y. Lin, and Ning Wang. CFD modeling of varying complexity for aerodynamic analysis of H-vertical axis wind turbines. *Renewable Energy*, 145:2658–2670, jan 2020.

[130] Hang Lei, Dai Zhou, Yan Bao, Ye Li, and Zhaolong Han. Three-dimensional Improved Delayed Detached Eddy Simulation of a two-bladed vertical axis wind turbine. *Energy Conversion and Management*, 133:235–248, feb 2017.

[131] Yutaka Hara, Naoki Horita, Shigeo Yoshida, Hiromichi Akimoto, and Takahiro Sumi. Numerical Analysis of Effects of Arms with Different Cross-Sections on Straight-Bladed Vertical Axis Wind Turbine. *Energies*, 12(11):2106, jun 2019.

[132] Amgad Dessoky, Thorsten Lutz, Galih Bangga, and Ewald Krämer. Computational studies on Darrieus VAWT noise mechanisms employing a high order DDES model. *Renewable Energy*, 143:404–425, dec 2019.

[133] Abdolrahim Rezaeiha, H. Montazeri, and Bert Blocken. CFD analysis of dynamic stall on vertical axis wind turbines using Scale-Adaptive Simulation (SAS): Comparison against URANS and hybrid RANS/LES. *Energy Conversion and Management*, 196:1282–1298, sep 2019.

[134] M. Sergio Campobasso, Jernej Drofelnik, and Fabio Gigante. Comparative assessment of the harmonic balance Navier–Stokes technology for horizontal and vertical axis wind turbine aerodynamics. *Computers & Fluids*, 136:354–370, sep 2016.

[135] Abdolrahim Rezaeiha, Ivo Kalkman, and Bert Blocken. CFD simulation of a vertical axis wind turbine operating at a moderate tip speed ratio: Guidelines for minimum domain size and azimuthal increment. *Renewable Energy*, 107:373–385, jul 2017.

[136] Abdolrahim Rezaeiha, Hamid Montazeri, and Bert Blocken. Towards accurate CFD simulations of vertical axis wind turbines at different tip speed ratios and solidities: Guidelines for azimuthal increment, domain size and convergence. *Energy Conversion and Management*, 156:301–316, jan 2018.

[137] László Daróczy, Gábor Janiga, Klaus Petrasch, Michael Webner, and Dominique Thévenin. Comparative analysis of turbulence models for the aerodynamic simulation of H-Darrieus rotors. *Energy*, 90:680–690, oct 2015.

[138] P. J. Roache. Perspective: A method for uniform reporting of grid refinement studies. *Journal of Fluids Engineering, Transactions of the ASME*, 116(3):405–413, sep 1994.

[139] K. M. Almohammadi, D. B. Ingham, L. Ma, and M. Pourkashanian. Effect of Transitional Turbulence Modelling on a Straight Blade Vertical Axis Wind Turbine. In *Alternative Energies: Updates on Progress*, pages 93–112. Springer, Berlin, Heidelberg, 2013.

[140] R Bravo, S Tullis, and S Ziada. Performance testing of a small vertical-axis wind turbine. *21st Canadian Congress of Applied . . .* , (June 2007):2–3, 2007.

[141] Rosario Lanzafame, Stefano Mauro, and Michele Messina. 2D CFD Modeling of H-Darrieus Wind Turbines Using a Transition Turbulence Model. *Energy Procedia*, 45:131–140, jan 2014.

[142] K.M. Almohammadi, D.B. Ingham, L. Ma, and M. Pourkashan. Computational fluid dynamics (CFD) mesh independency techniques for a straight blade vertical axis wind turbine. *Energy*, 58:483–493, sep 2013.

[143] Abdolrahim Rezaeiha, Ivo Kalkman, and Bert Blocken. CFD simulation of a vertical axis wind turbine operating at a moderate tip speed ratio: Guidelines for minimum domain size and azimuthal increment. *Renewable Energy*, 107:373–385, jul 2017.

[144] A. Rossetti and G. Pavesi. Comparison of different numerical approaches to the study of the H-Darrieus turbines start-up. *Renewable Energy*, 50:7–19, feb 2013.

[145] F. Trivellato and M. Raciti Castelli. On the Courant–Friedrichs–Lewy criterion of rotating grids in 2D vertical-axis wind turbine analysis. *Renewable Energy*, 62:53–62, feb 2014.

[146] Galih Bangga, Amgad Dessoky, Zhenlong Wu, Krzysztof Rogowski, and Martin O.L. Hansen. Accuracy and consistency of CFD and engineering models for simulating vertical axis wind turbine loads. *Energy*, 206:118087, jun 2020.

[147] Mazharul Islam, David S.K. Ting, and Amir Fartaj. Aerodynamic models for Darrieus-type straight-bladed vertical axis wind turbines. *Renewable and Sustainable Energy Reviews*, 12(4):1087–1109, may 2008.

[148] Xin Jin, Gaoyuan Zhao, KeJun Gao, and Wenbin Ju. Darrieus vertical axis wind turbine: Basic research methods. *Renewable and Sustainable Energy Reviews*, 42:212–225, feb 2015.

[149] Amin A Mohammed, Hassen M Ouakad, Ahmet Z Sahin, and Haitham M S Bahaidarah. Vertical Axis Wind Turbine Aerodynamics: Summary and Review of Momentum Models. *Journal of Energy Resources Technology*, 141:050801–1, 2019.

[150] Andrés Meana-Fernández, Irene Solís-Gallego, Jesús Manuel Fernández Oro, Katia María Argüelles Díaz, and Sandra Velarde-Suárez. Parametrical evaluation of the aerodynamic performance of vertical axis wind turbines for the proposal of optimized designs. *Energy*, 147:504–517, mar 2018.

[151] Sina Shamsoddin and Fernando Porté-Agel. Large eddy simulation of vertical axis wind turbine wakes. *Energies*, 7(2):890–912, 2014.

[152] J. H. Strickland, B. T. Webster, and T. Nguyen. A Vortex Model of the Darrieus Turbine: An Analytical and Experimental Study. *Journal of Fluids Engineering*, 101(4):500, dec 1979.

[153] D. Vandenberghe and E. Dick. A free vortex simulation method for the straight bladed vertical axis wind turbine. *Journal of Wind Engineering and Industrial Aerodynamics*, 26(3):307–324, jan 1987.

[154] A. C. Mandal and J. D. Burton. Effects of dynamic stall and flow curvature on the aerodynamics of Darrieus turbines applying the cascade model. *Wind Engineering*, 18(6):267–282, 1994.

[155] Frank Scheurich and Richard E Brown. Effect of Dynamic Stall on the Aerodynamics of Vertical-Axis Wind Turbines. 2011.

[156] David Marten, Georgios Pechlivanoglou, Christian Navid Nayeri, and Christian Oliver Paschereit. Nonlinear Lifting Line Theory Applied to Vertical

Axis Wind Turbines: Development of a Practical Design Tool. *Journal of Fluids Engineering*, 140(2), feb 2018.

[157] E Tingey and A Ning. Parameterized Vertical-Axis Wind Turbine Wake Model Using CFD Vorticity Data. *ASME Wind Energy Symposium*, 2016.

[158] Richard E. Brown. Rotor Wake Modeling for Flight Dynamic Simulation of Helicopters. *AIAA Journal*, 38(1):57–63, jan 2000.

[159] Brian Hand, Andrew Cashman, and Ger Kelly. A Low-Order Model for Offshore Floating Vertical Axis Wind Turbine Aerodynamics. *IEEE Transactions on Industry Applications*, 53(1):512–520, 2017.

[160] A. Sagharichi, T. Najafi Ghaghelestani, and S. Toudarbari. Impact of harmonic pitch functions on performance of Darrieus wind turbine. *Journal of Cleaner Production*, 241:118310, dec 2019.

[161] Li Zou, Kun Wang, Yichen Jiang, Aimin Wang, and Tiezhi Sun. Wind tunnel test on the effect of solidity on near wake instability of vertical-axis wind turbine. *Journal of Marine Science and Engineering*, 8(5), 2020.

[162] Delphine De Tavernier, Carlos Simão Ferreira, Ang Li, and Uwe Schmidt Paulsen. VAWT in double-rotor configuration: the effect on airfoil design. 2018.

[163] David W. MacPhee and Asfaw Beyene. Fluid–structure interaction analysis of a morphing vertical axis wind turbine. *Journal of Fluids and Structures*, 60:143–159, jan 2016.

[164] Jie Su, Yaoran Chen, Zhaolong Han, Dai Zhou, Yan Bao, and Yongsheng Zhao. Investigation of V-shaped blade for the performance improvement of vertical axis wind turbines. *Applied Energy*, 260, feb 2020.

[165] Leonardo Brito Kothe, Sérgio Viçosa Möller, and Adriane Prisco Petry. Numerical and experimental study of a helical Savonius wind turbine and a com-

parison with a two-stage Savonius turbine. *Renewable Energy*, 148:627–638, apr 2020.

[166] Marco Raciti Castelli, Alessandro Englaro, and Ernesto Benini. The Darrieus wind turbine: Proposal for a new performance prediction model based on CFD. *Energy*, 36(8):4919–4934, aug 2011.

[167] A. Arab, M. Javadi, M. Anbarsooz, and M. Moghiman. A numerical study on the aerodynamic performance and the self-starting characteristics of a Darrieus wind turbine considering its moment of inertia. *Renewable Energy*, 107:298–311, jul 2017.

[168] Peter Bachant and Martin Wosnik. Modeling the near-wake of a vertical-axis cross-flow turbine with 2-D and 3-D RANS. *Journal of Renewable and Sustainable Energy*, 8(5):053311, sep 2016.

[169] Matthieu Boudreau and Guy Dumas. Comparison of the wake recovery of the axial-flow and cross-flow turbine concepts. *Journal of Wind Engineering and Industrial Aerodynamics*, 165:137–152, jun 2017.

[170] H.F. Lam and H.Y. Peng. Study of wake characteristics of a vertical axis wind turbine by two- and three-dimensional computational fluid dynamics simulations. *Renewable Energy*, 90:386–398, may 2016.

[171] Andrés Bravo Cuesta, Francisco Javier Gomez-Gil, Juan Vicente Martín Fraile, Jesús Ausín Rodríguez, Justo Ruiz Calvo, and Jesús Peláez Vara. Feasibility of a simple small wind turbine with variable-speed regulation made of commercial components. *Energies*, 6(7):3373–3391, jul 2013.

[172] Nicolas Bons. Optimization of Vertical Axis Wind Turbine Farm Layout. *American Institute of Aeronautics and Astronautics*, 2010.

[173] Jan Bartl and Lars Saetran. Blind test comparison of the performance and wake flow between two in-line wind turbines exposed to different turbulent inflow conditions. *Wind Energ. Sci*, 2:55–76, 2017.

[174] Kyle Beland, Jeremy Bibeau, Christopher Gagnon, and Jacob Landry. Offshore Wind Turbine Array. Technical report, 2013.

[175] Cian Desmond, Jimmy Murphy, Lindert Blonk, and Wouter Haans. Description of an 8 MW reference wind turbine. In *Journal of Physics: Conference Series*, volume 753, 2016.

[176] Magdi Ragheb and Adam M. Wind Turbines Theory - The Betz Equation and Optimal Rotor Tip Speed Ratio. In *Fundamental and Advanced Topics in Wind Power*. InTech, jun 2011.

[177] Dylan Iverson, Matthieu Boudreau, Guy Dumas, and Peter Oshkai. Reprint of: Boundary layer tripping on moderate Reynolds number oscillating foils. *Journal of Fluids and Structures*, 89:267–278, 2019.

[178] Yan Zhang. Effects of distributed leading-edge roughness on aerodynamic performance of a low-Reynolds-number airfoil: an experimental study. *Theoretical and Applied Mechanics Letters*, 8(3):201–207, may 2018.

[179] Mats Wahl. *Designing an H-rotor type Wind Turbine for Operation on Amundsen-Scott South Pole Station*. PhD thesis, Uppsala University, 2007.

[180] Sina Shamsoddin and Fernando Porté-Age. A large-eddy simulation study of vertical axiswind turbine wakes in the atmospheric boundary layer. *Energies*, 9(5):1–23, 2016.

[181] Andrew Barnes, Daniel Marshall-Cross, and Ben Richard Hughes. Towards a standard approach for future Vertical Axis Wind Turbine aerodynamics research and development. *Renewable and Sustainable Energy Reviews*, 148:111221, sep 2021.

[182] Andrew Barnes, Daniel Marshall-Cross, and Ben Richard Hughes. Validation and comparison of turbulence models for predicting wakes of vertical axis wind turbines. *Journal of Ocean Engineering and Marine Energy 2021 7:4*, 7(4):339–362, jul 2021.